

Master's Programme in Geoengineering

Integrated evaluation of strength and moisture resistance in fly ash-bound rammed earth with incineration slag aggregate.

Manish Jaiswal

**Master's Thesis
2025**

Copyright ©2025 Manish Jaiswal

Author Manish Jaiswal

Title of thesis: Integrated evaluation of strength and moisture resistance in fly ash-bound rammed earth with incineration slag aggregate.

Programme Master's Programme in Geoengineering

Thesis supervisor Prof. Jouni Punkki

Thesis advisor(s) Senior Advisor Leena Korkiala-Tanttu , DSc. Anoosheh Iravanian

Collaborative partner City of Helsinki

Date 15.12.2025

Number of pages 65+34

Language English

Abstract

This thesis investigates the use of recycled materials, such as incineration slag and fly ash, in rammed earth construction as a sustainable alternative. The study focused on evaluating the strength, durability, and moisture resistance of stabilized rammed earth mixes using incineration slag as the aggregate and fly ash as the binder.

Various binder-to-aggregate ratios, moisture content, and aggregate mixes were tested. Key tests included uniaxial compressive strength (UCS), freeze-thaw resistance, ultrasonic pulse velocity (UPV), and calorimetry. The best performance was observed in a mix with a 1:4 binder-to-aggregate ratio and 16 % water, using incineration slag, crushed concrete, and Nilsiä sand, achieving a UCS of 11.1 MPa after 28 days. In comparison, mixes with only incineration slag reached 5.21 MPa. After 15 freeze-thaw cycles, the UCS of the 1:4 incineration slag only mixes increased by 41 % to 7.33 MPa, while the 1:5 mix increased by 33 % to 5.96 MPa. Hydrophobization reduced capillary water uptake by about 96 %.

Calorimetry tests indicated that higher binder content and adequate water significantly improved hydration. The 1:4 mix with 20 % water released about 220 J/g binder after 72 hours, while the same mix with 17 % water released 190 J/g binder, indicating more complete hydration and better pozzolanic activation of the fly ash. Further research is needed to assess the long-term performance of hydrophobization treatments and moisture control, as well as their application at a larger scale.

Keywords: Rammed earth, recycled materials, Incineration slag, Crushed concrete, fly ash, UCS Test, Freeze-thaw test, Saturation test.

Table of Contents

1	Introduction.....	8
2	Literature review	10
2.1	History.....	10
2.2	Composition in rammed earth method.....	12
2.3	Mechanical behavior of rammed earth.....	15
2.4	Case Study (i): (Kariyawasam et al., 2015)	16
2.5	Case Study (ii): Konala test Structure.....	19
2.5.1	Overview of the test structure	19
2.5.2	Results and analysis	20
3	Experimental study materials.....	24
3.1	Aggregates	24
3.2	Binder, activator and auxiliary material.....	26
4	Methodology	29
4.1	Sieving	30
4.2	Hydrophobization.....	32
4.3	Preparation for test samples	33
4.4	Freeze-thaw resistance	35
4.5	Capillary saturation	36
4.6	Uniaxial Compression Test.....	37
4.7	Calorimetry	38
4.8	Ultrasonic pulse velocity.....	39
5	Results.....	41
5.1	Uniaxial compressive strength.....	41
5.2	Secant modulus E_{50}	42
5.3	Effect of freeze and thaw	44
5.3.1	Effect of F-T on specimens with IS as sole aggregate	44
5.3.2	Effect of F-T on specimens with partially substituted aggregate mix	45
5.3.3	Effect of F-T on secant modulus (E_{50}) of the specimens	47
5.3.4	Combined effect of F-T and aggregate composition on stress-strain behavior	47
5.4	Capillary saturation and effect of hydrophobization.....	48
5.5	Relationship between UPV and UCS.....	50
5.6	Calorimetry test.....	53

6	Discussions and analysis	57
6.1	Conclusions from the lab test	57
6.2	Comparison with previous studies	58
6.3	Reliability of results	60
6.4	Suggestion for future research	61
	Attachments	66

Preface

Over the past few years, significant progress has been made in civil engineering using recycled materials. At Aalto University, research has focused on integrating recycled materials into construction. This work aims to demonstrate the feasibility of using recycled materials through lab tests with verifiable physical and mechanical properties. Building on previous successful studies, this thesis explores various mix-design options to identify the use of Incineration slag as aggregate in the rammed earth construction technique. The City of Helsinki has commissioned the research under the RAKISEI project.

I want to express my sincere thanks to Professor Jouni Punkki and Professor Leena Korkiala-Tanttu for acquiring this thesis topic and providing invaluable support throughout the process. I am also grateful to my advisor, Anoosheh Iravanian, for her constructive feedback and guidance. I give special thanks to Jukka Piironen from Aalto University's Concrete Lab for his assistance with the experiments. I would like to sincerely thank the City of Helsinki for funding this project and for their continued support of similar research initiatives at Aalto University over the past several years.

Finally, I want to thank my family and friends, whose encouragement has been essential during this journey. Thank you Otso for your valuable input along the way. A special thanks to my wife Renu and my boy Ahaan Olavi for their continued support and belief in me.

Espoo 15.12.2025

Manish Jaiswal

Abbreviations

CC	Crushed concrete
CE	Circular economy
CEB	Compressed earth blocks
CEM I	Portland cement, CEM I 52,5 R
CSRE	Cement Stabilised Rammed Earth
CW	Concrete waste
FA	Fly ash
F-T	Freeze-thaw
GHG	Green House Gas
IS	Incineration Slag
MSW	Municipal Solid Waste
NS	Nilsia sand
OPC	Ordinary Portland Cement
OWC	Optimal water content
PICB	Precast interlocking concrete block
PSD	Particle size distribution
QF	Quarry Fines
RE	Rammed earth
SRE	Stabilised rammed earth
UCT	Uniaxial compression test
UPV	Ultrasonic pulse velocity
VTT	Technical research centre of Finland
XRF	X-ray fluorescence

1 Introduction

The acceleration in the urbanization trend over the last several decades has fueled immense demand for construction materials and other natural resources, contributing to significant environmental degradation, depletion of available natural resources, and global warming. About 40 % of the GHG emissions and a third of all the waste generated in the EU can be attributed to the construction Industry. According to some estimates, up to 90 % of the construction waste can be recycled; however, less than a third is recycled. According to the Waste Framework, Directive 2008/98 (as amended by Directive (EU) 2018/851), a target was set for 55 % of the generated municipal waste to be recycled and prepared for reuse by 2025 (Country Profile, 2022). Europe is at the forefront of waste recycling and circularity, with the highest rate of circularity of any other region. However, it is a paltry 11.8 % as of 2023. (European Environmental Agency, 2024).

Globally, urbanization and rapid economic development have accelerated the world's natural resource consumption, thus accelerating solid waste production. During the first decade of the 21st century, about 35 % of municipal solid waste was recycled in Finland.(Fischer, 2013). During the following decade, the recycling rate varied from 39% to 43%, which is an improvement but still falls short of the EU directive's initial target of 50% MSW recycling by 2020. As mandated by EU directive 2018/851, Finland, like any other EU member state, is committed to recycling 55 % of the MSW by the year 2025, 60 % by 2030, and 65 % by the end of the year 2035(ymparisto.fi, 2024).

The history of studies on using recycled materials as substitutes for natural aggregates and frame materials in earth construction spans over five decades. Since the early 2000s, public-private partnerships have been ongoing in Finland to foster the use of recycled materials in earth construction. The program highlights the importance of recycled materials in earthworks and their potential to reduce the environmental impact of earth construction. (UUMA, 2006). According to a recent estimate, the annual consumption of natural materials for construction and earthworks stands at about 100 million tons in rock materials. In contrast, natural aggregates consume about 70 to 80 million tons. The environmental impact and GHG emissions for the whole lifecycle of these materials are significant. Finland produces roughly a similar quantity of recovered materials suitable for construction, providing ample opportunity to explore the possibilities. However, achieving this requires commercializing the process of recycled material production, developing the technology needed for adoption in construction technology, and standardizing the procurement and planning for the use of recycled materials. (UUMA Programs, 2024).

On the other hand, using recycled materials like Fly ash as a binding agent in concrete substitutes or rammed earth construction will be pivotal in achieving the GHG emissions goals. Globally, the production of Ordinary Portland Cement (OPC), the primary binder of concrete output, accounts for 8 % of the carbon emissions and 3 % of global energy consumption. Not only this, but the concrete industry is also the largest consumer of natural aggregates and fresh water. The multi-faceted implications of the concrete industry's effect on the environment require a robust and holistic approach to finding sustainable solutions addressing these issues. The multifaceted implications of the concrete industry's environmental impact require a robust, holistic approach to find sustainable solutions.(Sivakrishna et al., 2020).

At Aalto University, research on the reuse of recycled materials and the characterization of their physical and mechanical properties has progressed over several years. In addition to extensive laboratory specimen preparation and testing, this thesis synthesised and critically examined the outcomes and research directions of earlier Aalto University theses, with particular emphasis on the work of Kasper Holopainen, Rammed earth noise wall test structure with recycled materials (2022). The objective of this thesis was to investigate the following research questions.

- How do the physical properties of samples incorporating incineration slag (IS) as aggregate and fly ash as binder vary with incremental changes in activator dosage and differing water contents?
- What is the effect of hydrophobization treatment on the capillary saturation behavior of rammed earth samples?
- In addition to utilizing IS as an aggregate, how are the material properties affected by the inclusion of supplementary aggregates, such as crushed concrete, in combination with IS?

This study focuses on stabilized rammed earth samples prepared with incineration slag as the primary aggregate, fly ash as the binder, and rapid cement as the activator. The experiments were limited to laboratory-scale samples tested for uniaxial compressive strength, capillary water absorption, and freeze-thaw resistance. Long-term field performance, chemical leaching, and microstructural degradation under natural environmental exposure were outside the scope of this research.

2 Literature review

This chapter deals with the history of rammed earth construction and its significance. It also examines the physical characteristics and mechanical properties of rammed earth structures and the methodology of rammed earth construction. Earth and water were the most abundantly available resources now and during the early phase of civilization. Earth/soil is also the most straightforward construction material. These two materials were abundantly used for making early structures due to their abundance, availability, and ease of work. This construction method has been used throughout several civilizations to produce monolithic and homogeneous structures. In this thesis work, the main constituent will be incineration slag.

2.1 History

Earth construction and structures are still prevalent worldwide, with a significant population still living in earthen dwellings. Historical records of buildings with earth or soil are not well documented, but they date back several millennia from the Nile Valley civilization to the Indus Valley civilization. Several remains of earthen structures dating back to the early civilizations of Egypt, China, Mexico, and Peru, as well as in Mesopotamia and Babylonia, have been uncovered. When humankind initially went on to get away from the hunter-gatherer way of living to the agrarian way of living, they tended to settle along the banks of the rivers. This transition necessitated the need for permanent shelter and soil-earth-based construction, and shelter became an obvious choice due to the availability of those resources. (Reddy, 2022).

The use of earthen structures was not limited to building homes for shelter but was also used for religious buildings. Ramesseum, the Memorial temple of Ramesses II at Goruna, Egypt, is one such structure that dates back at least three millennia. Similarly, the citadel of Bam in Iran is one fine example of a structure made out of earth and other organic materials, also called adobe, dating back to the 6th- 4th century B.C. One of the world's seven wonders, "The Great Wall of China" is primarily a rammed earth structure dating back to the 7th century B.C during the reign of the Qin dynasty. However, later covering the exterior made it appear like a stone wall, which is a well-renowned earth structure. During 300 to 900 AD, the Sun Pyramid in Teotihuacan, Mexico, was built with its core mostly from 2 million tons of rammed earth. (Minke, 2006).

In Germany, after the Bronze Age discoveries, the earth was primarily used as infill in timber-framed houses and as a sealant for walls made of tree trunks. The oldest example of such a mud brick structure that still exists is found in Northern Europe near Lake Constance, Germany, which is estimated to date back to the 6th century BC. According to ancient texts of Pliny, several rammed earth forts existed in Spain by the end of year 100 BC. (Minke, 2006).



Figure 2.1. Citadel of Bam, Iran (Left) and Sun Pyramid in Teotihuacan, Mexico (Right).

Even in the modern era, there have been several examples of using rammed earth to build structures, one of which is the city of Shibam in Yemen. Roughly over three centuries ago, the residents began to build. Almost 500 of those buildings cross the 30-meter mark, a testament to the incredible versatility of rammed earth structures. The town of Tarim, near Shibam, Yemen, is home to the Al-Muhdhar Mosque, which features a minaret reaching 53 meters in height. Built as an adobe minaret, it is the tallest earthen structure constructed over a century ago, in 1914. (Jaquin Paul, 2012).

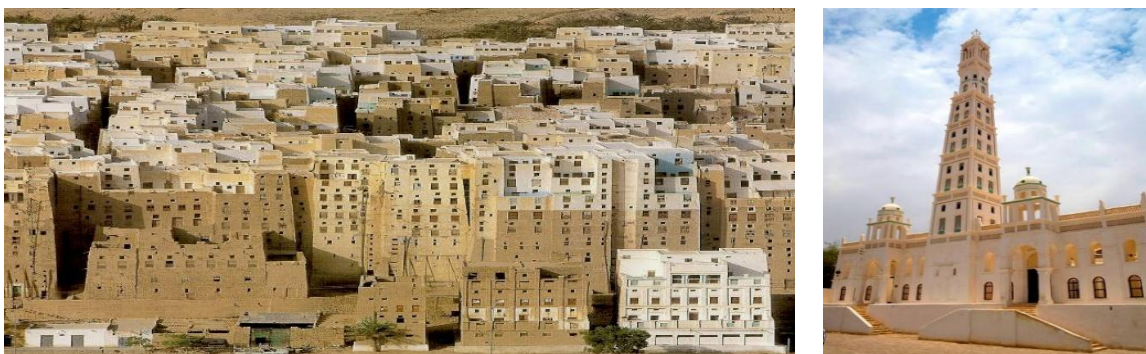


Figure 2.2. City of Shibam, Yemen (Left) and Al-Muhdhar Mosque, Yemen (Right).

At the end of the 18th century, Europe was experiencing a revolution against the ruling class, and freedom for the common person was the great cause for society. During this era, the rammed earth was 'rediscovered' and was made mainstream by the Frenchman Francios Cointeraux, who published a series of pamphlets about rammed earth in Lyon in 1791. (Jaquin Paul, 2012).

2.2 Composition in rammed earth method

At the very basic, rammed earth structures are made with earth/soil and an optimum amount of water. It can be stabilized or non-stabilized. Stabilizing the earth with either cement/cementitious materials or ramming it with suitable water content results in Cement stabilized rammed earth (CSRE); if the process involves using other binding materials, then we refer to it as stabilized rammed earth (SRE). The soil granulometry can vary, resulting in variations in the properties and characteristics. The stabilization can be physical, mechanical, or Chemical. Suitable particle size distribution with a good mix of constituent materials like gravel, sand, silt, and clay results in physical stabilization. Dynamic compaction using a manual or pneumatic compactor results in mechanical stabilization. Chemical stabilization is the addition of Cement or cementitious materials like lime, fly ash, or other materials to improve the strength and speed up the strengthening process. Builders utilize all three stabilization processes to achieve the best results. (Kariyawasam & Jayasinghe, 2016).

Mineral soil composition, grain size distribution, and binder type significantly affect the effectiveness and adaptability of rammed earth structures. Lime has been used as the prominent binding/stabilizing agent in rammed earth structures for over 2000 years, with the earliest documented uses dating back to ancient Greek and Roman architecture. In regions with rich clay content in the soil, lime became a popular additive to improve water resistance, cohesion, and long-term durability. When mixed with lime, soils rich in clay result in chemical improvement of these soils due to effective and permanent reaction between the Calcium compound and the pozzolanic fraction present in the soil.(Jaquin Paul, 2012). Lime stabilization loses its efficacy in areas like Northern Portugal, where the Kalolinitic clay is less than 10% in granitic soils. To mitigate this issue and minimize the dependence on environmentally harmful Cement, researchers have recently started using geopolymeric binders obtained via alkaline activation. Alkaline activation involves reacting aluminosilicate materials with alkaline solutions, such as sodium hydroxide (NaOH) or potassium silicate (K_2SiO_3), to produce a polymeric framework of Si-O-Al bonds. Adding water to the mix plays an important role as a catalyst in the stabilizing process. These chemical reactions allow for interparticle cohesion. (Cristelo et al., 2012)

In geotechnical engineering, materials are classified based on known mechanical and physical properties, which are initially used as a reference to identify suitable materials. The most important among those is the type of soil based on particle-size distribution. The type and proportion of soil used in compaction must maintain a proper balance between coarse material to provide strength and sufficient fine particles to facilitate pore formation via internal suction. Table 2.1 below illustrates soil types categorized by grain-size distribution range. It is also important to create a proper pore structure, in addition to using the optimum moisture level during compaction, to achieve cohesion and the required density after curing in the final structure. In the rammed earth method, the range of available materials can be vast, depending on availability, economic feasibility, and environmental suitability, and is not limited to compacted soil alone. It also includes stabilized soil, which differs from the traditional rammed earth structure primarily by the addition of Cement or cementitious materials, such as lime, for greater strength and rapid strength gain.(Walker, 2005).

Table 2.1. Classification of soil according to particle size fractions (SFS-EN ISO 14688-1:2018).

Soil Group	Fractions	Particle size range (mm)	Optimal composition
Coarse soil	Gravel	> 2.0 to ≤ 63	45% - 80%
	Sand	> 0.063 to ≤ 2	45% - 80%
Fine soil	Silt	>0.002 to ≤ 0.063	10% - 30%
	Clay	≤ 0.002	5% - 20%

Table 1 shows the types of soil based on grain-size distribution. Classification is primarily based on the grain size distribution, and the optimum % of each fraction that can be utilized as % of mass in the whole mix. Walker et al. (2005) presented the optimum grain-size distribution for the mix in rammed-earth construction, with upper and lower bounds for particle size and mass %. In addition to grain size distribution, the presence of organic constituents plays an important role in influencing the behavior of rammed earth structures. Soil collected from the upper layers of the ground, typically within the top 40 centimeters, often contains plant residues, humus, and peat. These materials include colloidal particles that are usually acidic, with pH values below 6, which can affect the stability and strength development of the mix. In some construction practices, dried plant matter such as straw is deliberately incorporated into the mixture to enhance its tensile and flexural performance. The fibrous structure of the straw contributes to crack resistance and ductility while also improving the thermal insulation properties of the finished rammed earth structure.(Minke, 2006)

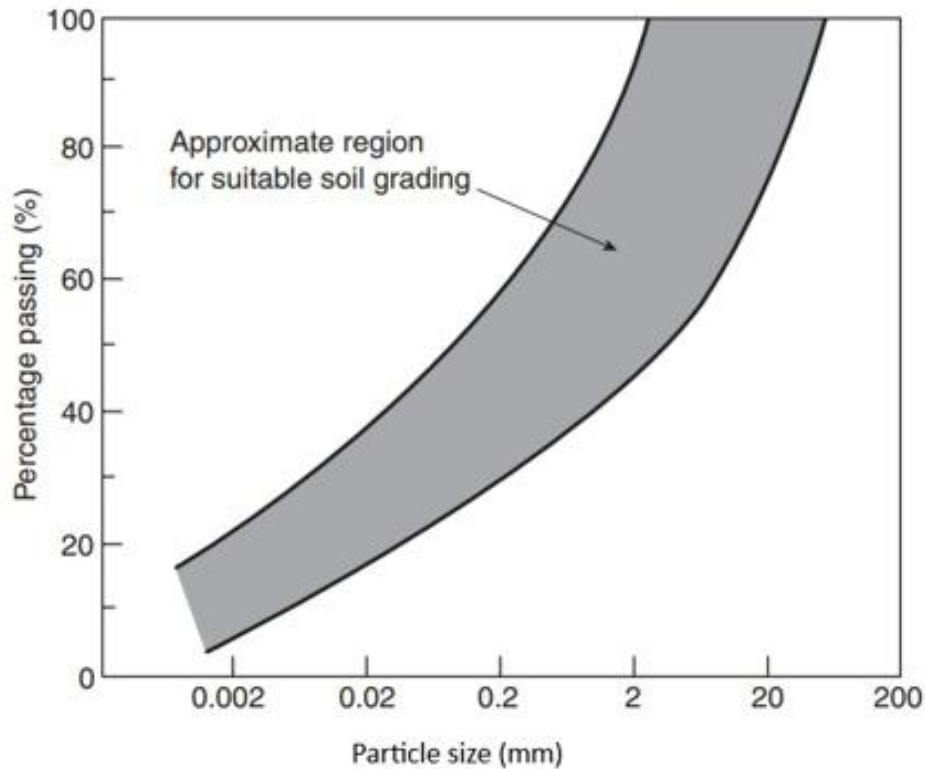


Figure 2.3. The optimal grain size distribution boundaries for rammed earth according to Walker, et al. (2005).

The suitability of soil materials for rammed-earth construction can be assessed with several geotechnical tests. One of the most commonly used parameters is the soil's particle size distribution (PSD). To evaluate the suitability of the soil for rammed earth construction, the yield limit, plastic limit, and shrinkage limit have to be defined. In 1907, Fuller and Thompson developed a widely accepted and used equation to describe the maximum gradation density for any given maximum fraction/aggregate size. Concrete technology can utilize this equation to achieve the theoretical maximum density and strength of any given mixture. The highest possible density for a given mixture increases the interaction between particles, i.e., internal forces that positively affect the material's strength.(Ciancio et al., 2013) . The equation is presented as

$$P = [d/D]^n \times 100$$

Where,

P = % passing a sieve of size d

d = Considered aggregate size

D = Maximum aggregate size in the mix

n = parameter, which adjusts the curve for fineness or coarseness (for maximum particle density $n \approx 0.5$ according to Fuller and Thompson)

However, the strength of a rammed-earth structure is not solely based on internal forces; there is little research evidence that links the density of the material to its strength. Walker (2005) recommends a plasticity limit between 2 and 30 and a yield limit below 45 for compacted soil. Keeping the shrinkage limit to less than 5 % is also recommended. When the compacted soil is stabilized with Cement, the plasticity value can be between 2 and 22 and below the yield limit of 40. According to Walker (2005), the best-suited material for stabilized rammed earth construction constitutes a mix of fine gravel (2-6.3 mm) 45-80 %, silt 15-30 %, and clay up to 20 %.

2.3 Mechanical behavior of rammed earth

In rammed-earth structures, the primary source of strength arises from the suction forces between soil particles and water in unstabilized conditions. The strength and behavior of rammed earth can be analyzed using principles of soil mechanics. In compacted earth construction, strength is commonly assessed through the Uniaxial Compressive Strength (UCS) test. Research consistently shows that the water content in the mixture significantly influences the final strength of the structure. (Jaquin et al., 2009).

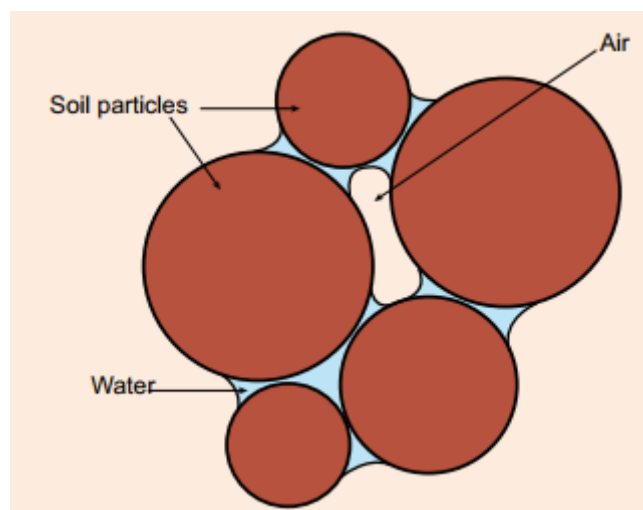


Figure 2.4. Simple model of unsaturated soil. (Jaquin et al. 2012)

Earthen materials are highly responsive to fluctuations in moisture, and this sensitivity has a direct influence on their mechanical behavior. When the moisture content increases, the cohesive forces between soil particles weaken, resulting in a measurable reduction in compressive strength and stiffness. Moisture ingress in earthen structures can occur through several pathways, including capillary rise from the foundation, roof leakage, or direct exposure to rainfall, particularly when surface detailing is inadequate. (Traoré et al., 2021).

Partially saturated soil contains three distinct phases: solid aggregates, pore water in the liquid state, and air occupying the remaining pore spaces. The interaction between these phases makes the development of effective stress considerably more complex than in either fully saturated or arid soils. In fully saturated soils, effective stress is defined as the difference between the total stress and the pore water pressure. However, in partially saturated soils, where both air and water coexist within the pore structure, a single, universally accepted definition of effective stress does not exist. (Fredlund & Rahardjo, 1993) Design shortcomings, such as applying impermeable coatings or elevating ground levels above the foundation line, can exacerbate this issue by restricting natural evaporation and disrupting the wall's moisture balance. Over time, these factors promote excessive water absorption, which may trigger surface erosion, progressive strength loss, and, in more severe cases, structural degradation of the earthen walls. (Traoré et al., 2021).

Freeze-thaw cycles induce frost damage, ground surface heave, and soil erosion in water-saturated environments. Frost heave occurs as freezing and thawing processes form ice lenses within the freezing zone, which expand the frozen soil volume and lift the ground surface. Soil qualifies as frost-susceptible when adequate moisture and freezing conditions promote substantial ice lens formation. During freezing, ice lenses extract water from the unfrozen zone at the frost line. Materials that form minimal ice lenses during freezing remain non-frost susceptible. Beyond ice lens formation, frost heave also develops when pore water freezes in situ within the soil matrix. (Pylkkänen & Nurmikolu, 2015). Freeze-thaw cycles significantly compromise the durability of rammed earth structures by causing spalling through the combined effects of moisture ingress and temperature fluctuations. At near-zero temperatures, water within soil pores freezes and expands, generating internal stresses that weaken the structural matrix. The inherently porous and permeable nature of rammed earth facilitates rapid moisture absorption, while repeated freeze-thaw events intensify surface spalling and cumulative material degradation. Experimental studies indicate that twelve freeze-thaw cycles between 21°C and -23°C can reduce wall mass by up to 2 %. The application of stabilizing agents, surface coatings, or insulation layers can effectively limit moisture intrusion and mitigate freeze-induced deterioration. (Fix & Richman, 2009).

2.4 Case Study (i): (Kariyawasam et al., 2015)

This chapter refers to an investigation by Kariyawasam et al. (2015) that assessed cement-stabilized rammed earth (CSRE) to determine whether it can serve as a viable alternative to traditional construction materials. This study involved assessing and establishing the strength properties of CSRE using

three types of laterite soil and varying cement percentages. Three types of laterite soils were sandy laterite, gravelly laterite, and clayey laterite. During the research, they identified all durability-related problems and determined remedial measures. They also assessed the embodied energy and contribution to the operational energy. The research also outlined the application of CSRE in pilot projects. The study evaluated the compressive strength of rammed earth wall panels prepared from selected soil types stabilized with cement contents of 6 %, 8 %, and 10 %. The samples were compacted at an optimum moisture range of 12 to 14 % and cured for 28 days under controlled conditions. Among the tested materials, the samples made with sandy laterite and 10 % cement content achieved the highest compressive strength of 3.7 MPa, demonstrating that increasing cement dosage within the tested range significantly enhanced the load-bearing capacity of the rammed earth panels.

The researchers mixed the selected soil type with a designated amount of cement as a dry mix. The dry mix and the optimum amount of water (12-14 %) were mixed and placed in the erected formwork layer by layer, compacting each layer before placing another layer on top. The formwork for CSRE was temporary and had sufficient strength, stiffness, and stability to resist the stresses exerted during erection, including placing the mix and ramming it with the hammer. Unlike the formwork for concrete structures, which must remain in place for a while after casting, the formwork for CSRE can be removed almost immediately after compacting. Two identical wall panels measuring 1000 mm long, 160 mm wide, and 650 mm high. The slenderness ratio was set to 4 in all cases to avoid nonuniformity in the test. The mixture was compacted manually using a 2.5 kg hand tamper. The compaction process followed the principle of compacting a 300 mm-high loose layer to a 150 mm-high compacted layer using the hammer, with an effective compaction ratio of 2.

In all cases, the effect of increased cement content was significant. Sandy laterite with 10 % cement, achieving the highest compressive strength of 3.71 MPa. The compressive strength obtained in the tests was satisfactory, considering the lowest average strength was recorded for Clayey laterite with 6 % cement at 1.66 MPa, and a typical two-storied load-bearing house, which accounts for stress at the plinth level, is 0.9 MPa. However, this assumption did not address safety factors in the load calculation. The researchers observed that the first cracks appeared at 60 % of the ultimate load during the compressive strength test.

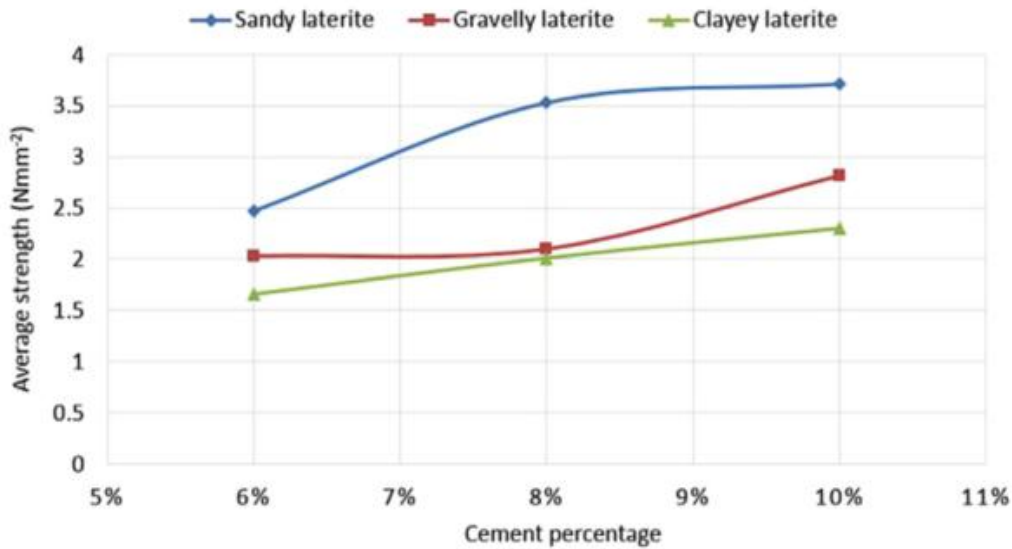


Figure 2.5. Variation of the strength of CSRE with soil type and cement % (Kariyawasam et al., 2015)

A flexural strength test was performed on the CSRE samples by applying out-of-plane loading parallel and perpendicular to the compacted layer. The testing process followed the guidelines provided by BS:5628, Part 1: 1992. For the flexural strength test, the researchers constructed a wall panel from sandy laterite soil with 8 % cement content and a wall thickness of 240 mm. To quantify the result and enable an appropriate comparison with traditional brick walls, the researchers cast a similar wall panel using burnt clay bricks and subjected it to the same test. Table 2.2 shows the flexural strength of CSRE and burnt clay bricks.

Table 2.2. Flexural strength of walling materials in two orthogonal directions.

Type of materials	Flexural strength (MPa)	
	Parallel to bed joints	Perpendicular to bed joints
Burnt clay bricks with water absorption >12 %	0.30	0.90
240 mm thick rammed earth wall made with sandy laterite	0.46	0.92

The flexural strength of the CSRE wall was 50 % higher than the conventional brick wall parallel to bed joints and was marginally better perpendicular to bed joints. These two strength tests at optimum water content do not provide hindsight on the structure's performance in adverse conditions. Like most earthen structures, the strength decreases after crossing the optimum water content level. Testing was done by preparing a CSRE wall panel measuring 240 mm long, 240 mm wide, and 140 mm high. To prepare the samples, the team mixed sandy laterite soil with 5 %, 6 %, and 8 %

cement. After preparing those samples, they were submerged in water for 24 hours and then subsequently tested for compressive strength test. Table 2.3 presents the wet and dry compressive strength values for different CSRE samples.

Table 2.3. Wet and dry compressive strength value for different CSRE samples

CSRE (% of cement content)	Wet strength (MPa)	Dry strength (MPa)	Ratio of wet/dry strength
CSRE Specimen (5% cement)	2.33	4.84	0.48
CSRE Specimen (6% cement)	1.22	2.34	0.52
CSRE Specimen (8% cement)	3.19	5.23	0.61

As shown above in table 2.3, wet strength is considerably weaker than dry strength, irrespective of the cement amount. The 6 % cement specimen unexpectedly underperformed compared to those with 5 % or 8 % cement, regardless of whether wet or dry. Following Earth Building Standard recommendations, every tested sample's wet/dry compressive strength ratio surpassed the 0.4 minimum. Better soil selection, higher compaction, and optimized cement/stabilizer could improve wet sample performance.

2.5 Case Study (ii): Konala test Structure

2.5.1 Overview of the test structure

This chapter documents the forensic study on a full-scale stabilised rammed earth test wall constructed in October 2021 at Konala, Helsinki. It was built in four distinct sections with four different stabilized rammed earth mixtures to study the suitability of different recycled materials in rammed earth construction and the long-term impact of using those materials, as investigated by Kasper Holopainen (2022). A long-term evaluation of the Konala test structure was conducted by Otso Laurila (2024).

Table 2.4. Detailed Mix Composition of Wall Sections Prepared in Konala

Parameter	Wall Section 1 (CC + Fly ash)	Wall Section 2 (CC + Fly ash)	Wall Section 3 (IS + Fly ash)	Wall Section 4 (IS + Fly ash)
Binder to aggregate ratio	1:5	1:5	1:4	1:5
Aggregate (saturated) [kg]	3047	3060	2609	2609
Aggregate w %	9.4	9.4	19.4	19.4
Water in aggregate [kg]	262	263	424	424
Aggregate dry weight [kg]	2785	2797	2185	2185
Fly ash [kg]	473	476	464	372

Cement [kg]	84	84	82	66
Planned w %	10	10	17	17
Added water [kg]	104	104	90	108
Actual w %	11	11	19	20

Each section of the test structure was 2.5 m long, 0.5 m wide and 1.2 m high separated by plywood boards in between. The mixes were rammed into a mold made from swan timber. The top of the section was covered with 1 m wide HDPE film forming 0.25 m eaves on both sides of the test structure.



Figure 2.6. Section of Konala Test structure

2.5.2 Results and analysis

As part of the long-term evaluation of the test structure, Otso Laurila (2022) made a detailed analysis of the test structure and samples taken from each test structure. Three samples from each and 12 in total were collected from the test structure. All the test samples were from the top of the structure, as it was not easy to retrieve the sample by cutting the test structure with a circular saw. General erosion assessment of the test structure was made, UPV test were performed on the Test structure and on the test samples. Test samples were also subjected to UCS to compare the results against the lab sample with a 28-day curing period vs the 975 days for the test structure.

Table 2.5. UPV comparison between Konala test structure and the corresponding laboratory samples.

Mix No.	Mix Composition	UPV, test structure average [m/s]	UPV, lab sample average [m/s]	Δ UPV (Test Structure VS Lab sample) [%]
1	CC + Fly ash (Helen) (1:5)	1661.9	2013.3	-17.4%
2	CC + Fly ash (UPM) (1:5)	1491.5	2261.1	-34.1%
3	IS + Fly ash (Helen) (1:4)	735.7	661.1	+11.3%

4	IS + Fly ash (Helen) (1:5)	806.6	731.1	+10.3%
---	----------------------------	-------	-------	--------

Table 2.5. presents the measured UPV values for both the Konala test structure and the corresponding laboratory samples. Measurements were carried out using the A1410 Pulsar handheld UPV device, applying the direct transmission method. The device manufacturer specifies a minimum threshold of 1000 m/s for reliable readings. As shown in the table, the incineration slag (IS) based mixes, IS + Fly ash (Helen) (1:4) and IS + Fly ash (Helen) (1:5), recorded structure velocities of 735.7 m/s and 806.6 m/s, thus the accuracy of the results for the IS-based samples can't be relied upon. In contrast, the crushed concrete (CC) based mixes, CC + Fly ash (Helen) and CC + Fly ash (UPM), showed substantially higher structure velocities of 1661.9 m/s and 1491.5 m/s, closer to those typically observed in weak concrete.

The difference between structure and sample readings highlights the influence of field exposure and material composition. The IS-based mixes showed positive deviations of 11.3 % and 10.3 %, where structure readings were slightly higher than laboratory samples, possibly due to differences in compaction or localized densification in the field or the fact that the curing period was much longer for the test structure samples. Conversely, the CC based mixes exhibited negative deviations of 17.4 % and 34.1 %, meaning their field structure readings were significantly lower than those from laboratory samples. This reduction is likely caused by microcracking, surface erosion, and moisture ingress that developed over time under natural environmental exposure, leading to signal attenuation. Overall, the data confirm that the crushed concrete mixtures maintained a denser and more coherent internal structure than the incineration slag mixtures, but the effects of weathering and heterogeneity reduced their in-situ UPV values compared to laboratory conditions.

Table 2.6. Comparison of Uniaxial Compressive Strength (UCS) Between 28-Day (Holopainen, 2022) and 975-Day Samples

Mix No.	Mix Composition	Sample	UCS (975d) [MPa]	UCS (28d) [MPa]	UCS Average (975d) [MPa]	UCS Average (28d) [MPa]
1	CC + Fly ash (Helen)	Sample 1	5.51	3.41	5.87	3.68
1	CC + Fly ash (Helen)	Sample 2	2.88	4.19		
1	CC + Fly ash (Helen)	Sample 3	7.39	3.43		
1	CC + Fly ash (Helen)	Sample 4	7.71			
2	CC + Fly ash (UPM)	Sample 1	2.47	3.25	4.48	3.08
2	CC + Fly ash (UPM)	Sample 2	5.17	2.96		
2	CC + Fly ash (UPM)	Sample 3	5.79	3.03		
3	IS + Fly ash (Helen) (1:4)	Sample 1	0.37		0.44	

3	IS + Fly ash (Helen) (1:4)	Sample 2	0.57			
3	IS + Fly ash (Helen) (1:4)	Sample 3	0.39			
4	IS + Fly ash (Helen) (1:5)	Sample 1	0.48	1.32		
4	IS + Fly ash (Helen) (1:5)	Sample 2	0.41	1.15	0.46	1.25
4	IS + Fly ash (Helen) (1:5)	Sample 3	0.5	1.28		

Table 2.6. presents the uniaxial compressive strength (UCS) values measured from both the Konala test structure (975-day samples) and the laboratory-prepared samples (28-day samples) as reported by Holopainen (2022). The results demonstrate that the crushed concrete (CC) based mixtures achieved substantially higher UCS values compared to the incineration slag (IS) based mixtures. Among all tested mixes, the CC + Fly ash (Helen) recipe exhibited the highest long-term strength with an average of 5.87 MPa after 975 days, followed by CC + Fly ash (UPM) with 4.48 MPa. In contrast, the IS + Fly ash (Helen) (1:4) and (1:5) mixtures recorded markedly lower strengths of 0.44 MPa and 0.46 MPa, respectively. When comparing the short-term and long-term results, the crushed concrete mixes show a clear strength gain over time, reflecting the ongoing hydration of the cementitious components within the structure, while the IS-based mixes show a decline, likely due to weaker particle bonding and structural degradation.

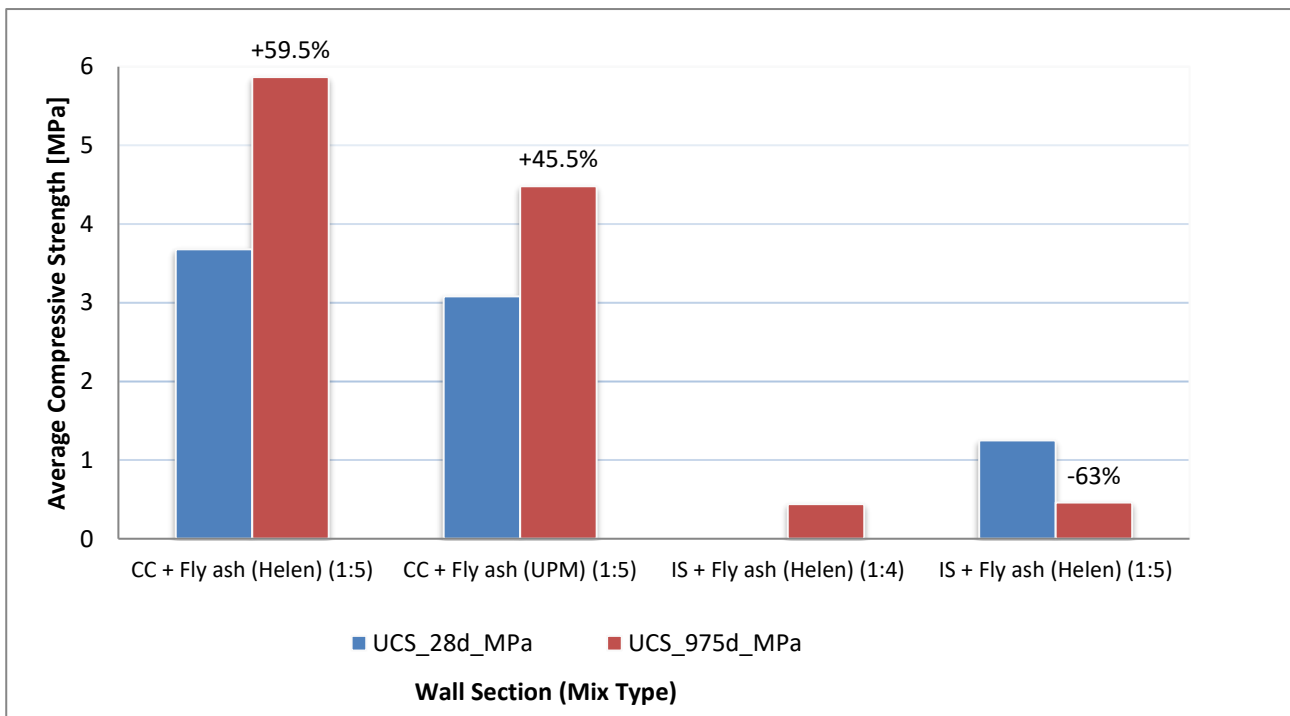


Figure 2.7. Average Uniaxial Compressive Strength (UCS) of lab samples (28 days) vs Konala Test Wall 975 Days.

The figure 2.7. visualizes these differences more clearly, illustrating the distinct performance of each mix between 28 and 975 days. The CC + Fly ash (Helen) and CC + Fly ash (UPM) mixtures show strength increases of approximately 59 % and 45 %, respectively, indicating effective long-term hydration and matrix densification. Conversely, the IS + Fly ash (Helen) (1:4) and (1:5) mixes show sharp reductions of more than 63 %, highlighting their structural vulnerability over time. The contextual analysis supports that these discrepancies arise from variations in field compaction, aggregate gradation, and moisture conditions. The crushed concrete sections benefited from ongoing cement hydration and better cohesion, while the incineration slag mixtures suffered from poor bonding, uneven moisture distribution, and disturbances from nearby site activities. As also noted by Holopainen (2022), section 3 appeared notably drier and dustier than laboratory samples, suggesting suboptimal water content and reduced binder activation. Overall, both Table 3.4 and Figure 2.7. demonstrate the superior long-term stability and durability of crushed concrete aggregates compared to the weaker, degradation-prone incineration slag mixtures.

3 Experimental study materials

This chapter outlines the experimental plan and laboratory methods employed in the study. The procedures for sample preparation, compaction, curing conditions, and testing are detailed. Test methods for compressive strength, ultrasonic pulse velocity, capillary saturation, freeze-thaw resistance, and calorimetry are described, with references to relevant standards and previous studies where appropriate. The objective is to ensure transparency and reproducibility of the data generation process.

3.1 Aggregates

Waste incineration slag (0-2 mm)

In the Uusimaa region, municipal mixed waste is collected and transported by the Helsinki Region Environmental Services Authority (HSY) to the waste-to-energy plant operated by Vantaan Energia in Vantaa. After incineration, the resulting slag is delivered to HSY's processing facility at the Ämmässuo landfill site in Espoo. There, the slag undergoes treatment, which includes the removal of ferrous and non-ferrous metals, crushing, and sieving into defined grain size fractions.

The processed fractions at Ämmässuo landfill site in Espoo include 0-2 mm, 2-5 mm, 5-16 mm, 16-50 mm, and a 2-50 mm mixed fraction. While larger fractions are often utilized in constructing structural layers at the landfill site, the 0-2 mm fraction remains underutilized, despite its growing accumulation and limited storage capacity. This master's thesis focuses on the 0-2 mm fraction of municipal solid waste (MSW) incineration slag, selected due to its limited current applications and increasing availability (Figure 3.1). The material has been processed at the Ämmässuo site according to the MARA regulation, which requires sampling in 5,000-tonne batches. According to leaching tests, the leaching values are too high for chromium (Cr), mercury (Hg), molybdenum (Mo), antimony (Sb), F⁻ (fluoride ion), SO₄ (sulfate) and TDS (total dissolved solids) for the incineration slag to be considered as inert waste. However, none of the values are high enough to cause the slag to be considered as dangerous waste. The complete result sheet is presented in the appendices.



Figure 3.1. Dried incineration slag 0-2 mm

The study aims to examine the mechanical behavior of samples in which this slag fraction serves as the primary aggregate. By evaluating its mechanical properties, the research seeks to determine the suitability of this recycled material as a potential replacement for conventional aggregates in construction applications.

Crushed concrete

In the study, the Crushed concrete also referred to as CC used as part of aggregate during the sample preparation was sourced from the crushing and recycling plant located in Vantaa and operated by Rudus Oy. Crushed concrete is considered as waste in Finland even after processing it. Which in practice entails the requirement for environmental permits to use them in construction or otherwise. However, government directive 843/2017 also called MARA-directive exempt the need for environmental permits to use crushed concrete is the construction of roads with restricted condition.



Figure 3.2. Crushed concrete aggregate (0-16 mm)

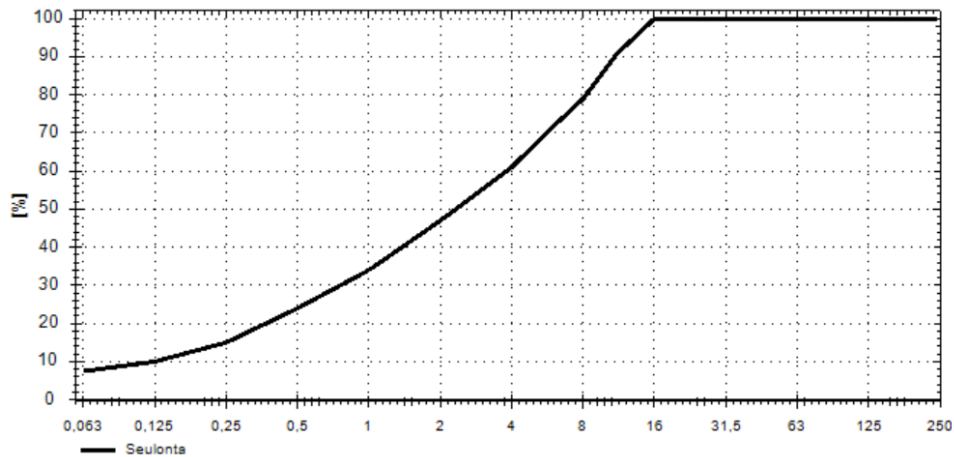


Figure 3.3. Gradation curve of Crushed concrete aggregate used in this study (Rudus Oy, 2024)

3.2 Binder, activator and auxiliary material

Fly ash

Fly ash is considered a primary pollutant produced in coal-fired power plants and thermal power plants. It is composed mainly of metallic oxides of metals such as silicon, Aluminum, Iron, and Calcium. In the coal-fired power plants, electrostatic precipitators or bag filters are generally used to collect the fly ash. (Zeynali et al., 2023). Several studies have demonstrated the potential of using fly ash as a binder material, particularly when it is coarse, has a high loss on ignition, or is conditioned. It is also possible to use fly ash in multi-binder systems to improve performance. Additionally, use of fly ash for grouting and masonry is on par with the results obtained by using Portland cement. (Mccarthy & Dhir, 1998).



Figure 3.6. Fly ash sourced from Rudus Oy

In all sample preparations conducted during this study, fly ash was used as the sole binder, with CEM I 52,5R acting as the chemical activator. The fly ash, supplied by Rudus Oy, is a byproduct of a coal-

fired power plant. Based on the X-ray fluorescence (XRF) analysis, it was found that silicon oxides made up approximately 50 % of the constituent materials, while aluminum, iron, and calcium oxides together accounted for around 40 %. A detailed breakdown of the XRF results is included in the appendices.

Rapid cement CEM I 52,5 R

Cement is a finely divided inorganic material primarily used as a binding component in concrete, along with aggregates and water. Its primary raw materials are limestone and naturally occurring minerals. Chemically, cement is composed of calcium, silicon, aluminum, iron, and sulfate compounds. The manufacturing process involves grinding the raw materials into a fine powder and heating them in a kiln at approximately 1450 °C. During this process, the minerals partially melt and react to form clinkers, which primarily consist of calcium silicates. Simultaneously, carbon dioxide is released from the limestone. The resulting clinker is then ground into a fine powder to produce the final cement product. (Suomen Betoniyhdistys ry, 2016 s.28, Betoniteollisuus ry 2019).



Figure 3.7. Rapid cement CEM I 52,5 R

The cement type used in the study was rapid-hardening cement CEM I 52.5 R. Rapid-hardening cement is a very fast-setting Portland cement. In this study, rapid-hardening cement was used directly as a binder in stabilized test samples, and additionally as an activator together with fly ashes from

coal combustion and biofuel combustion. The properties of the rapid-hardening cement, its additives, and the chemical composition of the clinker are listed in the table below Table 3.1.

Table 3.1: Rapid cement CEM I 52.5 R physical properties, additives and chemical composition, Finnsementti Oy 2019

Properties of Rapid-hardening Cement	Results	Units	Additives of Rapid-hardening Cement	
Strength 7d	41...46	MPa	Additive	%
Strength 28d	57...68	MPa	Limestone	0...5 %
Initial setting time	120...180	min	Blast furnace slag	-
Volume stability	0...2.0	mm	Chemical Composition of Clinker	
Fineness (Blaine)	490...570	m ² /kg	Compound	%
Loss on ignition	1.8...3.0	%	Calcium oxide (CaO)	63...65 %
Insoluble residue	0.3...0.9	%	Silicon dioxide (SiO ₂)	20...22 %
SO ₃	3.5...3.9	%	Aluminium oxide (Al ₂ O ₃)	4.0...5.4 %
Chloride content	≤ 0.08	%	Iron(III) oxide (Fe ₂ O ₃)	2.8...3.3 %
Cr ⁶⁺	0...2	mg/kg	Magnesium oxide (MgO)	2.5...3.2 %

4 Methodology

This chapter presents the laboratory research plan. The experimental study included the preparation of 102 samples in 28 series with variations in binder-to-aggregate ratio, water content %, cement %, and aggregate constituents as seen in table 4.1. The Uniaxial Compressive Strength test served as the fundamental test for each series. Selected series underwent additional testing, including capillary saturation, Freeze-thaw, and Ultrasonic Pulse Velocity. Calorimetry tests were conducted on design mixes from four series, namely M_5, M_6, M_17, and M_18. All tests adhered to established research standards, which were applied as necessary.

Table 4.1. The laboratory test matrix. M_11 and M_12 are Hydrophobized series.

Identification	Aggregate	Binder	Binder to Aggregate ratio	Cement (%)	Water (as % of dry mass)	Curing age (days)	Tests Performed
M_1_(1_3)	IS 0-2 mm	Rudus FA	1:04	3	20	28	UCT
M_2_(1_3)	IS 0-2 mm	Rudus FA	1:05	2.47	20	28	UCT
M_3_(1_3)	IS 0-2 mm	Rudus FA	1:04	6.75	20	28	UCT
M_4_(1_3)	IS 0-2 mm	Rudus FA	1:05	5.67	20	28	UCT
M_5_(1_3)	IS 0-2 mm	Rudus FA	1:04	10	20	28	UCT, Calorimetry
M_6_(1_3)	IS 0-2 mm	Rudus FA	1:05	8.17	20	28	UCT, Calorimetry
M_7_(1_3)	IS 0-2 mm	Rudus FA	1:04	10	20	28	F-T, UCT
M_8_(1_3)	IS 0-2 mm	Rudus FA	1:05	8.17	20	28	F-T, UCT
M_9_(1_3)	IS 0-2 mm	Rudus FA	1:04	10	20	28	SAT, UCT
M_10_(1_3)	IS 0-2 mm	Rudus FA	1:05	8.17	20	28	SAT, UCT
M_11_(1_3)**	IS 0-2 mm	Rudus FA	1:04	10	20	28	SAT, UCT
M_12_(1_3)**	IS 0-2 mm	Rudus FA	1:05	8.17	20	28	SAT, UCT
M_13_(1_3)	IS 0-2 mm	Rudus FA	1:04	3	17	28	UCT
M_14_(1_3)	IS 0-2 mm	Rudus FA	1:05	2.47	17	28	UCT
M_15_(1_3)	IS 0-2 mm	Rudus FA	1:04	6.75	17	28	UCT
M_16_(1_3)	IS 0-2 mm	Rudus FA	1:05	5.67	17	28	UCT
M_17_(1_3)	IS 0-2 mm	Rudus FA	1:04	10	17	28	UCT, Calorimetry
M_18_(1_3)	IS 0-2 mm	Rudus FA	1:05	8.17	17	28	UCT, Calorimetry
M_19_(1_3)	IS 0-2 mm	Rudus FA	1:04	10	17	28	F-T, UCT
M_20_(1_3)	IS 0-2 mm	Rudus FA	1:05	8.17	17	28	F-T, UCT
M_21_(1_3)	IS 0-2 mm	Rudus FA	1:04	10	17	28	SAT, UCT
M_22_(1_3)	IS 0-2 mm	Rudus FA	1:05	8.17	17	28	SAT, UCT
M_23_(1_3)	50% IS + 25% CC + 25% NS	Rudus FA	1:04	6.75	14	28	F-T, UPV, UCT
M_24_(1_3)	50% IS + 25% CC + 25% NS	Rudus FA	1:04	6.75	16	28	F-T, UPV, UCT
M_25_(1_3)	50% IS + 25% CC + 25% NS	Rudus FA	1:04	6.75	18	28	F-T, UPV, UCT
M_23_(4_6)	50% IS + 25% CC + 25% NS	Rudus FA	1:04	6.75	14	28	UPV, UCT, SAT
M_24_(4_6)	50% IS + 25% CC + 25% NS	Rudus FA	1:04	6.75	16	28	UPV, UCT, SAT
M_25_(4_6)	50% IS + 25% CC + 25% NS	Rudus FA	1:04	6.75	18	28	UPV, UCT, SAT
M_26_(1_3)	50% IS + 50% NAT AGG	Rudus FA	1:04	6.75	8	28	F-T, UPV, UCT
M_27_(1_3)	50% IS + 50% NAT AGG	Rudus FA	1:04	6.75	10	28	F-T, UPV, UCT
M_28_(1_3)	50% IS + 50% NAT AGG	Rudus FA	1:04	6.75	12	28	F-T, UPV, UCT
M_26_(4_6)	50% IS + 50% NAT AGG	Rudus FA	1:04	6.75	8	28	UPV, UCT, SAT
M_27_(4_6)	50% IS + 50% NAT AGG	Rudus FA	1:04	6.75	10	28	UPV, UCT, SAT
M_28_(4_6)	50% IS + 50% NAT AGG	Rudus FA	1:04	6.75	12	28	UPV, UCT, SAT

As shown in Table 4.1, the experimental study included the preparation of 102 samples in 28 series with variations in binder-to-aggregate ratio, water content %, cement %, and aggregate constituents. Cement was used as activator and the % of cement in mix with 1:5 binder to aggregate ratio is proportionally reduced compared to 1:4 binder to aggregate ratio mixes. The Uniaxial Compressive Strength test served as the fundamental test for each series. Selected series underwent additional testing, including capillary saturation, Freeze-thaw, and Ultrasonic Pulse Velocity. Calorimetry tests were conducted on design mixes from four series, namely M_5, M_6, M_17, and M_18. All tests followed existing research standards, which were applied as required.

4.1 Sieving

The grain size distribution of the incineration slag was determined by dry sieving in accordance with SFS-EN 933-1. The oven-dried samples were weighed, poured into stacked sieves, and shaken for 15 minutes. The retained mass on each sieve was measured and expressed as a % of the dry mass. The cumulative passing percentages were then used to construct the grain size distribution curves. Nilisiä sand used in some specimen preparation also had sieving done previously by Abdi Wayu (2023) at Aalto University and the gradation curve for that is presented in fig (3.4).



Figure 4.1. Sieving setup at Aalto University, Espoo

Sieve analysis for used crushed concrete and the grain size distribution for it was provided by Rudus Oy. Sieving setup is presented in figure 4.1. Incineration slag had over 90% of the particles between 0.063 and 2 mm and the gradation curve for the incineration slag is presented in Figure 4.2. According to SFS 13793:2001, curve located entirely in area 1 is highly susceptible to frost whereas the curve under 1L is moderately susceptible to frost. Incineration slag entirely falls under area 3 that is not frost-susceptible.

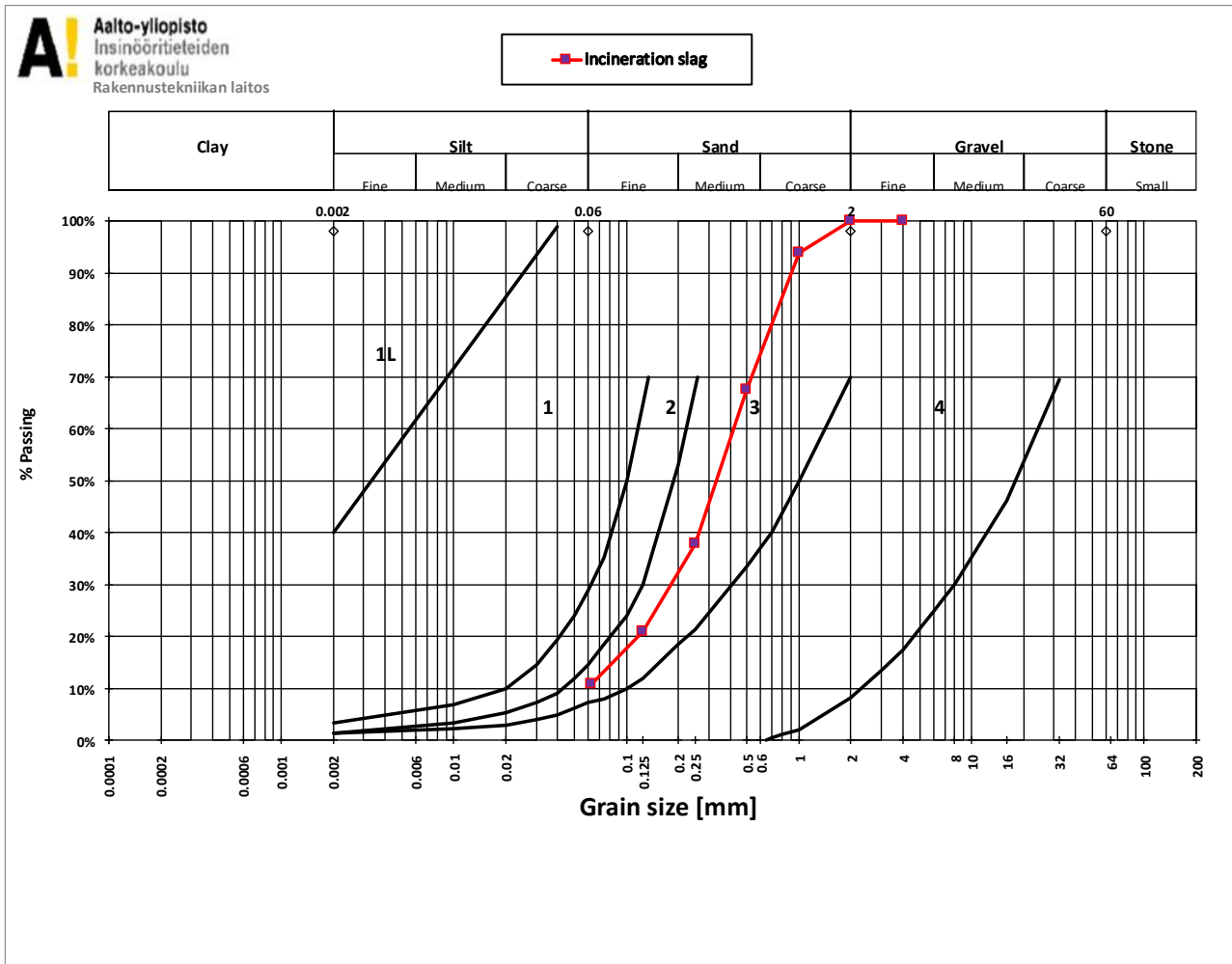


Figure 4.2. Gradation curve of Incineration slag.

In the first phase of the specimen preparation, all 66 samples were made with incineration slag as the sole aggregate. In second phase of the study, samples were prepared where half the mass of aggregate was made up of Incineration slag and remaining half the mass was made up of equal part Crushed concrete and Nilsjä sand. Comparative samples with natural aggregates were made in a way that half the dry mass of specimen was made up of Incineration slag and remaining half was made up of Natural aggregates and fines in such a proportion that will have similar granularity curve as it was with the ones made from Incineration slag, Crushed concrete and Nilsjä sand as represented in figure 4.3.

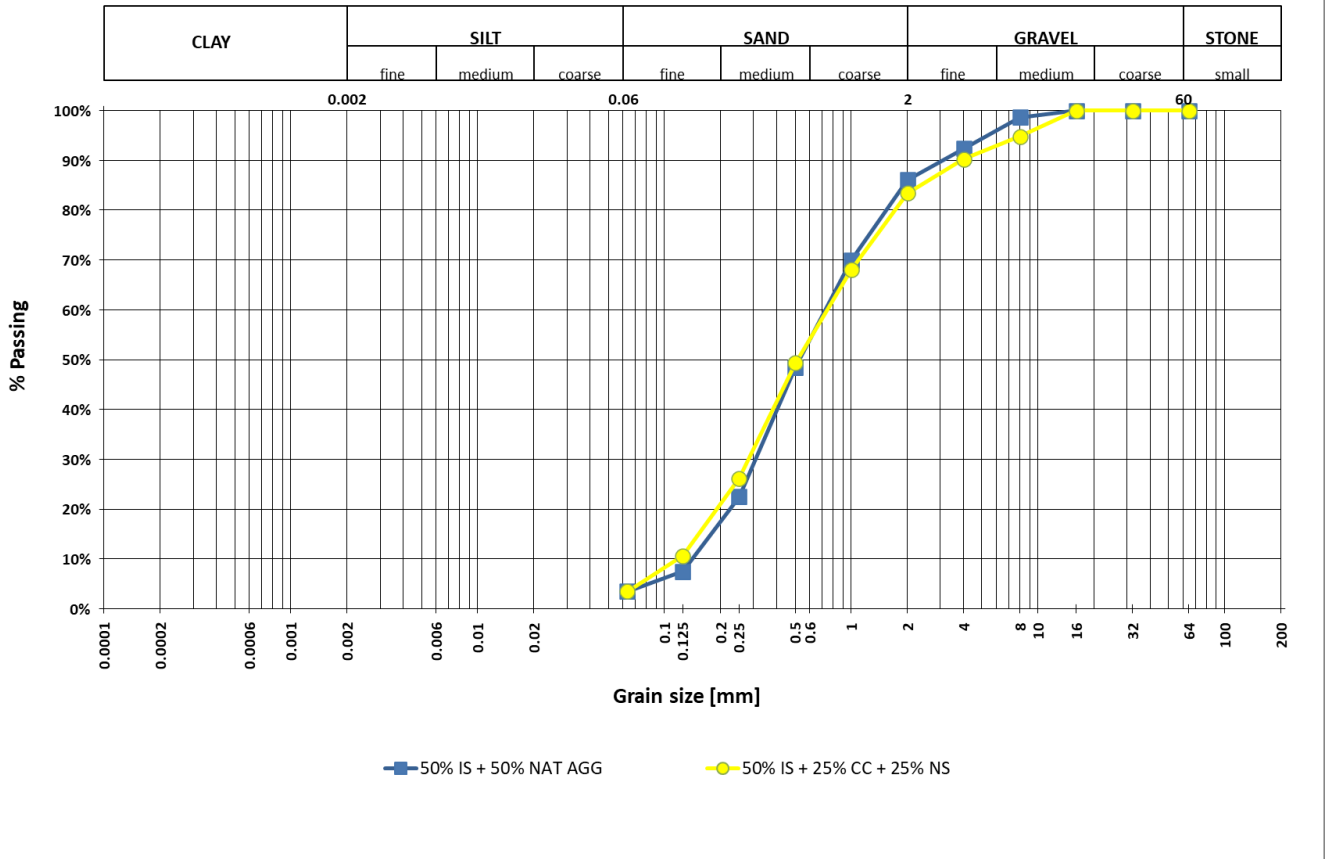


Figure 4.3. Gradation curve of mixed aggregates

4.2 Hydrophobization

The incineration slag was oven dried overnight at 100 °C to remove residual moisture and then pulverized to a powder form. Ethanol was then measured into a glass beaker, and the mass of slag per batch was adjusted to two-thirds of the ethanol mass. Subsequently, stearic acid corresponding to 3 % of the ethanol weight was added. The mixture was stirred magnetically and gently heated until the stearic acid fully dissolved in the ethanol, producing a clear and homogeneous solution. Gentle heat was applied to the base of the beaker through the stirrer apparatus to accelerate the dissolution of stearic acid. Once the solution became homogeneous, the stirring rod was removed, and the ethanol stearic acid mixture was transferred to a separate container containing the pulverized incineration slag.

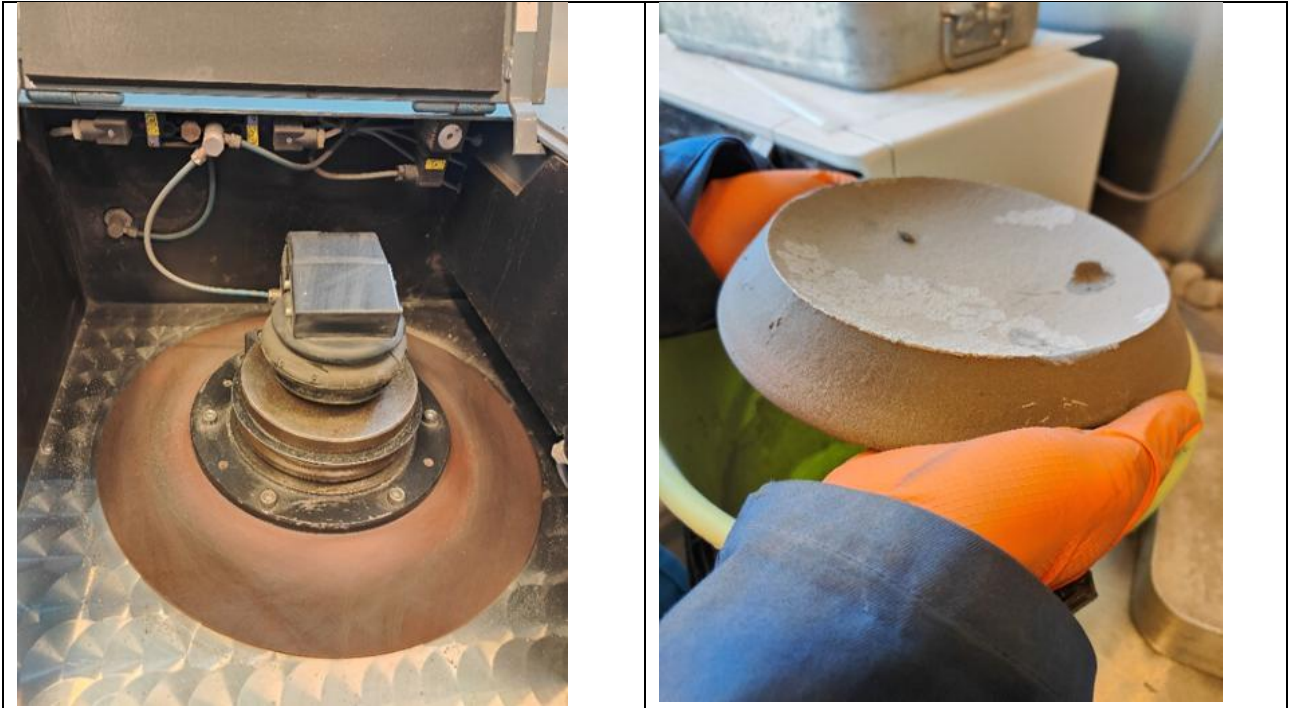


Figure 4.4. Grinding Incineration slag (Left); Incineration slag powder mixed and dried with the mixture of ethanol and stearic acid (Right)

The mixture was manually stirred for five minutes using a wooden rod, after which it was placed under a ventilation hood to allow ethanol evaporation. During evaporation, the mixture was intermittently stirred to enhance the drying process. Before use, the hydrophobized slag was blended in a Hobart bench mixer to disintegrate agglomerates formed during evaporation and mixed to the specimen where it accounted for 20% of the total mass of aggregate.

4.3 Preparation for test samples

All research samples, except for the calorimetry samples, were prepared using the VTT hammer. Each specimen had a uniform diameter of 100 mm, while the height averaged 165 mm and ranged between 140 mm and 180 mm. This variation in height resulted from the consistent wet mass of approximately 2.2 kg applied to all samples, combined with differences in density determined by the design mix. Previous research at Aalto University on the rammed earth technique demonstrated that cubical samples were unsuitable, as the mixture adhered to the mould walls and the samples were damaged during demoulding. Consequently, cylindrical samples were adopted as the standard for all sample preparation.



Figure 4.5. Mixing of ingredients in Hobart Mixer (Left); Specimen preparation by using VTT hammer to compact the stabilized rammed earth mixture in mould (Right).

Specimen preparation followed a four-step process. First, all ingredients were gathered. Aggregate materials were oven dried at 105 °C for 24 hours to eliminate residual moisture. Hydrophobized fractions were produced as described in Chapter 4.3. Once dried, the required amounts were weighed into a steel mixing pan. To prevent rapid water absorption by the aggregates, the pan was pre-wetted. The ingredients were blended in a Hobart plane mixer equipped with a flat beater blade. Dry materials were mixed for 30 seconds, followed by the addition of the target water amount and an additional 60 seconds of mixing. The pan walls were then scraped to dislodge any adhering material, and mixing continued for 30 seconds at the second highest speed. Simultaneously, the moulds were prepared. ICT moulds with cylindrical bodies, base plates, and top plates were used. A plastic sheet was placed on each base plate, and the inside walls of the moulds were lightly oiled to facilitate later sample removal.

The second half of the process involved compaction and curing. Each specimen was constructed in five layers, with approximately 440 grams of fresh mix per layer. Each layer was compacted using 20 blows from the VTT hammer, which features a 4 kg drop weight and a 0.45-meter drop height. Prior to adding each subsequent layer, the surface of the previous layer was gently scratched with a

knife to promote interlocking and minimize weak interfaces. After compacting the final layer, a jacking device was used to remove the samples from the moulds, which were then placed on rigid plastic sheets. The specimens were immediately covered with plastic bags and cured for 28 days at 21 °C and over 95 % relative humidity to ensure adequate hydration. Following curing, additional procedures for freeze-thaw testing, saturation measurements, and calorimetry were conducted as outlined in Chapters 4.4, 4.5, and 4.7.

4.4 Freeze-thaw resistance

The objective of the freeze-thaw resistance test is to determine how much of a specimen loses its compressive strength because of freeze-thaw stress. The freeze-thaw resistance of the rammed earth samples was evaluated in accordance with CEN/TS 13286-54: EN. After curing for 28 days under controlled temperature and humidity, the samples were transferred to a climate-controlled chamber and subjected to 15 freeze-thaw cycles of 24 hours each. Following the cycles, they were allowed to equilibrate to room temperature before compressive strength testing. For the freeze-thaw test, samples were removed from the curing room, surface moisture was eliminated, and the specimens were securely wrapped in plastic cling film. The wrapped samples were then placed in a freeze-thaw device, as shown in figure 4.5. Prior to testing, the apparatus was calibrated using a reference container filled with 8-16 mm crushed rock aggregate and water added a few centimeters above the surface. The container, equipped with a thermocouple and sealed with a lid, was placed at the chamber's center, and the standard freeze-thaw schedule was applied to verify that the equipment functioned within the specified limits. Altogether 30 samples of 10 different series were subjected to f-t test.



Figure 4.6. Freeze-thaw chamber with test samples.

4.5 Capillary saturation

Capillary saturation in fine-grained soils occurs when strong intermolecular forces between water molecules and soil particles drive water upward through narrow pores. Soils rich in particles smaller than 0.02 mm have pores tight enough to hold continuous water films, allowing steady capillary rise. The surface tension of water keeps these films intact and supports ongoing moisture movement within the soil. In rammed earth, fine-grained fractions enhance capillary flow, influencing how moisture spreads and stays within the compacted mass. Controlling the grain-size distribution and limiting excess fines helps regulate moisture behavior and maintain both dimensional and mechanical stability in rammed earth structures. (Ehrola, 1996). In the capillary test, the test cylinder had a uniform diameter of 100mm. Height of samples from same series were within 1-2 mm difference and there were 3 samples per series. Altogether 12 series went through capillary saturation test. Capillary rise was measured according to the procedure specified in EN 13057:2002.



Figure 4.7. Samples after Capillary saturation test

The samples were dried at 40 °C until the mass variation stabilized below 0.2% over a two-hour period, at which point the constant mass was recorded. The specimen was then placed on metallic support bars within a vessel containing a shallow water layer, ensuring approximately 1 mm of submersion at the base. Capillary rise was observed as a visible dark band along the specimen surface. Measurements of rise height and corresponding time were performed at intervals specified by EN 13057 (12 min, 30 min, 1 h, 2 h, 4 h, and 24 h). The specimen surface was divided into equal segments to quantify spatial variation in capillary rise. After each measurement, excess surface moisture was removed, the mass was recorded, and the specimen was returned to the vessel for continued testing.

4.6 Uniaxial Compression Test

The mechanical properties of the test samples, particularly the uniaxial compressive strength and the secant modulus (E_{50}), were determined through uniaxial compression testing conducted in accordance with the standard SFS-EN 13286-41. Altogether, there were 102 samples that were tested for their peak force before failure. All samples were cured for 28 days in the curing room with over 95% humidity and 21 °C. Some samples were subjected to 15 24-hour freeze-thaw cycles in climate-controlled setup then allowed to return to room temperature before being subjected to Uniaxial compression test. Some samples also went through capillary saturation test and the subjected to UCS test.



Figure 4.8. Zwick & Roell Uniaxial Compression Test setup, Aalto University

Along with determining the maximum compressive strength, the Secant modulus (E_{50}) was evaluated for the test samples. E_{50} represents the slope of the linear portion of the stress-strain curve and is calculated by dividing the stress corresponding to 50% of the peak stress by the strain measured at that point. In geotechnical studies, E_{50} is a key parameter for describing the mechanical behavior of soils and similar materials. A higher E_{50} value indicates a stiffer, less compressible material that undergoes smaller elastic deformations under load, whereas a lower E_{50} value signifies a softer, more compressible material with greater elastic deformation when subjected to stress.

4.7 Calorimetry

A calorimeter measures the heat released during the hydration of cementitious materials and enables precise evaluation and comparison of binder and mixture performance. The instrument maintains a constant temperature within an insulated chamber and receives the samples immediately after water addition. During hydration, temperature sensors continuously record the thermal energy generated. In an isothermal calorimeter, the sample directly contacts a heat flow sensor, which transfers heat to a constant-temperature sink. The device simultaneously measures a reference sample with equivalent heat capacity and reports the difference between the sample and reference signals, reducing noise and transient effects while improving measurement accuracy. (Linderoth et al., 2021). The calorimetry tests were conducted on four different mixes to evaluate the influence of binder ratio and water content on hydration behavior.



Figure 4.9. Calorimetry test setup

Two mixes were prepared with 20 % water content, and the remaining two with 17 % water content. Within each subgroup, one mix had a 1:4 binder-to-aggregate ratio, while the other had a 1:5 ratio, allowing a direct comparison of binder concentration effects. All samples weigh 208 g, corresponding to the maximum tube capacity of the calorimeter. In each mix, cement acted as the activator and fly ash as the primary binder; however, for result representation, the combined mass of cement and fly ash was considered as the total binder.

4.8 Ultrasonic pulse velocity

Ultrasonic Pulse Velocity (UPV) testing is a widely adopted nondestructive method used to indirectly evaluate the strength and uniformity of cementitious materials, including concrete and stabilized rammed earth. This technique enables rapid assessment of material quality by measuring the velocity of ultrasonic waves propagating through the specimen, which correlates with its density, elasticity, and internal integrity. Higher pulse velocities typically indicate a denser and more homogeneous material with fewer internal defects such as voids or cracks.(Al-Neshawy, 2021). In the second phase, a total of 36 samples from series M_23 to M_28, each consisting of six samples, were tested using the UPV method.



Fig 4.10. UPV testing setup

After the designated curing period, the samples were removed from the curing room and placed on the testing table to stabilize at room temperature. Once conditioned, the diameter, height, and weight of each specimen were measured before performing the UPV test to assess their mechanical properties.

5 Results

This chapter presents the principal laboratory results, including compressive strength and ultrasonic pulse velocity for various mixes and curing conditions, both before and after freeze-thaw cycles and capillary saturation. The effects of hydrophobization and varying water contents on strength and moisture behavior are examined. Calorimetry and saturation results are also included to elucidate hydration and moisture transport. The findings are interpreted in relation to the material compositions described previously, to link mechanical and durability performance.

5.1 Uniaxial compressive strength

Figure 5.1 illustrates the variation in uniaxial compressive strength (UCS) with cement content for mixes with binder-to-aggregate ratios of 1:5 and 1:4, tested at moisture contents of 17 % and 20 %. For the 1:5 mixes at 17 % moisture, UCS increases from 1.32 MPa at 2.47 % cement to 2.70 MPa at 5.67 % and 4.49 MPa at 8.17 %. At 20 % moisture, the same cement contents yield higher strengths: 1.52, 3.59, and 5.21 MPa, respectively. These results indicate that increasing water content within the workable range enhances strength.

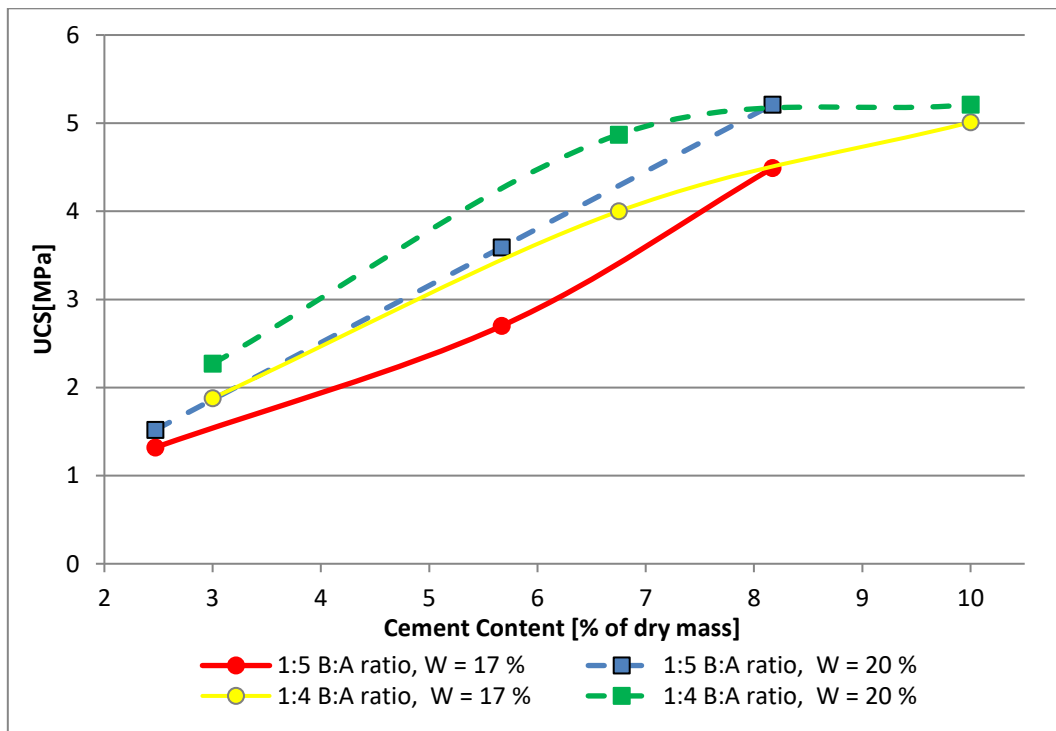


Figure 5.1. Relationship between cement content and uniaxial compressive strength for incineration slag-based rammed earth at binder-to-aggregate ratios of 1:4 and 1:5, with moisture contents of 17 % and 20 % after 28-day curing.

The 1:4 mixes exhibit a comparable trend. At 17 % moisture, UCS rises from 1.88 MPa at 3 % cement to 4.00 MPa at 6.75 % and 5.01 MPa at 10 %. At 20 % moisture, these values increase to 2.27, 4.87, and 5.21 MPa. The data demonstrates a substantial, nearly linear increase in UCS with cement content at lower and intermediate levels, with the rate of increase diminishing between approximately 8 % and 10 % cement, particularly for the wetter mixes. The 1:4 mixes consistently achieve higher strengths than the 1:5 mixes at equivalent cement contents. This pattern, as shown in Figure 5.1, is consistent with observations in cement-stabilised earth and soil-cement systems, where strength increases with additional cement until a continuous cemented skeleton forms, after which further cement additions yield diminishing returns. Curing at or near the optimum moisture content maximises both compaction and hydration.

Comparable findings are reported in other studies on cement-stabilised rammed earth. (Tuyan et al., 2014). The pronounced influence of water content on strength is also well established in experimental research on rammed earth mixtures. When cement and fly ash are combined, a similar trend is observed: rapid strength gains at low binder contents, followed by a gradual plateau at higher levels. (Nguyen & Phan, 2021) The higher UCS values at 20 % moisture compared to 17 % in the present results indicate that 17 % is below the optimum moisture content for these mixes. Increased water facilitates particle rearrangement during compaction and supplies additional water for hydration, particularly at intermediate cement contents. The greater binder fraction in the 1:4 mixes produces thicker, more continuous cementitious bridges around the aggregate, thereby enhancing the load-bearing capacity.

5.2 Secant modulus E_{50}

Figure 5.2. illustrates the variation in the secant modulus E_{50} with cement content for mixes with binder-to-aggregate ratios of 1:5 and 1:4 at moisture contents of 17 % and 20 %. For the 1:5 mixes, E_{50} increases with cement content at both moisture levels, indicating that even small increases in cement content enhance material stiffness. At 20 % moisture, E_{50} values consistently exceed those at 17 % for the same cement content, suggesting that 17 % is below the optimum moisture content for these mixes. The 1:4 mixes exhibit a similar trend but achieve higher E_{50} values than the 1:5 mixes at equivalent cement contents. An increased binder fraction results in greater material stiffness, characterized by a pronounced increase in E_{50} at low and medium cement contents, followed by a reduced rate of stiffness gain at the highest cement levels. This behaviour aligns with previous findings on cement-stabilized rammed earth and soil-cement materials, where increases in cement content

and appropriate compaction moisture result in simultaneous gains in strength and stiffness until a continuous cemented framework is established. Beyond this point, additional cement yields diminishing returns. (Nguyen & Phan, 2021)

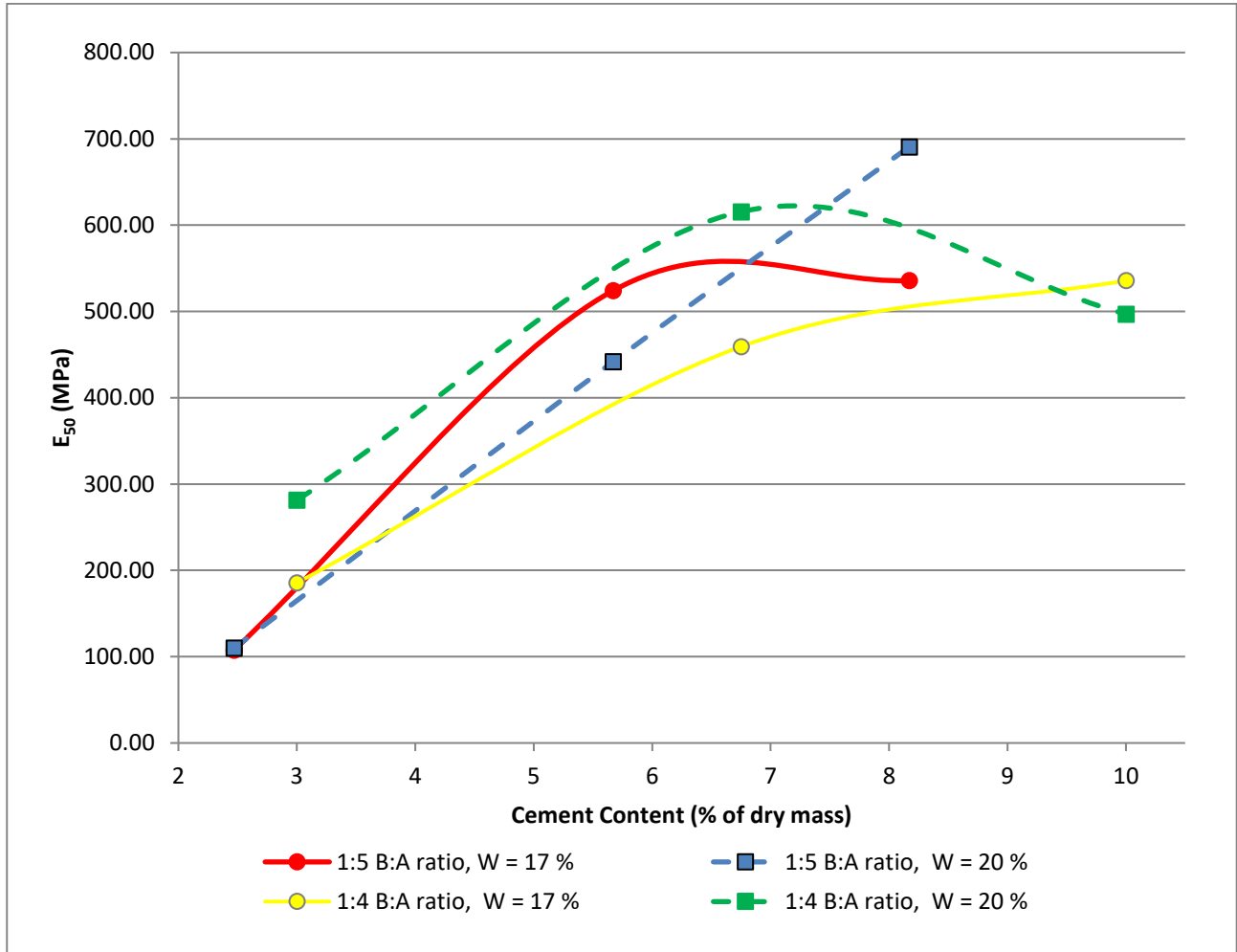


Figure 5.2. Relationship between cement content and Secant modulus E_{50} for incineration slag based rammed earth at binder to aggregate ratios 1:4 and 1:5, moisture contents 17 % and 20 % after 28-day curing.

Other studies on rammed earth have also demonstrated that mixtures compacted closer to optimum moisture content achieve higher elastic or secant moduli, attributed to improved particle rearrangement and more effective hydration of cementitious phases (Anssi Luoma, 2023). The higher E_{50} values observed for the 1:4 mixes and for specimens compacted at 20 % moisture in the present study are therefore consistent with earlier research and support the initial hypothesis regarding the influence of cement content, moisture, and binder ratio on the stiffness of cement-stabilized rammed earth.

5.3 Effect of freeze and thaw

5.3.1 Effect of F-T on specimens with IS as sole aggregate

Figure 5.3 presents the uniaxial compressive strength (UCS) and bulk densities measured prior to UCS testing for mixtures containing only incineration slag as aggregate. At 20 % water content, both binder-aggregate ratios (1:4 and 1:5) achieve a UCS of 5.21 MPa after 28 days. Following 15 freeze-thaw cycles, the UCS of the 1:4 mix increases to 7.33 MPa, representing a 41 % improvement, while the 1:5 mix rises to 5.96 MPa. Specimens subjected to freeze-thaw cycles consistently exhibit slightly higher densities than reference specimens. For instance, the 1:4 mix with 20 % water content increases in density from 1,725.71 to 1,772.13 kg/m³. This increase is likely attributable to the presence of sufficient free water and un-hydrated binder after 28 days.

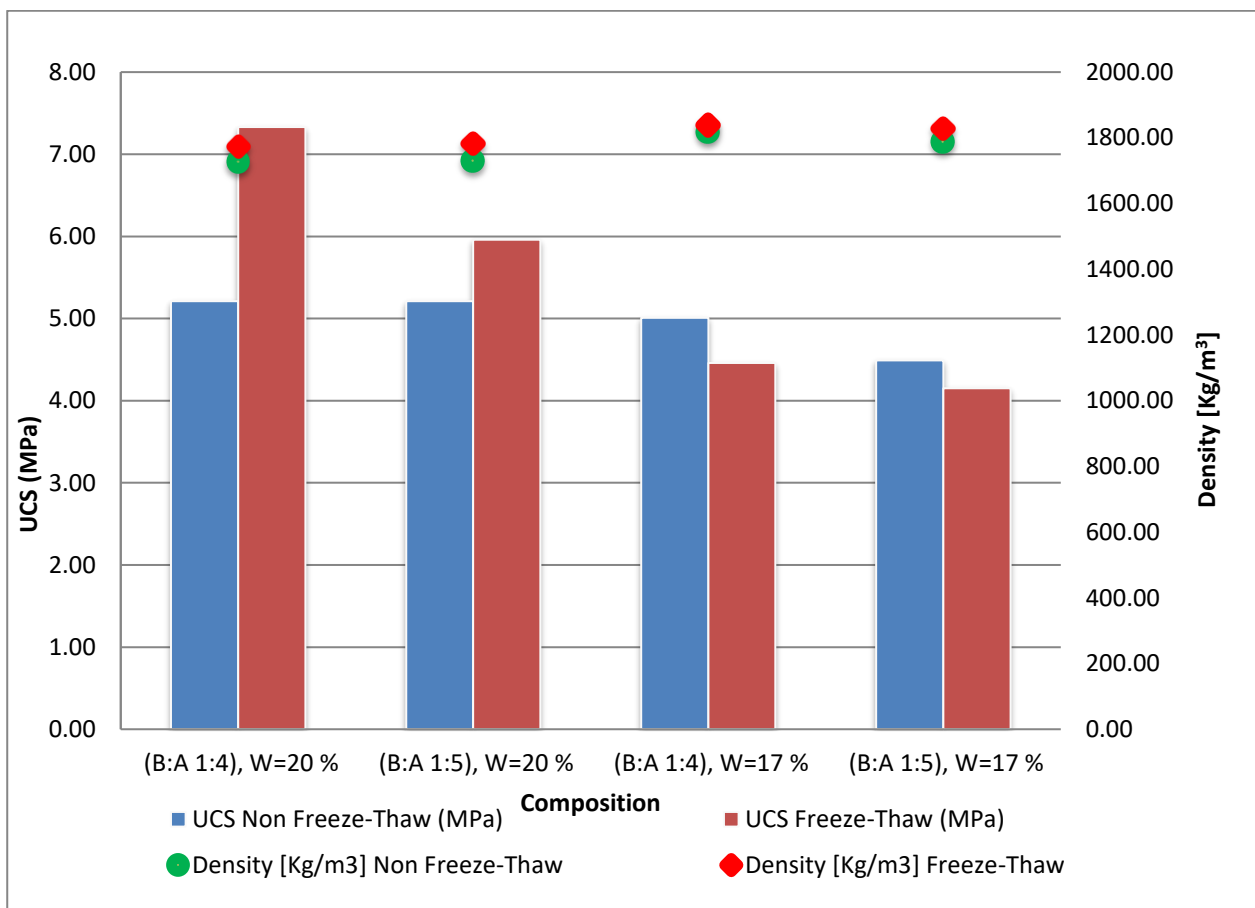


Figure 5.3. Comparison of uniaxial compressive strength UCS and bulk density values for stabilized rammed earth mixtures with varying binder to aggregate ratios and moisture contents, using incineration slag as the sole aggregate, under freeze and thaw and non-freeze- thaw conditions.

The specimens were wrapped in cling film prior to placement in the freeze-thaw chamber, ensuring they remained sealed and maintained high humidity. As the chamber temperature increased, the

retained moisture facilitated continued cement hydration and enabled ongoing pozzolanic reactions, resulting in a denser microstructure. This additional curing can partially compensate for, or in some cases surpass, the microcracking damage caused by freeze-thaw cycles. Consequently, certain mixtures exhibited a slight overall increase in strength. Comparable effects have been documented in cementitious systems with internal curing water or rehydration following freeze-thaw cycles. (Dhunge et al., 2023). At 17 % water content, the observed trend reverses. Both mixes initially display slightly higher densities than the 20 % water content mixes; however, their UCS values decrease following freeze-thaw cycles. Specifically, the UCS of the 1:4 mix declines from 5.01 to 4.46 MPa, and the 1:5 mix decreases from 4.49 to 4.15 MPa. Densities continue to increase slightly prior to testing, for example, from 1,816.52 to 1,838.03 kg/m³. Higher initial density suggests tighter particle packing and reduced pore volume, yet limited water availability restricts further hydration and diminishes the matrix's capacity to relieve stresses induced by ice formation. Under these conditions, freeze-thaw cycles are likely to induce microcracking that is not compensated by the formation of new binding phases, resulting in a net loss of strength. Comparable outcomes, in which density increases while strength decreases after freeze-thaw exposure, have been reported in stabilized earth materials and other cementitious composites. In such cases, microstructural damage outweighs any beneficial curing effects. (Bruno et al., 2022).

5.3.2 Effect of F-T on specimens with partially substituted aggregate mix

Figure 5.4 presents the uniaxial compressive strength (UCS) and bulk density measured immediately prior to testing. All mixes maintain a binder-to-aggregate ratio of 1:4, with only the moisture content varying between the two aggregate systems. In the first system, composed of 50 % incineration slag and 50 % natural aggregate, the UCS after 28 days increases from 4.20 MPa to 4.63 MPa at 8 % water following 15 freeze-thaw cycles. The density also rises from approximately 1,935 kg/m³ to 1,952 kg/m³. At higher water contents, the trend reverses. At 10 % water, UCS decreases from 5.47 MPa to 4.79 MPa, and density declines from approximately 1,966 kg/m³ to 1,937 kg/m³. At 12 % water, strength falls from 8.10 MPa to 6.58 MPa, accompanied by a slight reduction in density. These results are consistent with laboratory findings indicating that the optimal water content for this system is approximately 10 %. When the mix is drier than this optimum, repeated wetting and curing during freeze-thaw cycles appear to promote further hydration and slight densification, which can offset early microcracking and result in a modest strength increase. When the water content is at or above the optimum, freeze-thaw cycles induce greater microcracking and surface scaling, which outweigh any continued hydration. These observations align with previous studies demonstrating that moisture

and saturation significantly influence freeze-thaw damage in cement-based and stabilized earth materials.(Ge et al., 2022)

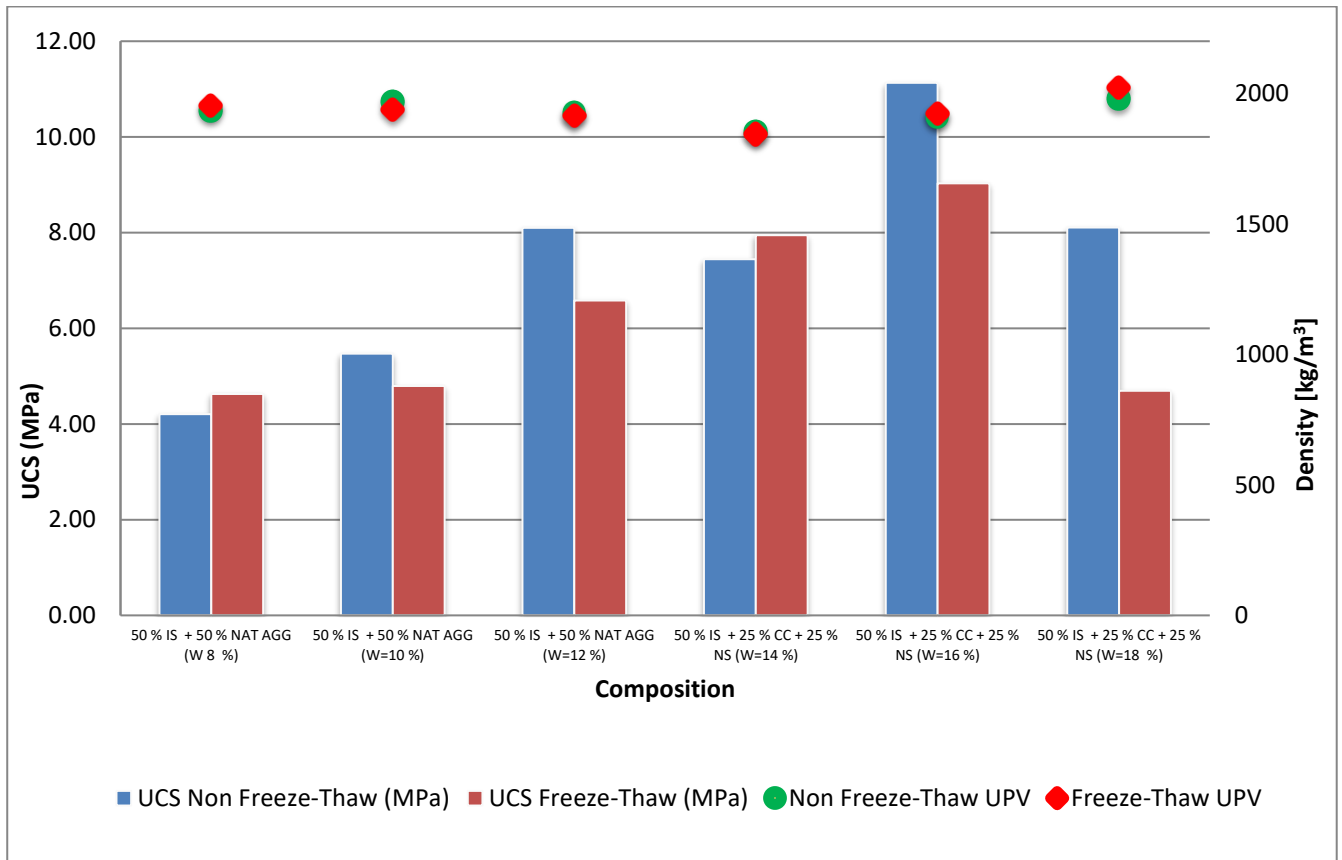


Figure 5.4. Comparison of uniaxial compressive strength (UCS) and bulk density values for stabilized rammed earth mixtures with varying moisture contents, mixed aggregate composition under freeze-thaw and non-freeze-thaw conditions.

The second aggregate system consists of 50 % incineration slag, 25 % crushed concrete, and 25 % Nilsia sand. Water contents of 14, 16, and 18 % were tested, with the optimal value identified at approximately 16 %. At 14 % water, the UCS increases from 7.45 MPa to 7.94 MPa after freeze-thaw cycling, while density decreases slightly from 1,853 kg/m³ to 1,844 kg/m³. This outcome indicates that additional hydration along the primary structure can compensate for moderate microstructural damage. At 16 and 18 % water, freeze-thaw cycles result in pronounced strength losses, from 11.13 MPa to 9.03 MPa and from 8.10 MPa to 4.70 MPa, respectively. Densities remain relatively stable or even increase, reaching approximately 1,921 kg/m³ and 2,022 kg/m³. The observation that density remains constant or increases while strength declines demonstrates that pore filling and ongoing hydration do not compensate for the propagation of cracks at the interfaces between slag, crushed concrete, and sand. This phenomenon is consistent with findings in recycled aggregate concrete, where

freeze-thaw cycles induce increased microcracking in the old mortar and at the aggregate-paste interfaces, resulting in strength loss that is not reflected in bulk density measurements. (Tuyan et al., 2014)

5.3.3 Effect of F-T on secant modulus (E_{50}) of the specimens

Table 5.1. Secant modulus (E_{50}) values of the samples. Non-F-T Values have been measured after 28 days of curing. For F-T samples, values have been measured after an additional 15 freeze-thaw cycles.

Aggregate	Binder	Binder to Aggregate ratio	Moisture content (as % of dry mass)	Secant modulus E_{50}	%CV	Secant modulus E_{50}	%CV	E_{50} Ratio
				Non F-T [MPa]		F-T [MPa]		
IS	Fly Ash	01:04	20	496.96	33.91	972.97	60.65	0.51
IS	Fly Ash	01:04	20	690.67	21.23	802.7	28.26	0.86
IS	Fly Ash	01:05	17	580.35	16.96	187.42	31.6	3.10
IS	Fly Ash	01:05	17	535.73	27.39	326.42	33.91	1.64
50% IS + 25% CC + 25% NS	Fly Ash	01:04	14	626.83	32.69	807.45	10.95	0.78
50% IS + 25% CC + 25% NS	Fly Ash	01:04	16	823.81	39.91	605.93	34.95	1.36
50% IS + 25% CC + 25% NS	Fly Ash	01:04	18	377.46	9.1	489.18	25.34	0.77
50% IS + 50% NAT AGG	Fly Ash	01:04	8	442.83	48.04	330.77	8.27	1.34
50% IS + 50% NAT AGG	Fly Ash	01:04	10	556.31	23.62	358.25	38.82	1.55
50% IS + 50% NAT AGG	Fly Ash	01:04	12	876.88	39.2	543.36	31.54	1.61

Table 5.1. shows how the secant modulus E_{50} changes before and after freeze-thaw for the main aggregate and binder combinations in this test program. The IS-only mixes do not follow a single pattern. At a 1:4 ratio with 20 % moisture, E_{50} nearly doubles after undergoing freeze-thaw cycles. But at 17 % moisture and in the 1:5 mixes, the stiffness after freeze-thaw is either lower or only slightly higher than before. The hybrid aggregates also behave differently. The 50 % IS + 25 % CC + 25 % NS mixes usually lose stiffness after freeze-thaw. In contrast, the 50 % IS + 50 % NAT AGG specimens tend to keep or slightly increase their E_{50} , which is why the E_{50} ratios are higher for these mixes. There is significant variation between specimens, especially for E_{50} after freeze-thaw, which is reflected in high coefficients of variation.

5.3.4 Combined effect of F-T and aggregate composition on stress-strain behavior

Figure 5.5. presents a comparison of the stress-strain curves for three incineration slag mixes, illustrating the effects of aggregate type and freeze-thaw cycling on their mechanical behavior. The mix containing 50 % incineration slag (IS), 25 % crushed concrete (CC), and 25 % Nilsjö sand (NS) demonstrates the highest performance under all conditions. This mix achieves peak stresses approaching 12 MPa prior to freeze-thaw exposure and remains above 9 MPa afterward. The mix with 50 % IS and 50 % natural aggregate displays intermediate characteristics, with peak stresses of

approximately 8 to 9 MPa in the reference state and 6 to 7 MPa following freeze-thaw cycles. In contrast, the 100 % IS mix is the weakest, with peak stresses of 5-6 MPa that decrease further after cycling.

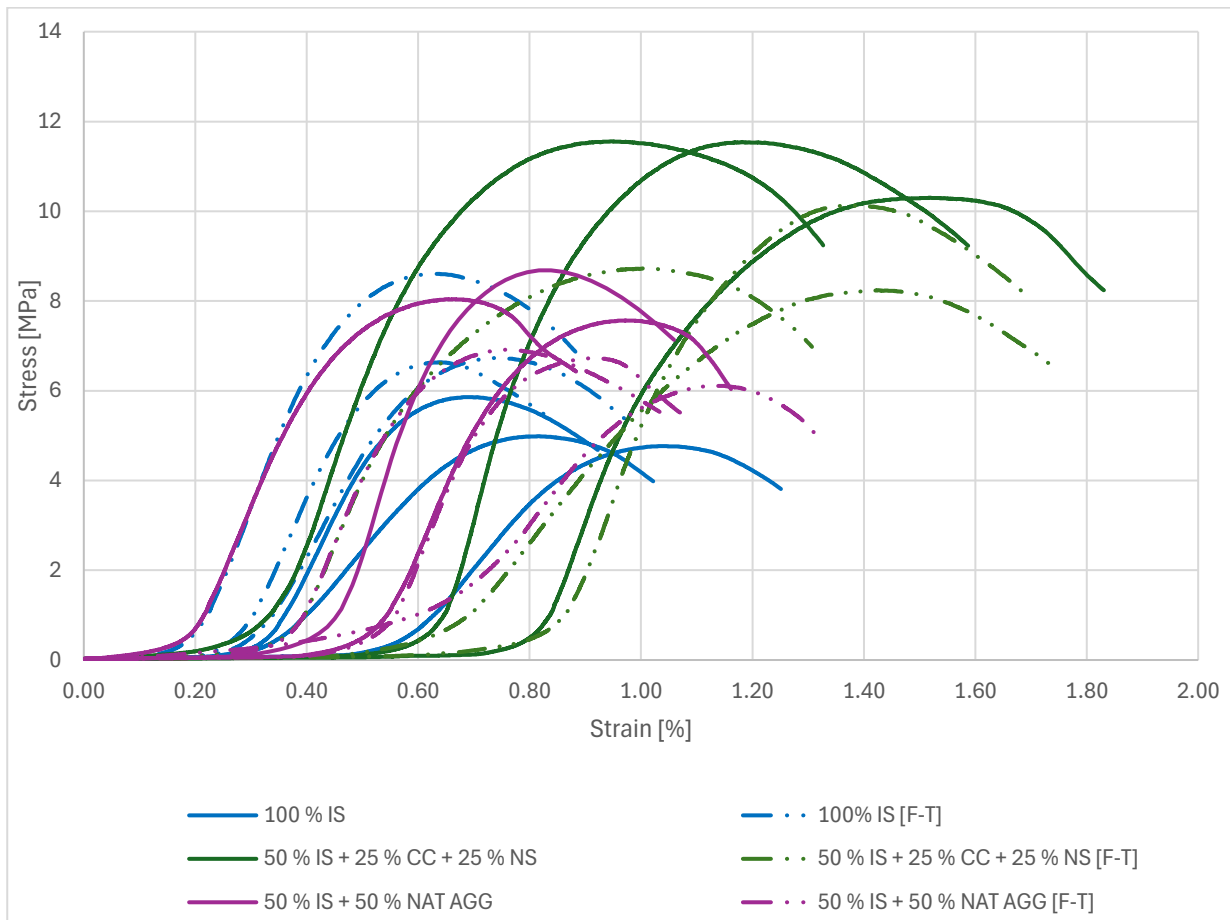


Figure 5.5. Stress strain curves of mixes before and after f-t cycles. Values have been measured after 28 days of curing, and for f-t specimens after an additional 15 f-t cycles.

For all mixes, the peak stress occurs at small strains of approximately 0.6 to 1.0 %, indicating that freeze-thaw cycling primarily reduces load-carrying capacity, while the overall deformation pattern remains consistent. These results indicate that incorporating recycled aggregates, particularly crushed concrete and Nilsjö sand, with incineration slag enhances both initial stiffness and strength, and provides superior residual performance after freeze-thaw exposure compared to mixes containing only incineration slag or incineration slag with natural aggregates.

5.4 Capillary saturation and effect of hydrophobization

Figure 5.6. demonstrates that cumulative water uptake increases almost linearly with the square root of time, a characteristic behaviour of capillary-driven flow in porous materials. The hydrophobized

mixes, M₁₁ and M₁₂, exhibit the lowest capillary activity, with water uptake values of 2.66 and 2.59 kg/m² after 4.90 h^{0.5}, respectively. In contrast, non-hydrophobized mixes with identical aggregate and binder content absorb significantly more water. At W = 20 %, the 1:4 mix M₉ reaches 12.75 kg/m², while the 1:5 mix M₁₀ attains 29.76 kg/m². The drier mixes at W = 17 % (M₂₁ and M₂₂) display the highest uptake, at 30.04 and 43.70 kg/m², respectively. These findings indicate that hydrophobic treatment disrupts liquid water pathways within the slag matrix. Additionally, lower initial water content enhances capillary suction, resulting in more rapid and greater moisture ingress, even when aggregate content remains constant.

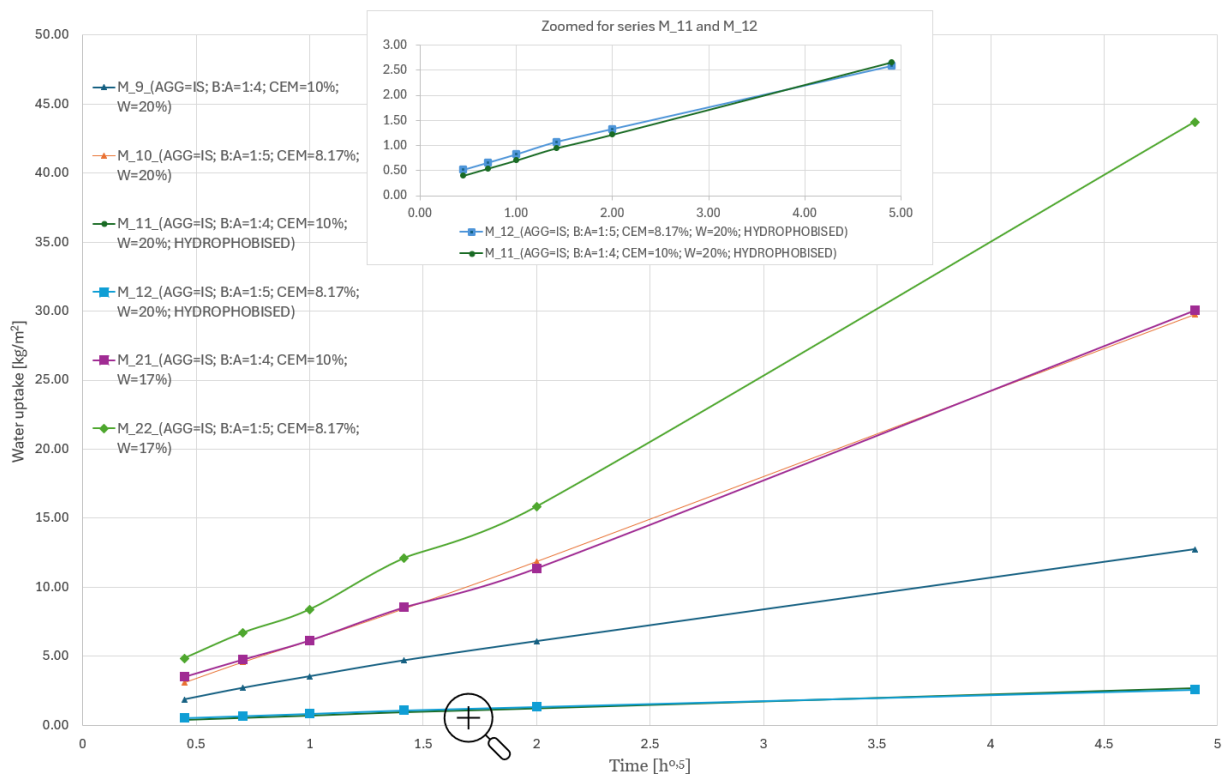


Figure 5.6. Capillary water uptake in incineration slag-only mix with varying binder-to-aggregate ratios, cement contents, and water contents. The inset provides a magnified view of the hydrophobized mixtures M₁₁ and M₁₂.

Figure 5.7. demonstrates the results for capillary water uptake in mixtures where incineration slag was partially replaced by Nilsjö sand and Crushed Concrete in one series and by natural aggregates in the other, maintaining a binder-to-aggregate ratio of 1:4 and a cement content of 6.75 %. In all cases, water uptake increases approximately linearly with the square root of time, indicating that capillary action governs the transport process. The IS + CC + NS mixtures (M₂₃ - M₂₅) exhibit lower water uptake than the IS + Natural aggregates (M₂₆ - M₂₈) at equivalent time intervals. This observation indicates that the combination of crushed concrete and Nilsjö sand produces a capillary network with lower conductivity compared to that formed by the laboratory aggregate. Among the IS

+ CC + NS mixtures, the sample with 16 % water (M_24) absorbs the least water, approximately 17.2 kg/m² after 4.9 h^{0.5}. Both the drier mixture with 14% water (M_23) and the wetter mixture with 18% water (M25) absorb more water, at approximately 28.2 and 22.1 kg/m², respectively, suggesting the existence of an optimal moisture content that minimizes absorptivity. The IS + natural aggregates display a different trend as the initial water content increases from 8 % to 12 %, total water uptake decreases from approximately 37.8 kg/m² (M_26) to 34.7 and 32.9 kg/m² (M_27 and M_28). These results suggest that lower initial water content enhances capillary suction, resulting in faster and greater moisture uptake in this more open aggregate system.

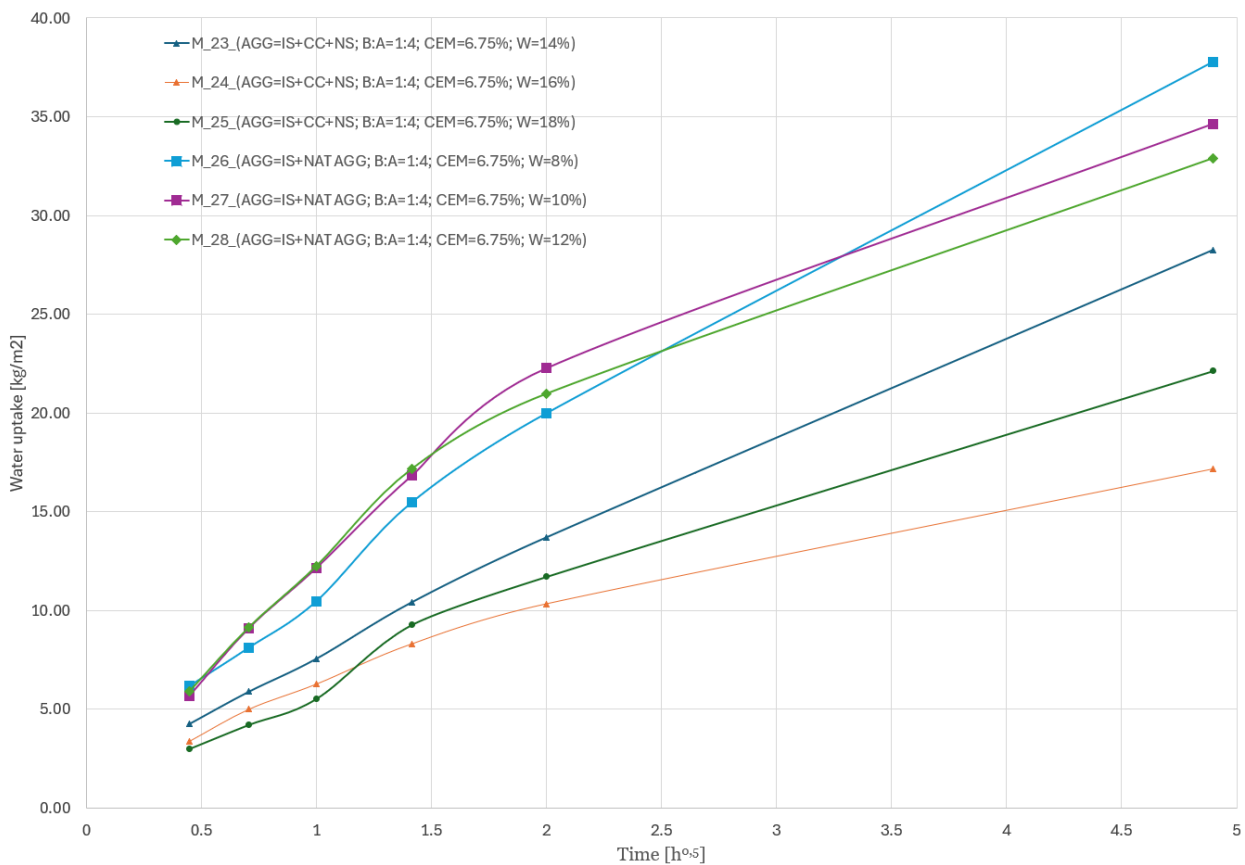


Figure 5.7. Capillary water uptake of mixes with partial incineration slag replacement (B:A = 1:4, CEM = 6.75 %) and varying moisture content.

5.5 Relationship between UPV and UCS

The relationship between ultrasonic pulse velocity (UPV) and uniaxial compressive strength (UCS) was investigated for two distinct stabilized rammed earth mix using incineration slag (IS) as primary aggregate and fly-ash as binder activated with 6.75 % rapid cement by dry mass. Each mix series was

tested at three moisture contents selected from laboratory observations of compaction behavior 14 %, 16 %, 18 % for IS + CC + NS and 8 %, 10 %, 12 % for IS + LA. The UPV and UCS tests were carried out consecutively on the same samples within two hours, ensuring a constant moisture state between the two measurements. In Figure 5.1., the 16 % series (identified as the optimum) exhibited an average UPV of 2819 m/s and a UCS of 11.13 MPa, whereas the 18 % series showed a comparable UPV of 2873 m/s but a markedly lower UCS of 8.10 Mpa, approximately 37 % weaker despite a 2 % higher velocity.

In Figure 5.8. for the samples without F-T, R^2 value was less than 0.3, the fact that samples with 18% water content have high scatter caused by microstructural heterogeneity and moisture-dependent effects within the compacted earth matrix. In rammed earth, the presence of partially saturated pores allows ultrasonic waves to propagate efficiently even when particle-binder bonding and dry density differ significantly between samples. Consequently, UPV remains relatively high in water-rich samples while UCS varies widely, reducing the statistical fit of the regression model. After 15 freeze-thaw cycles, UPV decreased by 24 % and UCS by 19 % at 16 % water, while the 18 % series suffered losses of 41 % and 42 %, respectively, yielding a strong correlation ($R^2 \approx 0.78$). In Figure 5.2, where crushed concrete and Nilsjö sand were replaced with laboratory-designed fractions of controlled gradation, the initial correlation was already high ($R^2 \approx 0.90$). The 12 % mix produced the highest strength, about 37 % greater than the 10 % mix with an average UPV of 2657 m/s and UCS of 8.10 MPa. Following freeze-thaw exposure, both parameters declined by 20-30 % but maintained a consistent relationship ($R^2 \approx 0.70$).

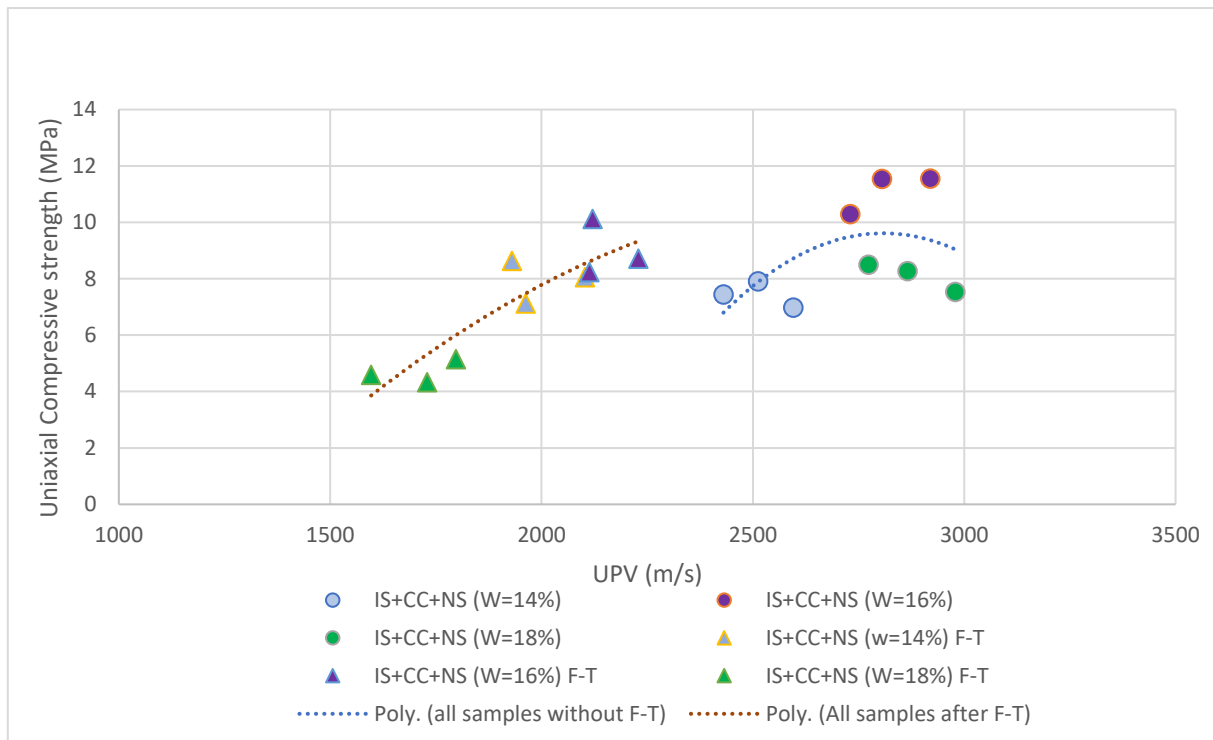


Figure 5.8. The correlation between UPV values and the UCS values of the samples made by ramming. Aggregate: IS+CC+NS. Values have been measured after 28 days of curing. For F-T samples values have been measured after additional 15 freeze-thaw cycles.

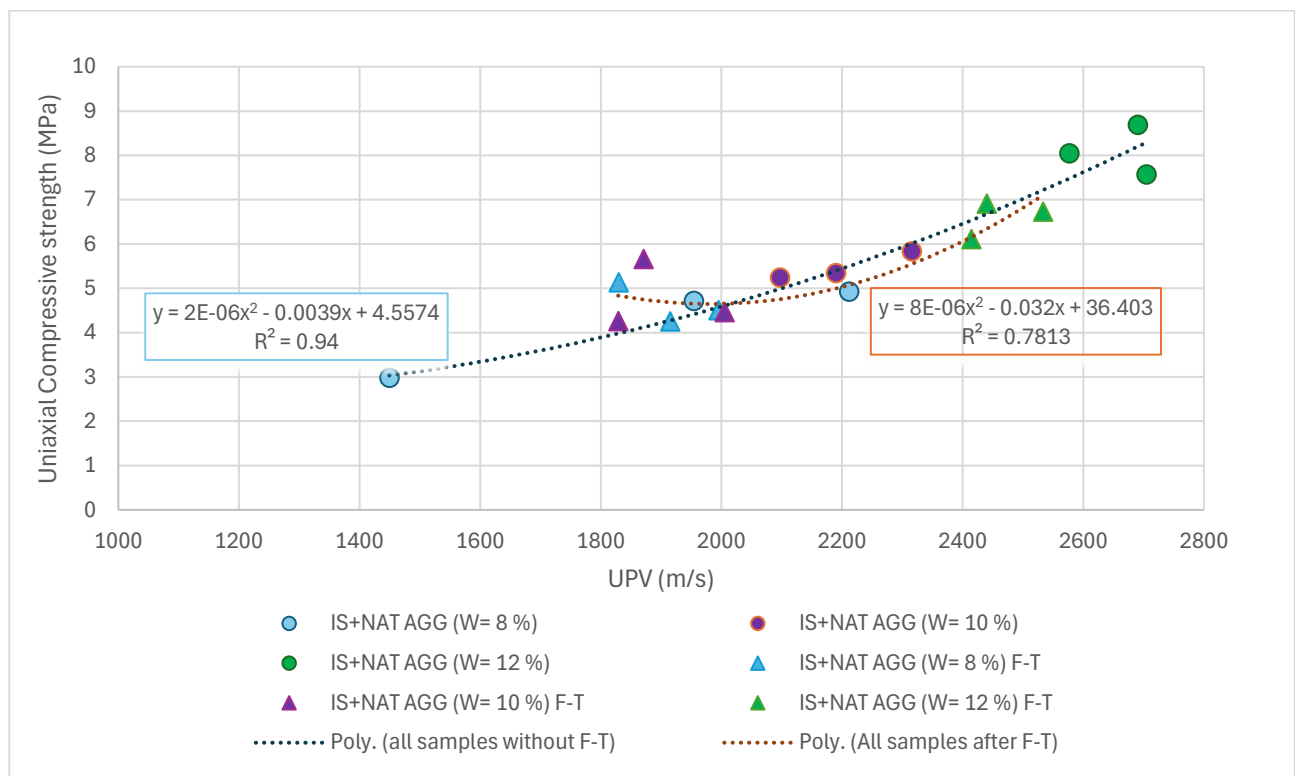


Figure 5.9. The correlation between UPV values and the UCS values of the samples made

by ramming. Aggregate: IS+NAT AGG. Values have been measured after 28 days of curing. For F-T samples values have been measured after additional 15 freeze-thaw cycles.

Since UPV and UCS tests were performed under the same moisture state, the observed discrepancies arise from the internal microstructure rather than transient drying. The higher velocity yet lower strength at 18 % water content in Figure 5.8. demonstrates the masking effect of pore-water coupling: when water exceeds the optimum compaction level, it occupies capillary voids and enhances ultrasonic transmission without improving the mechanical contact network. Similar behavior has been documented in cementitious and earthen materials where water-filled pores increase wave velocity but reduce stiffness (Hall & D.Hoff, 2022). At the 16 % optimum, the balance between lubrication and binder hydration promotes denser packing and stronger particle-to-binder interfaces, producing concurrent increases in UPV and UCS. Conversely, at 18 % water, excess moisture induces segregation and incomplete pozzolanic bonding of fly ash, resulting in up to 40 % loss in both velocity and strength after freeze-thaw. For the IS + NA series in Figure 5.9., the controlled aggregate gradation improves particle packing and stress transfer, thus lowering the optimum water content to 10-12 %. This refined structure limits pore connectivity and enhanced resistance to freeze-thaw deterioration, consistent with findings by (Mehta & Monteiro, 2014), who reported that better gradation and reduced void ratio increase both UPV reliability and frost durability.

5.6 Calorimetry test

Table 5.2. The composition of the calorimetry mix.

Sample ID	M_5	M_6	M_17	M_18
Channel No	01	02	03	04
Mix Time	01-Oct-2024 08:40:00	01-Oct-2024 08:50:00	01-Oct-2024 08:59:00	01-Oct-2024 09:07:00
Sample Mass, g	208.000	208.000	208.000	208.000
Water Mass, g	34.670	34.670	30.220	30.220
Cement Type	CEM I 52,5 R	CEM I 52,5 R	CEM I 52,5 R	CEM I 52,5 R
Cement Mass, g	17.330	14.160	17.780	14.520
Suppl 1 Type	Fly ash	Fly ash	Fly ash	Fly ash
Suppl 1 Mass, g	17.330	14.730	17.780	14.510
Inert Solids Type	Inceneration slag	Inceneration slag	Inceneration slag	Inceneration slag
Inert Solids Mass, g	138.670	144.440	142.220	148.140
Comment	Binder to agg (1:4) w20%	Binder to agg (1:5) w20%	Binder to agg (1:4) w17%	Binder to agg (1:5) w17%
Instrument Type	ICal 4000H	ICal 4000H	ICal 4000H	ICal 4000H
Instrument S/N	A0162404	A0162404	A0162404	A0162404
Temp Control	On	On	On	On
Calibr Name	A0162404 20240708	A0162404 20240708	A0162404 20240708	A0162404 20240708
Start Time	01-Oct-2024 08:32:11	01-Oct-2024 08:32:13	01-Oct-2024 08:32:14	01-Oct-2024 08:32:16
Stop Time	04-Oct-2024 09:39:43	04-Oct-2024 09:39:46	04-Oct-2024 09:39:48	04-Oct-2024 09:39:51

Table 5.2 presents the four calorimetry mixes used to investigate early heat release in cement-activated fly ash, with incineration slag serving as the inert aggregate. Each sample mix weighed 208 g and were tested in the ICal 4000H calorimeter under identical temperature conditions. Mixes M_5 and M_6 contained binder to aggregate ratios of 1:4 and 1:5 with 20% water, while M_17 and M_18 used the same ratios with 17% water. In all mixes, Incineration slag was used as the sole aggregate constituent, fly ash as the binder, and Rapidcement CEM 152.5R as the activator. This experimental design enables analysis of the effects of binder content and initial water content on the calorimetric response.

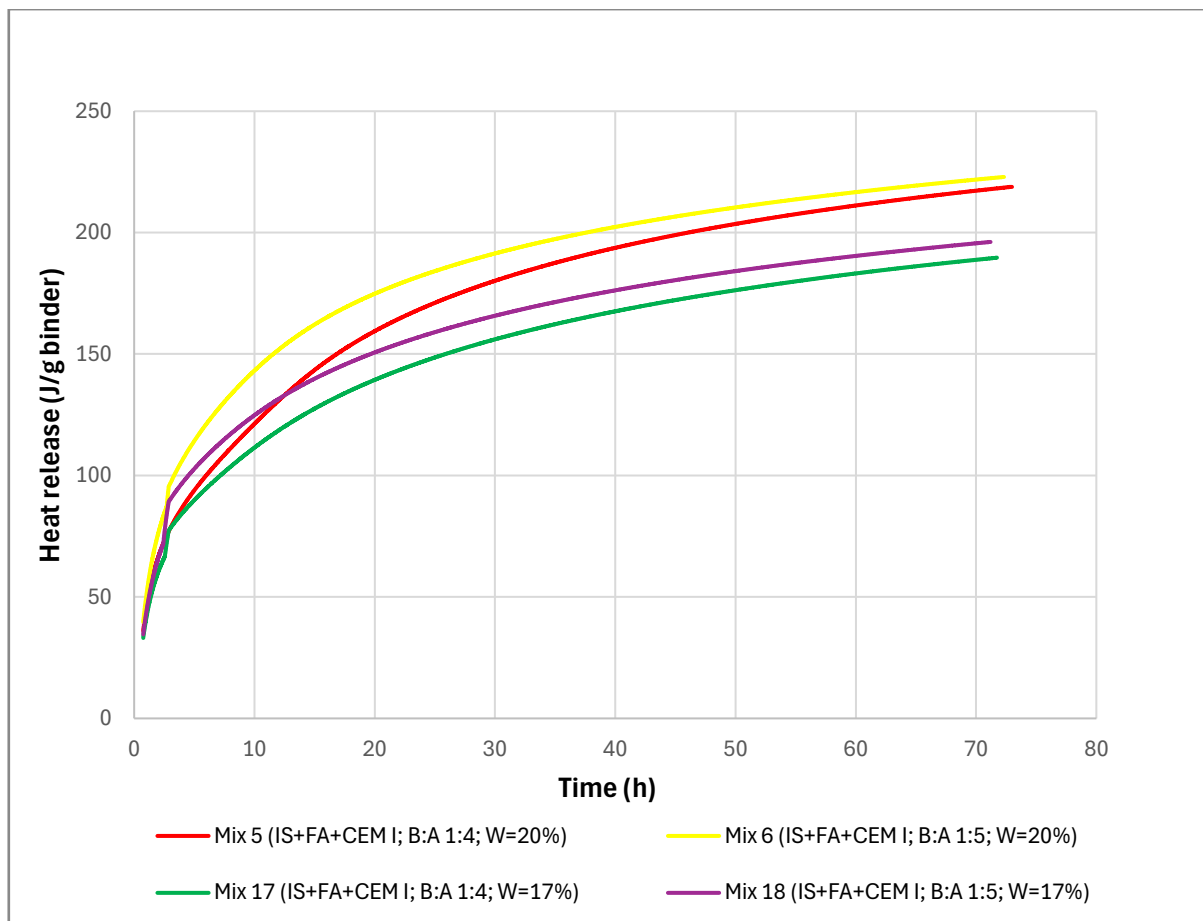


Figure 5.10. The cumulative heat release of the mixes against time after 45 minutes.

Figure 5.10. illustrates the cumulative heat release (J/g binder) of the cement-activated fly ash mixture. The results show that both the binder ratio and water content exert distinct influences on hydration kinetics and total heat evolution. Mixtures with a 1:4 binder-to-aggregate ratio (M_5 and M_17) released more heat overall than those with a 1:5 ratio (M_6 and M_18), confirming that higher binder availability enhances the extent of hydration reactions. Among these, M_5, which contained 20 % water, produced the highest cumulative heat, approximately 220 J/g binder after 72 h, indicating more

complete hydration and pozzolanic activation of fly ash. In contrast, the lower water counterpart M_17 (17 % water) displayed a slower rate and lower total heat release, suggesting that reduced moisture limits ion mobility and delays the dissolution of reactive phases.

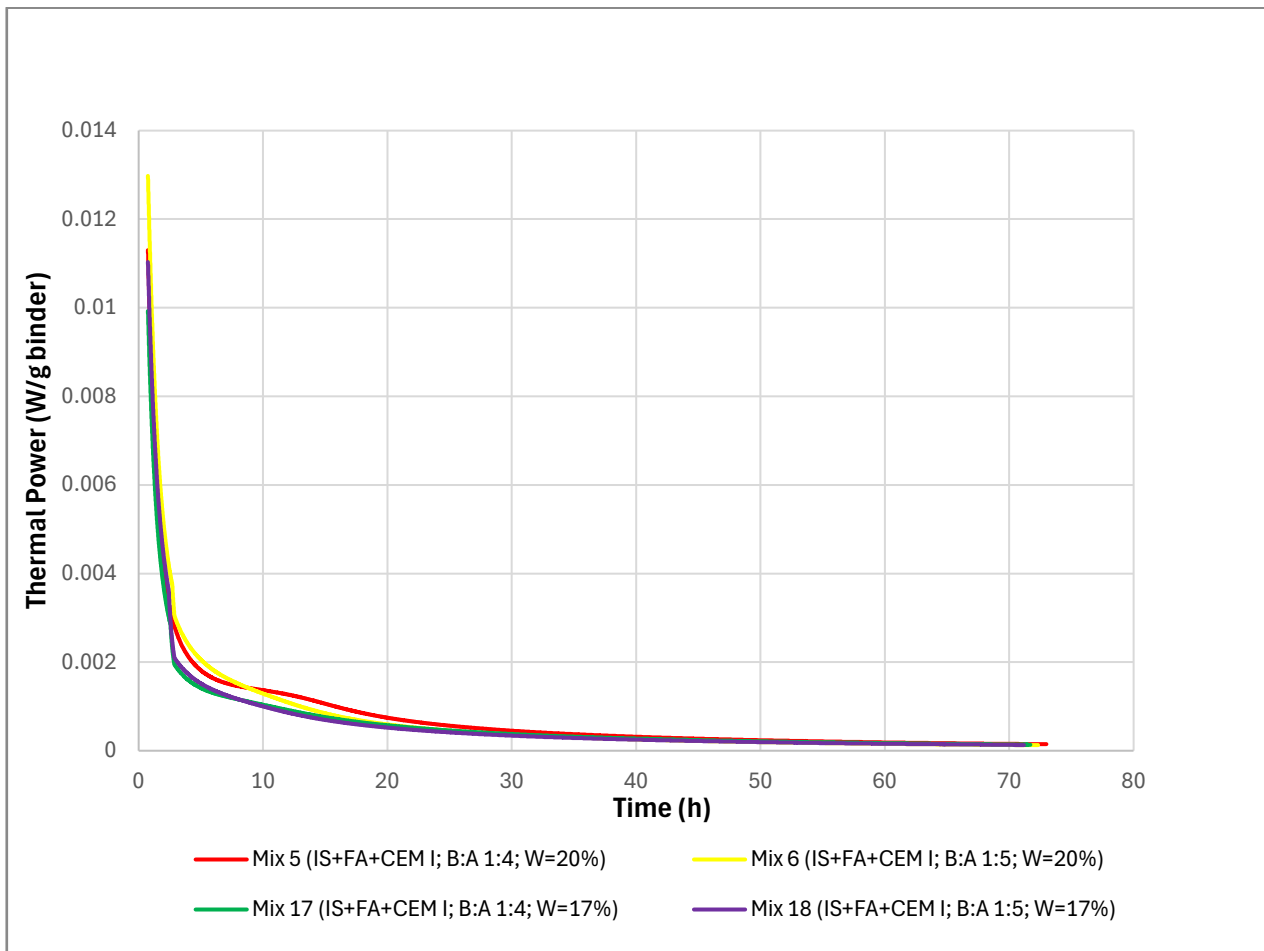


Figure 5.11. Thermal power against time after 45 minutes.

Figure 5.11. presents the corresponding thermal power (W/g binder) curves recorded at 20 °C. All samples exhibit a pronounced initial peak within the first few hours, corresponding to the early dissolution of cement and the onset of calcium-silicate-hydrate (C-S-H) formation. Mixtures with higher water content (M_5 and M_6) reached this peak slightly earlier and with greater magnitude, reflecting faster hydration kinetics under improved workability and dispersion conditions. Conversely, the 17% water mixes (M_17 and M_18) displayed a dampened, slightly delayed heat-flow peak, indicating diffusion-controlled hydration driven by reduced pore-water availability. Beyond the first 24 h, heat flow gradually diminished for all mixes, consistent with the deceleration stage typical of blended binders. The higher cumulative heat of the 1:4 mixes also confirms that a greater binder proportion yields a denser hydration network and enhanced reactivity between cement and fly ash. Overall, the calorimetry results demonstrate that cement effectively activates the latent

hydraulic potential of fly ash, and both increased binder content and adequate moisture are critical for achieving complete and sustained hydration in these cement-activated fly-ash mixtures.

6 Discussions and analysis

This chapter summarizes the key findings from the results obtained by all the lab tests and situates the results within a broader context by comparing the performance of the studied mixes with previous research on rammed earth and recycled materials by Aromaa (2021), Holopainen (2022), Luoma (2023) and Laurila (2024), and other recent studies. The chapter assesses data reliability and limitations and discusses implications for practical design, with particular attention to the benefits of fly ash-bound rammed earth with incineration slag for durability and resource efficiency. The results indicate that incorporating incineration slag and recycled aggregates enhances freeze-thaw resistance and strength, supporting their use as sustainable alternatives to conventional aggregates in cement-stabilized earth. The chapter also identifies key gaps in current knowledge and outlines how these findings can guide future research and promote wider adoption of recycled materials in earth construction.

6.1 Conclusions from the lab test.

The mechanical performance of fly ash-bound rammed earth incorporating incineration slag aggregate is primarily determined by aggregate composition and moisture condition. Stress-strain analyses demonstrate that partial replacement of incineration slag with crushed concrete and Nilsjö sand yields the most robust mechanical behavior, achieving peak stresses near 11.2 MPa prior to freeze-thaw exposure and maintaining values above 9 MPa after 15 f-t cycles. In contrast, mixtures containing only incineration slag display the lowest peak stresses and experience the greatest reductions following freeze-thaw cycling. Notably, when incineration slag serves as the sole aggregate, freeze-thaw exposure can result in strength gains if sufficient moisture is present to enable continued hydration, as evidenced by the 1:4 mixture at 20 % water, which increased from 5.21 MPa to 7.33 MPa after 15 f-t cycles. These findings indicate that blending recycled aggregates enhances both initial and residual strength under freeze-thaw conditions compared with systems that use only slag. Incineration slag requires additional research to clarify how its high aluminum content affects hydration. Telén (2023) reports that using incineration slag as the sole aggregate limits strength development, so mix designs should restrict its proportion.

Moisture resistance results further support this design rationale, demonstrating that capillary transport is highly sensitive to both initial water content and hydrophobic treatment. Water uptake increased nearly linearly with the square root of time, and hydrophobized specimens exhibited the lowest uptake

values, approximately 2.66 kg/m² and 2.59 kg/m². In comparison, non-hydrophobized mixtures showed uptake values ranging from 12.75 kg/m² to 29.76 kg/m² under similar binder and aggregate conditions. Within the mixed recycled aggregate series, an optimal moisture level is apparent, as the specimen with 16 % water absorbed less water than both drier and wetter counterparts. This suggests that absorptivity is minimized when compaction, pore structure, and binder interaction are optimally balanced. These findings support the conclusion that hydrophobization interrupts liquid water pathways, while moisture content regulates pore connectivity and capillary suction.

Calorimetry data provide insight into the observed strength and durability trends, revealing that water content significantly affects hydration kinetics and total evolution. Mixtures with a 1:4 binder-to-aggregate ratio with 20 % water released approximately 220 J/g binder after 72 hours, compared to about 190 J/g binder for the 1:4 binder-to-aggregate mix with 17 % moisture content. This result indicates more complete hydration and greater pozzolanic activation compared to mixtures with lower water content. Collectively, these findings demonstrate that optimal performance is achieved through careful control of moisture content, adequate binder availability, and well-graded recycled aggregate blends. Hydrophobization is identified as a particularly effective strategy for reducing capillary water uptake and enhancing durability under moisture exposure.

6.2 Comparison with previous studies

The comparison of the highest uniaxial compressive strength (UCS) values achieved in previous studies is presented in Figure 6.1. All samples included in this assessment were prepared using the rammed earth technique, compacted with the VTT hammer, and cured for 28 days under controlled laboratory conditions. Each study examined different combinations of recycled aggregates and low-emission binders, which led to variation in mechanical properties. Although the moisture content and binder proportions differed slightly among the works, this comparison focuses on the best-performing mixtures reported by each researcher. The evaluated materials include crushed concrete, quarry fines, foundry sand, and incineration slag as aggregates, along with binders such as CEM III/B, fly ash, and Ecolan Infra 80. Together, these studies reflect the development of stabilized rammed earth materials through continuous improvement in the selection of recycled aggregates and supplementary binders.

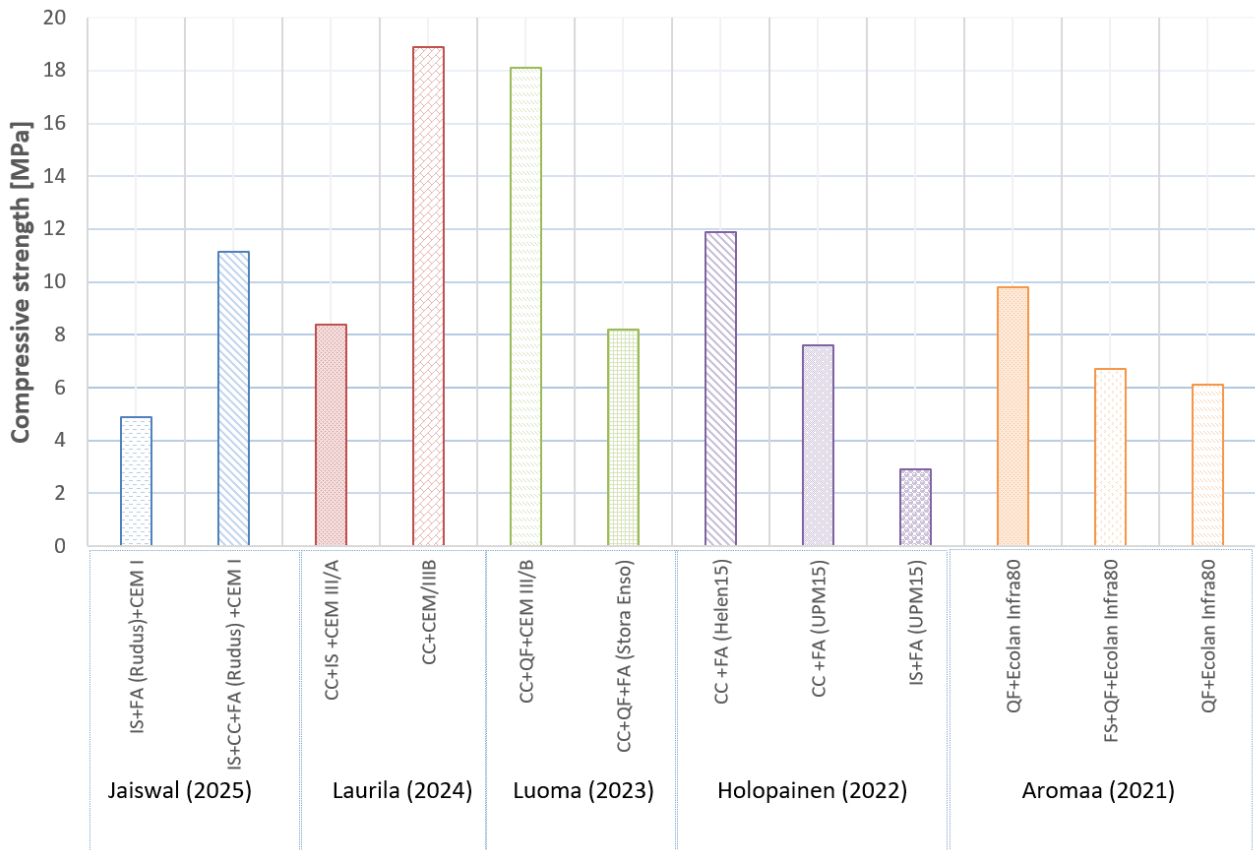


Figure 6.1. Comparison of compressive strengths between previous studies all made up of different materials however, utilized rammed earth technique and cured for 28 days. (IS= Incineration slag; FA= Fly ash (From multiple sources); CC= Crushed concrete; QF= Quarry Fines; FS= Foundry sand)

(Aromaa, 2021) investigated the potential of industrial by-products as stabilizing agents in rammed earth construction by employing the commercial binder Ecolan Infra 80, composed of approximately 80 % fly ash and 20 % cementitious additives. The study systematically explored very low binder contents, with binder-to-aggregate ratios ranging from 1:9 to 1:15.5, to evaluate the efficiency of the binder under resource-conserving conditions. The mix combining quarry fines (QF) with Ecolan Infra 80 at a 1:9 ratio achieved a uniaxial compressive strength (UCS) of about 9.8 MPa, marking the highest performance in the series. When foundry sand (FS) and quarry fines were used together in equal proportions as aggregates with the same binder ratio, the UCS reached approximately 6.7 MPa. A third set, which utilized quarry fines as the sole aggregate and a 1:15.5 binder-to-aggregate ratio, still attained a remarkable strength of 6.2 MPa, considering the significantly reduced binder content. These results demonstrate that optimized particle gradation and binder efficiency can yield structurally viable materials even at minimal binder dosages, underscoring the potential of industrial side-streams as sustainable alternatives in stabilized rammed earth applications.

(Holopainen, 2022) expanded the work by studying crushed concrete, waste incineration slag, and a mixture of fly ash with desulphurization by-products as potential aggregates. The binders used were fly ash from Helsingin Energia (Helen) and bio-based fly ash from UPM. Among all combinations, only the crushed concrete-based mixtures showed satisfactory results. The mixture of crushed concrete and Helen fly ash achieved a compressive strength of 11.9 MPa, while the combination with UPM fly ash reached 7.6 MPa. In contrast, the use of incineration slag with UPM fly ash resulted in only 2.9 MPa. These findings highlighted the critical role of aggregate selection in the performance of stabilized rammed earth, showing that crushed concrete provides a more effective reactive surface for binder hydration and bonding.

(Anssi Luoma, 2023) focused on the influence of binder type on strength development in stabilized rammed earth containing crushed concrete and quarry fines (0-3 mm) as aggregates. When CEM III/B was used as the binder at a binder-to-aggregate ratio of 1:6, the samples achieved a uniaxial compressive strength exceeding 18 MPa, demonstrating the high potential of slag-based cements in achieving strong and durable low-carbon materials. When fly ash was used as the binder with a ratio of 1:5, the strength decreased to 8.2 MPa. The results emphasized that binder composition has a significant effect on hydration reactions and that ground-granulated blast furnace slag binders outperform fly ash-based systems under identical preparation and curing conditions.

(Laurila, 2024) continued this development by combining crushed concrete and incineration slag in proportions of 80 and 20 %, respectively, using CEM III/A and CEM III/B as the binder with a binder-to-aggregate ratio of 1:6. Laurila's tests showed that the reference mix with 100 % crushed concrete and CEM III/B binder had the highest density, about 2130 kg/m³, and the highest uniaxial compressive strength at 18.9 MPa. This mix outperformed all the others. When 20 % of the crushed concrete was replaced with incineration slag, the best results came from mixes with CEM III/B and CEM III/A, which reached average UCS values of 7.43 MPa and 8.40 Mpa, respectively. These strengths are less than half of the 100 % crushed concrete and CEM III/B mix. The mix with incineration slag and the ash-based E65 binder had much lower strength, around 3.8 MPa. Laurila explains this by the lower reactivity of E65 compared to the slag-cement binders.

6.3 Reliability of results

Several steps were taken to improve the test results' reliability, but there are still limitations. The specimens were made using a set compaction method, fixed layer thickness, and controlled curing room conditions to reduce variation in density and moisture. Using three samples per mix for most tests gives a basic idea of scatter, and keeping the same loading rate, UPV device, and calorimetry setup across all mixes helps with comparability. However, the small sample size and noticeable scatter in UCS, E50, and water uptake for some mixes affect reliability. Changes in specimen mass during curing are a key source of uncertainty. Many samples gained additional mass in the curing room, indicating they absorbed more moisture. As a result, the actual water content at testing was not always the same as the designed value, so some differences in strength and stiffness may be due to the final moisture state, not just the mix design. The freeze-thaw procedure is a simplified representation of real climate, so the damage and moisture patterns may not fully match what occurs in actual foundations or walls.

There are several ways to improve reliability and reduce uncertainty in future work. Measuring and controlling both mass and moisture content for each specimen right before testing would help separate the effects of mix design from those of moisture uptake and drying. This could mean preconditioning specimens to a set humidity or sealing some batches to see the direct effect of moisture gain. Microstructural analysis, such as thin-sectioning, image analysis, or electron microscopy, could confirm links between pore structure, hydration, and transport properties, rather than relying solely on indirect measures like UV-Vis and calorimetry. Field-scale or larger-element tests would also help determine whether lab-cylinder results match real rammed-earth walls, where conditions are more complex. Together, these steps would make it clearer that the observed trends in strength and durability are real properties of the material, not just results of how the specimens were made or tested.

6.4 Suggestion for future research

Future research should take a few straightforward steps. The best mixes with incineration slag and recycled aggregates need to be tested with more samples and a slightly wider range of binder ratios and water contents. This will make the results more reliable and easier to repeat. Curing should be controlled more closely. For example, it would help to measure and record the moisture content or at least the mass of each specimen at mixing, after curing, and just before testing. Preconditioning samples to a target relative humidity could also be useful. This way, it is easier to see the effect of the mix design without the extra moisture from the curing room. Long-term performance should be checked under more realistic conditions, such as additional freeze-thaw cycles, combinations of

freezing and wetting/drying, or by keeping small test walls outdoors and monitoring them over time. Simple microstructural checks, such as basic microscopy and image analysis, can show how the pore structure and hydrates develop and how this relates to strength and moisture uptake. It would also be helpful to consider other types of fly ash and local industrial byproducts as binders, so the concept can be used with abundantly available materials.

References

- Al-Neshawy, F. , A. H. , & P. J. (2021). *Defining concrete compressive strength by combining the results of different NDT methods*.
- Anssi Luoma. (2023). *Mechanical properties of recycled materials in non-load bearing wall structure*.
- Aromaa, R. (2021). *Freeze-thaw resistance of hydraulically bound noise barrier wall built of secondary materials*.
- Bruno, A. W., Gallipoli, D., & Perlot, C. (2022). Effect of freezing-thawing cycles on the physical and mechanical properties of fired and unfired earth bricks. *Journal of Building Engineering*, 52, 104501. <https://doi.org/10.1016/j.jobe.2022.104501>
- Ciancio, D., Jaquin, P., & Walker, P. (2013). Advances on the assessment of soil suitability for rammed earth. *Construction and Building Materials*, 42, 40–47. <https://doi.org/10.1016/j.conbuildmat.2012.12.049>
- Country profile*. (2022).
- Cristelo, N., Miranda, T., & Oliveira, D. V. (2012). *Residual granitic soil improvement for rammed earth construction*. <https://www.researchgate.net/publication/258221211>
- Ehrola, E. (1996). *Liikenneväylien rakennesuunnittelun perusteet*.
- European Environmental Agency. (2024, December 5). *Europe's circular economy in facts and figures*. <https://doi.org/10.2800/5163049>
- Fischer, C. (2013). *Municipal waste management in Finland EEA project manager Almut Reichel Author affiliation*. <http://www.cri.dk/>
- Fix, S., & Richman, R. (2009). *Viability of Rammed Earth Building Construction in Cold Climates*.
- Fredlund, D. G. ., & Rahardjo, H. . (1993). *Soil mechanics for unsaturated soils*. Wiley.
- Ge, X., Ke, M., Liu, W., Wang, H., Lu, C., Mei, G., & Yang, H. (2022). Effect of the Internal Humidity of Concrete on Frost Resistance and Air Void Structure under Different Low Temperature Conditions. *Materials (Basel, Switzerland)*, 15(15). <https://doi.org/10.3390/ma1515225>
- Hall, C., & D.Hoff, W. (2022). *water transport in brick stone and concrete*.
- Holopainen, K. (2022). *Geoengineering maisteriohjelman Uusiomateriaaleista sulotun maan teknikkalla valmistettu meluseinäkoerakenne*.
- Jaquin, P. A., Augarde, C. E., Gallipoli, D., & Toll, D. G. (2009). The strength of unstabilised rammed earth materials. *Geotechnique*, 59(5), 487–490. <https://doi.org/10.1680/geot.2007.00129>
- Jaquin Paul, A. C. (2012). *3.P. Jaquin. earth building history science and conservation*.

- Kariyawasam, K. K. G. K. D., & Jayasinghe, C. (2016). Cement stabilized rammed earth as a sustainable construction material. *Construction and Building Materials*, *105*, 519–527. <https://doi.org/10.1016/j.conbuildmat.2015.12.189>
- Laurila, O. (2024). *Feasibility of treated recycled materials for rammed earth structures*.
- Linderoth, O., Wadsö, L., & Jansen, D. (2021). Long-term cement hydration studies with isothermal calorimetry. *Cement and Concrete Research*, *141*, 106344. <https://doi.org/10.1016/j.cemconres.2020.106344>
- Mccarthy, M. J., & Dhir, R. K. (1998). *Towards maximising the use of fly ash as a binder*.
- Mehta, P. K., & Monteiro, P. J. M. (2014). *Concrete*. <https://doi.org/10.1036/0071462899>
- Minke, G. (2006). *Introduction 1 Building with Earth Appendices 3 Building with Earth Design and Technology of a Sustainable Architecture Birkhäuser-Publishers for Architecture Basel · Berlin · Boston*.
- Nguyen, D. T., & Phan, V. T. A. (2021). Engineering properties of soil stabilized with cement and fly ash for sustainable road construction. *International Journal of Engineering*, *34*(12). <https://doi.org/10.5829/ije.2021.34.12c.12>
- Pylkkänen, K., & Nurmikolu, A. (2015). *Routa ja routiminen ratarakenteessa*.
- Reddy, B. V. V. (2022). *Springer Transactions in Civil and Environmental Engineering Compressed Earth Block & Rammed Earth Structures*. <https://doi.org/https://doi.org/10.1007/978-981-16-7877-6>
- Roy, S., Chah, C. N., Banerjee, A., Bordoloi, S., & Sekharan, S. (2025). Hydrophobized Iron Tailings–Based Cementitious Composites for External Applications. *Journal of Materials in Civil Engineering*, *37*(8). <https://doi.org/10.1061/JMCEE7.MTENG-18706>
- Sivakrishna, A., Adesina, A., Awoyera, P. O., & Kumar, K. R. (2020). Green concrete: A review of recent developments. *Materials Today: Proceedings*, *27*, 54–58. <https://doi.org/10.1016/j.matpr.2019.08.202>
- Suomen Betoniyhdistys ry. (2016). *Betoniteollisuus ry 2019*.
- Telén, B. (2023). *Review of city of Helsinki's plastic flow in street and park projects*.
- Traoré, L. B., Ouellet-Plamondon, C., Fabbri, A., McGregor, F., & Rojat, F. (2021). Experimental assessment of freezing-thawing resistance of rammed earth buildings. *Construction and Building Materials*, *274*, 121917. <https://doi.org/10.1016/J.CONBUILDMAT.2020.121917>
- Tuyan, M., Mardani-Aghabaglou, A., & Ramyar, K. (2014). Freeze–thaw resistance, mechanical and transport properties of self-consolidating concrete incorporating coarse recycled concrete aggregate. *Materials & Design*, *53*, 983–991. <https://doi.org/10.1016/J.MATDES.2013.07.100>
- UUMA. (2006). *UUMA*. <https://Uma.Kiertotaloussuomi.Fi/Briefly-in-English/>. <https://uusi-omaarakentaminen.fi/uuma-ohjelma/>
- UUMA Programs. (2024). *UUMA programs*. <https://uuma.kiertotaloussuomi.fi/briefly-in-english/>

Walker, Peter. (2005). *Rammed earth : design and construction guidelines*. BRE Bookshop.

Wayu, A. (2024). *Technical properties of fine-grained sand from Nilsjö quarry and its use in earth construction*.

ymparisto.fi. (2024, July 10). *Municipal waste*. <https://www.ymparisto.fi/fi/kestava-kierto-ja-bio-talous/kierratys-ja-jatteet/valtakunnallisen-jatesuunnitelman-seuranta/yhdyskuntajatteet>

Zeynali, Y., Niroumand, H., & Ziaie Moayed, R. (2023). Stabilizing cohesive soils with Micro- and Nano- fly ash as Eco-friendly Materials: An experimental study. *Construction and Building Materials*, 399. <https://doi.org/10.1016/j.conbuildmat.2023.132490>

Attachments

Attachment 1: List of UCS results from Lab test

Attachment 2: Technical data sheet of CEM I from Finnsementti

Attachment 3: Incineration slag leaching test results

Attachment 4: Chemical composition quantification results for Fly ash

17.09.24

Aalto-yliopisto
Insinööritieteiden korkeakoulu
Rakennustekniikan laitos

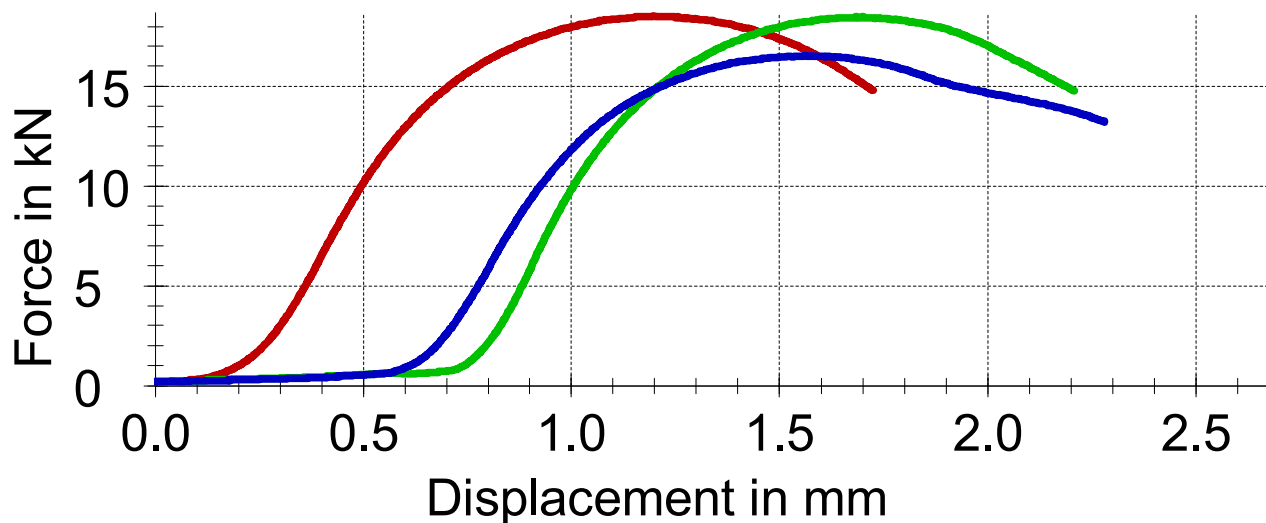
Test report

Customer : Aalto/CE/Soil Lab. Pre-treatment :
 Group : M1 Tester : Manish Jaiswal
 Material : Incenerated slag + Fly ash + Cement Notes... :
 Specimen type : Rammed earth cylinder
 Pre-load : 200 N
 Test speed : 3 mm/min

Test results:

Legends	Nr	Specimen identifier	d ₀ mm	h ₀ mm	ρ ₀ kg/m ³	Mass g	F _{max} kN	σ _M N/mm ²	dL at F _{max} mm
■	1	M1_1	100,00	172,3	1203	2258	18,50	2,36	1,2
■	2	M1_2	100,00	173,2	1190	2245	18,47	2,35	1,7
■	3	M1_3	100,00	171,3	1188	2215	16,53	2,10	1,6

Series graph:



Statistics:

Series	ρ ₀ kg/m ³	σ _M N/mm ²
n = 3		
\bar{x}	1194	2,27
s	8,422	0,14
v	0,71	6,33

17.09.24

Aalto-yliopisto
Insinööritieteiden korkeakoulu
Rakennustekniikan laitos

UCS Test for series M2

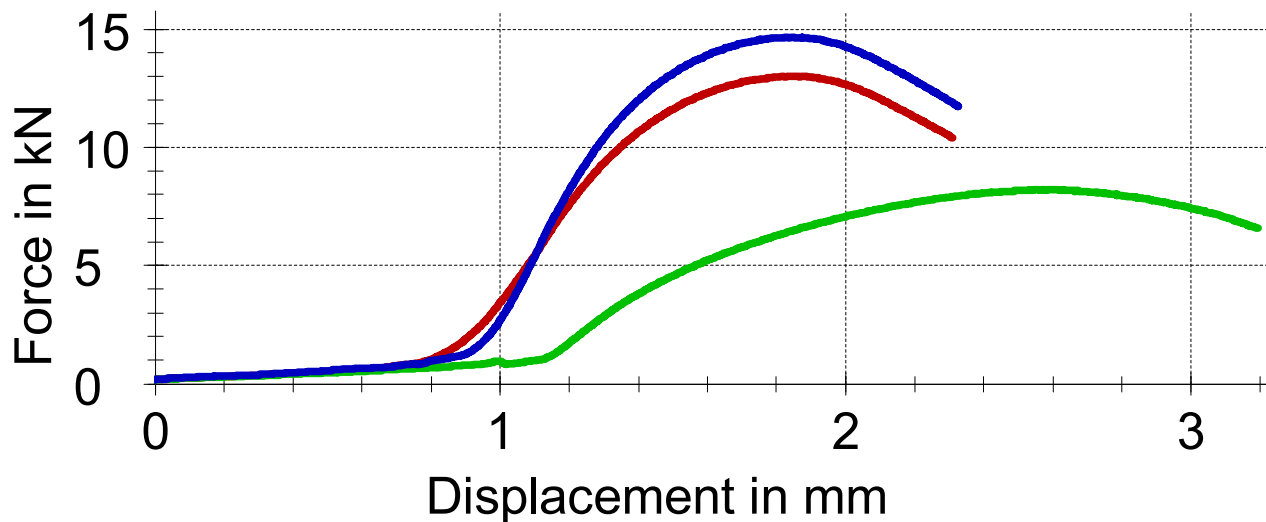
Heading : UCS Test for series M2 Specimen type : Rammed earth cylinder
Customer : Aalto/CE/Soil Lab. Pre-treatment :
Group : M2 Tester : Manish Jaiswal
Material : Inceneration slag + Fly ash + Cement Notes...

Pre-load : 200 N
Test speed : 3 mm/min

Test results:

Legends	Nr	Specimen identifier	d_0 mm	h_0 mm	ρ_0 kg/m ³	Mass g	F_{max} kN	σ_M N/mm ²	dL at F_{max} mm
■	1	M2_1	100,00	174,9	1296	2469	13,01	1,66	1,8
■	2	M2_2	100,00	177,7	1287	2490	8,20	1,04	2,6
■	3	M2_3	100,00	173,3	1301	2456	14,67	1,87	1,8

Series graph:



Statistics:

Series	ρ_0 kg/m ³	σ_M N/mm ²
n = 3		
\bar{x}	1295	1,52
s	7,009	0,43
v	0,54	28,07

17.09.24

Aalto-yliopisto
Insinööritieteiden korkeakoulu
Rakennustekniikan laitos

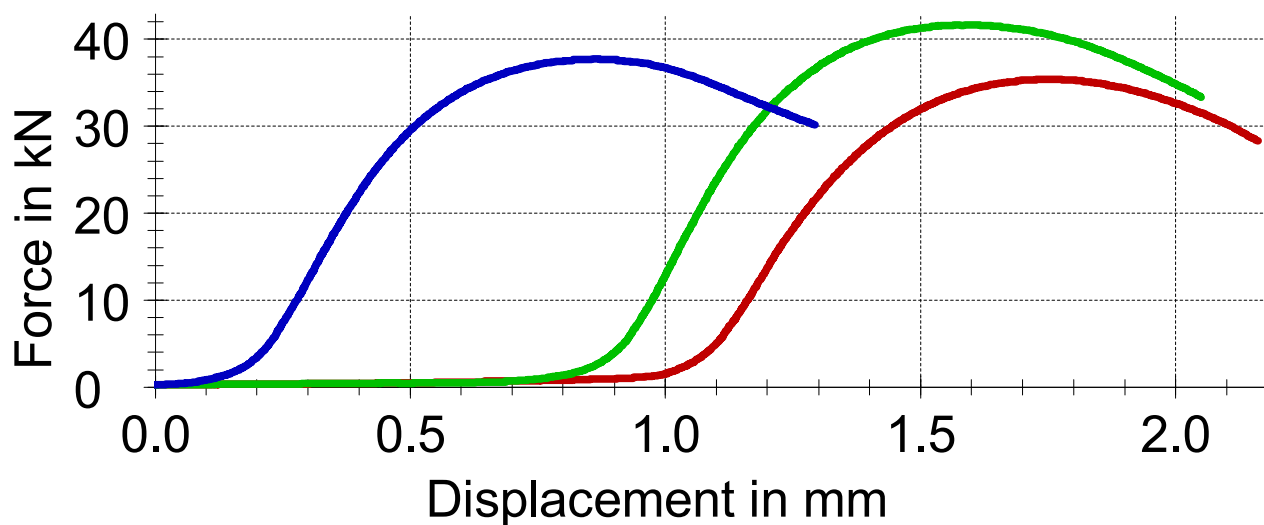
UCS Test for Series M3

Heading : UCS Test for Series M3 Specimen type : Rammed earth cylinder
Customer : Aalto/CE/Soil Lab. Pre-treatment :
Group : Tester : Manish Jaiswal
Material : Incenerated slag + Fly ash + Cement Notes... :
Pre-load : 200 N
Test speed : 3 mm/min

Test results:

Legends	Nr	Specimen identifier	d_0 mm	h_0 mm	ρ_0 kg/m ³	Mass g	F_{max} kN	σ_M N/mm ²	dL at F_{max} mm
■	1	M3_1	100,00	170,1	1303	2415	35,39	4,51	1,8
■	2	M3_2	100,00	169,5	1287	2376	41,62	5,30	1,6
■	3	M3_3	100,00	169,4	1310	2416	37,70	4,80	0,9

Series graph:



Statistics:

Series	ρ_0 kg/m ³	σ_M N/mm ²
n = 3		
\bar{x}	1300	4,87
s	11,75	0,40
v	0,90	8,24

18.09.24

Aalto-yliopisto
Insinööritieteiden korkeakoulu
Rakennustekniikan laitos

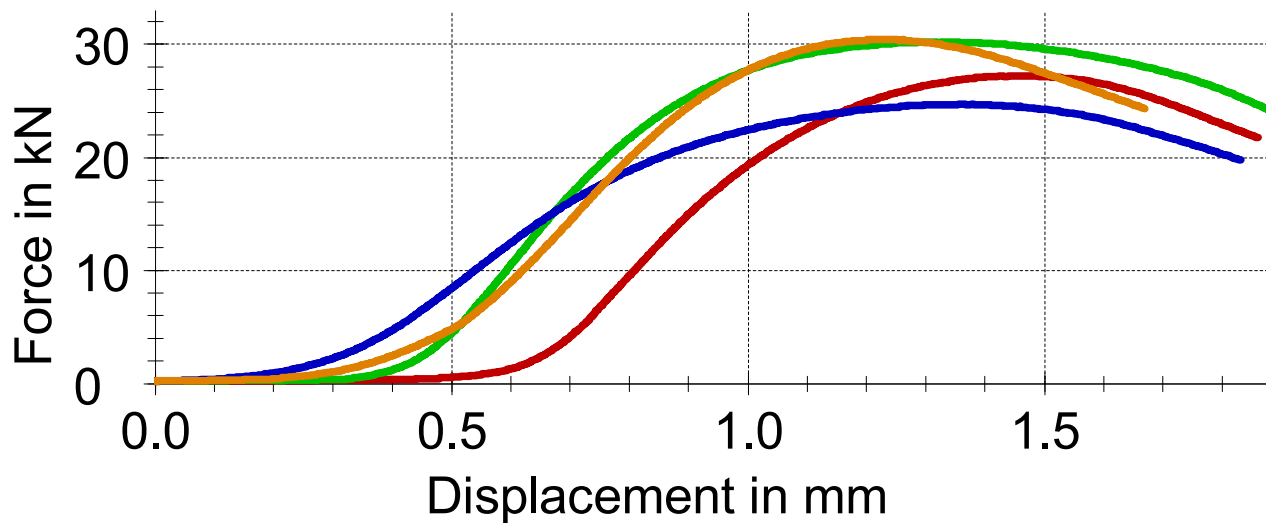
UCS Test series M4

Heading : UCS Test series M4 Specimen type : Rammed earth cylinder
 Customer : Aalto/CE/Soil Lab. Pre-treatment :
 Group : Tester : Manish Jaiswal
 Material : Incenerated slag + Fly ash + Cement Notes... :
 Pre-load : 200 N
 Test speed : 3 mm/min

Test results:

Legends	Nr	Specimen identifier	d ₀ mm	h ₀ mm	ρ ₀ kg/m ³	Mass g	F _{max} kN	σ _M N/mm ²	dL at F _{max} mm
■	1	M4_1	100,00	173,3	1253	2364	27,23	3,47	1,5
■	2	M4_2	100,00	174,6	1292	2458	30,22	3,85	1,3
■	3	M4_3	100,00	175,0	1287	2451	24,72	3,15	1,4
■	4	M4_4	100,00	170,4	1280	2376	30,44	3,88	1,2

Series graph:



Statistics:

Series	ρ ₀ kg/m ³	σ _M N/mm ²
n = 4		
\bar{x}	1278	3,58
s	17,6	0,35
v	1,38	9,66

18.09.24

Aalto-yliopisto
Insinööritieteiden korkeakoulu
Rakennustekniikan laitos

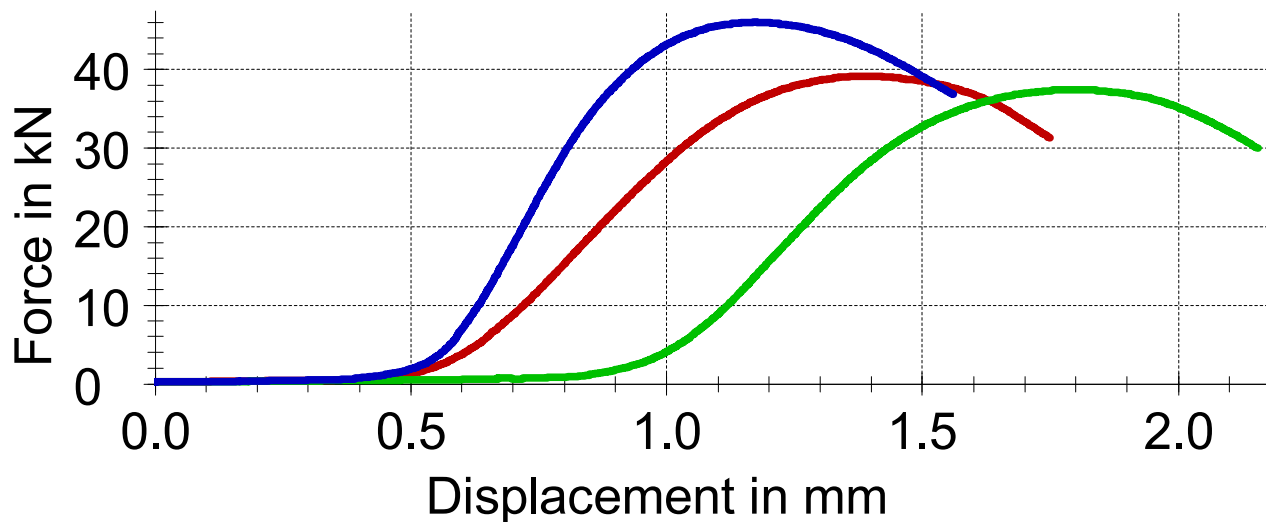
UCS Test for series M5

Heading : UCS Test for series M5 Specimen type : Rammed earth cylinder
Customer : Aalto/CE/Soil Lab. Pre-treatment :
Group : Tester : Manish Jaiswal
Material : Incenerated slag + Fly ash + Cement Notes... :
Pre-load : 200 N
Test speed : 3 mm/min

Test results:

Legends	Nr	Specimen identifier	d ₀ mm	h ₀ mm	ρ ₀ kg/m ³	Mass g	F _{max} kN	σ _M N/mm ²	dL at F _{max} mm
■	1	M5_1	100,00	171,2	1258	2344	39,16	4,99	1,4
■	2	M5_2	100,00	172,3	1177	2210	37,45	4,77	1,8
■	3	M5_3	100,00	169,2	1299	2393	46,03	5,86	1,2

Series graph:



Statistics:

Series	ρ ₀ kg/m ³	σ _M N/mm ²
n = 3		
\bar{x}	1245	5,20
s	61,66	0,58
v	4,95	11,11

18.09.24

Aalto-yliopisto
Insinööritieteiden korkeakoulu
Rakennustekniikan laitos

UCS Test series M6

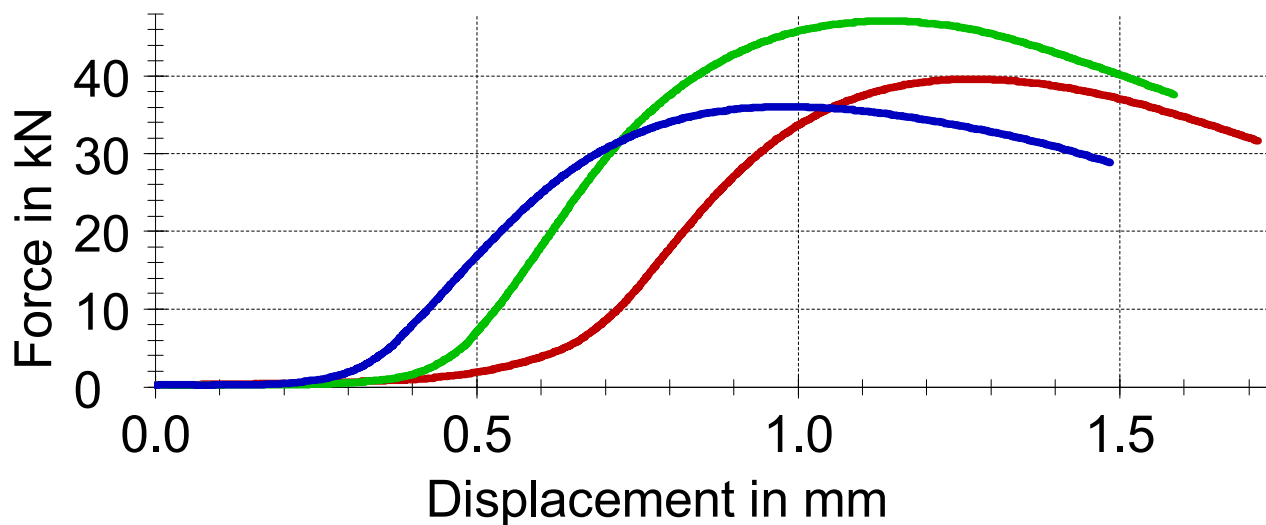
Heading : UCS Test series M6 Specimen type : Rammed earth cylinder
Customer : Aalto/CE/Soil Lab. Pre-treatment :
Group : Tester : Manish Jaiswal
Material : Incenerated slag + Fly ash + Cement Notes... :

Pre-load : 200 N
Test speed : 3 mm/min

Test results:

Legends	Nr	Specimen identifier	d ₀ mm	h ₀ mm	ρ ₀ kg/m ³	Mass g	F _{max} kN	σ _M N/mm ²	dL at F _{max} mm
■	1	M6_1	100,00	169,8	1232	2277	39,61	5,04	1,3
■	2	M6_2	100,00	169,8	1299	2402	47,10	6,00	1,2
■	3	M6_3	100,00	170,6	1212	2250	36,10	4,60	1,0

Series graph:



Statistics:

Series	ρ ₀ kg/m ³	σ _M N/mm ²
n = 3		
\bar{x}	1248	5,21
s	46,04	0,72
v	3,69	13,73

04.10.24

Aalto-yliopisto
Insinöörیتieteiden korkeakoulu
Rakennustekniikan laitos

Test report

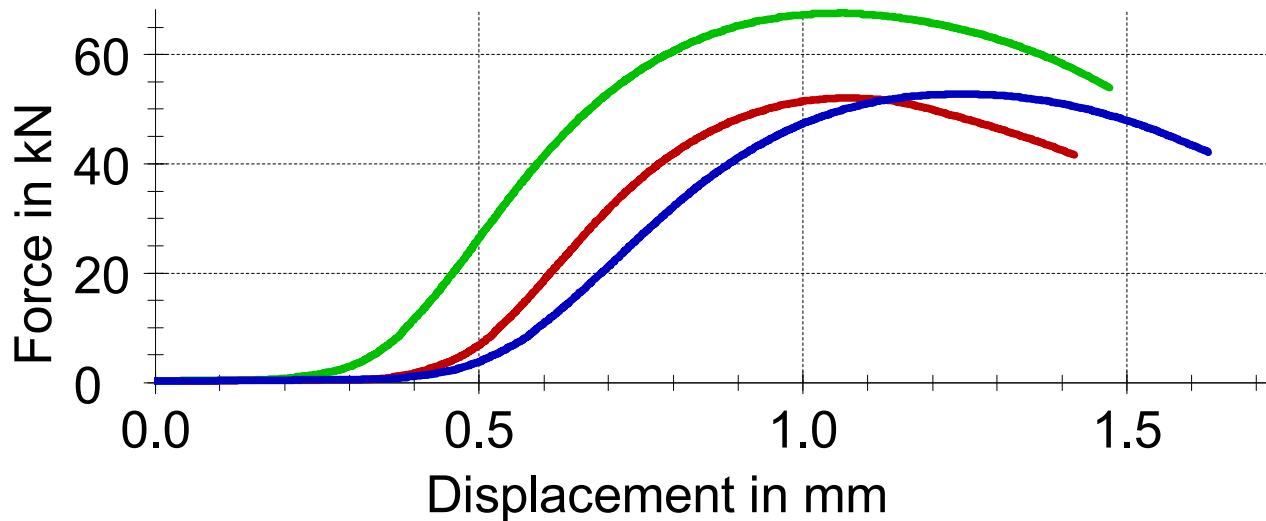
Customer : Aalto/CE/Soil Lab.
Group :
Material : Inceneration slag + Fly ash + Cement (1:4)
Specimen type : Cylindrical rammed earth
Pre-treatment :
Tester : Manish Jaiswal
Notes... :

Pre-load : 200 N
Test speed : 3 mm/min

Test results:

Legends	Nr	Specimen identifier	d_0 mm	h_0 mm	ρ_0 kg/m ³	Mass g	F_{max} kN	σ_M N/mm ²	dL at F_{max} mm
■	1	M_7_1	100,00	168,2	1257	2303	52,11	6,63	1,1
■	2	M_7_2	100,00	167,0	1313	2388	67,58	8,60	1,1
■	3	M_7_3	100,00	167,4	1264	2304	52,84	6,73	1,2

Series graph:



Statistics:

Series	ρ_0 kg/m ³	σ_M N/mm ²
n = 3		
\bar{x}	1278	7,32
s	30,6	1,11
v	2,39	15,18

04.10.24

Aalto-yliopisto
 Insinöörیتieteiden korkeakoulu
 Rakennustekniikan laitos

Test report

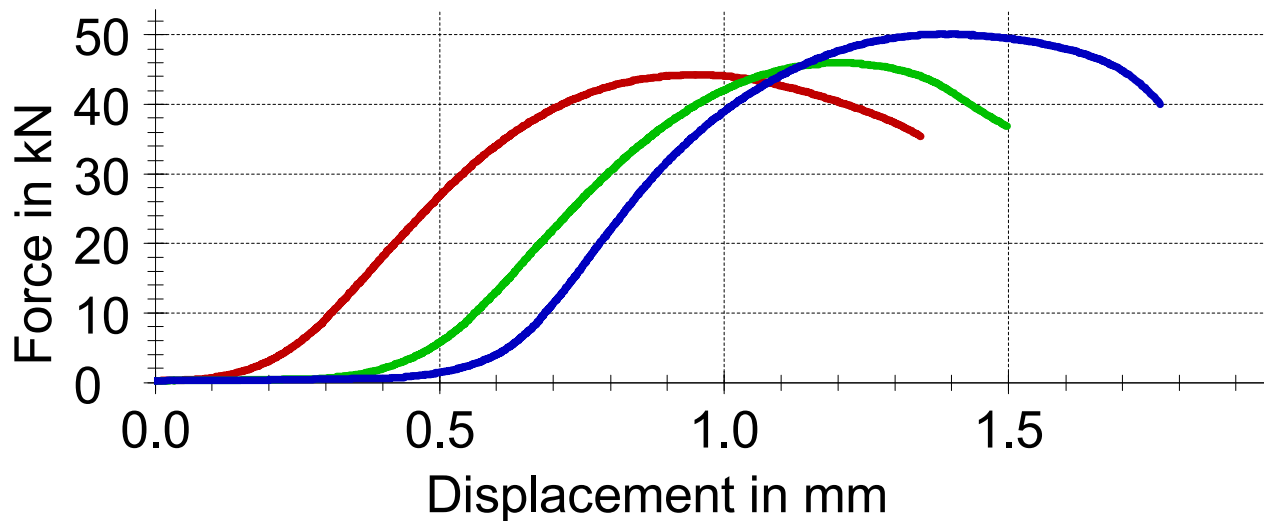
Customer : Aalto/CE/Soil Lab.
 Group :
 Material : Inceneration Slag + Fly ash + Cement (1:5)
 Specimen type : Cylindrical rammed earth
 Pre-treatment :
 Tester : Manish Jaiswal
 Notes... :

Pre-load : 200 N
 Test speed : 3 mm/min

Test results:

Legends	Nr	Specimen identifier	d ₀ mm	h ₀ mm	ρ ₀ kg/m ³	Mass g	F _{max} kN	σ _M N/mm ²	dL at F _{max} mm
■	1	M_8_1	100,00	168,0	1249	2287	44,28	5,64	1,0
■	2	M_8_2	100,00	168,4	1301	2386	46,02	5,86	1,2
■	3	M_8_3	100,00	169,2	1307	2408	50,11	6,38	1,4

Series graph:



Statistics:

Series	ρ ₀ kg/m ³	σ _M N/mm ²
n = 3		
\bar{x}	1286	5,96
s	31,56	0,38
v	2,45	6,39

02.10.24

Aalto-yliopisto
Insinöörیتieteiden korkeakoulu
Rakennustekniikan laitos

Test report

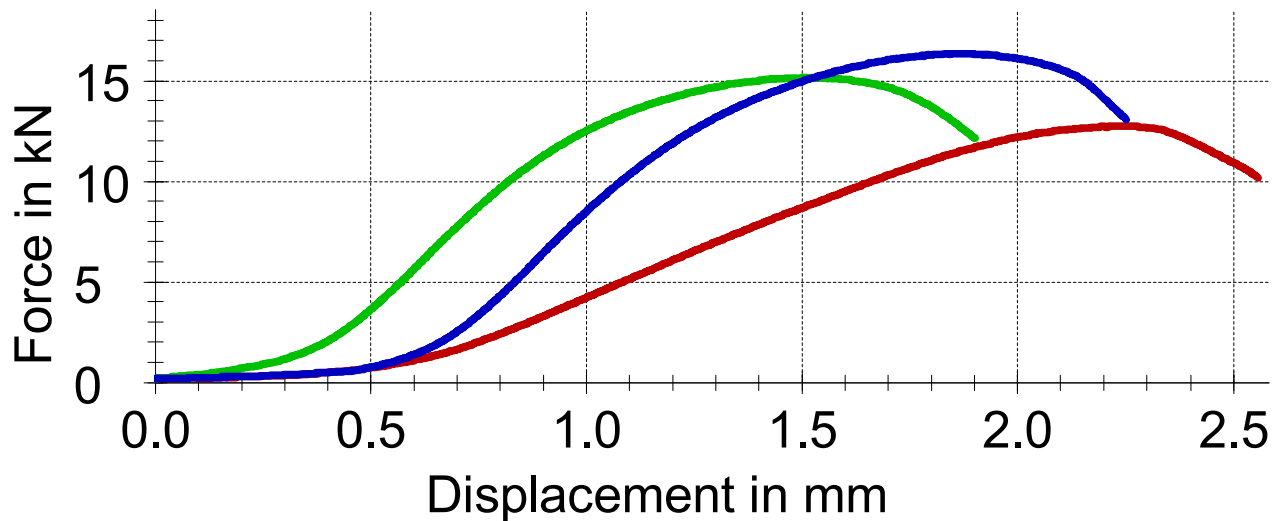
Customer : Aalto/CE/Soil Lab.
Group :
Material : Inceneration slag + Fly ash + Cement (1:4)
Specimen type : Cylindrical rammed earth
Pre-treatment :
Tester : Manish Jaiswal
Notes... :

Pre-load : 200 N
Test speed : 3 mm/min

Test results:

Legends	Nr	Specimen identifier	d ₀ mm	h ₀ mm	ρ ₀ kg/m ³	Mass g	F _{max} kN	σ _M N/mm ²	dL at F _{max} mm
■	1	M_13_1	100,00	180,0	1304	2558	12,75	1,62	2,2
■	2	M_13_2	100,00	177,6	1309	2531	15,16	1,93	1,5
■	3	M_13_3	100,00	179,6	1300	2542	16,35	2,08	1,9

Series graph:



Statistics:

Series	ρ ₀ kg/m ³	σ _M N/mm ²
n = 3		
\bar{x}	1304	1,88
s	4,612	0,23
v	0,35	12,45

02.10.24

Aalto-yliopisto
Insinööritieteiden korkeakoulu
Rakennustekniikan laitos

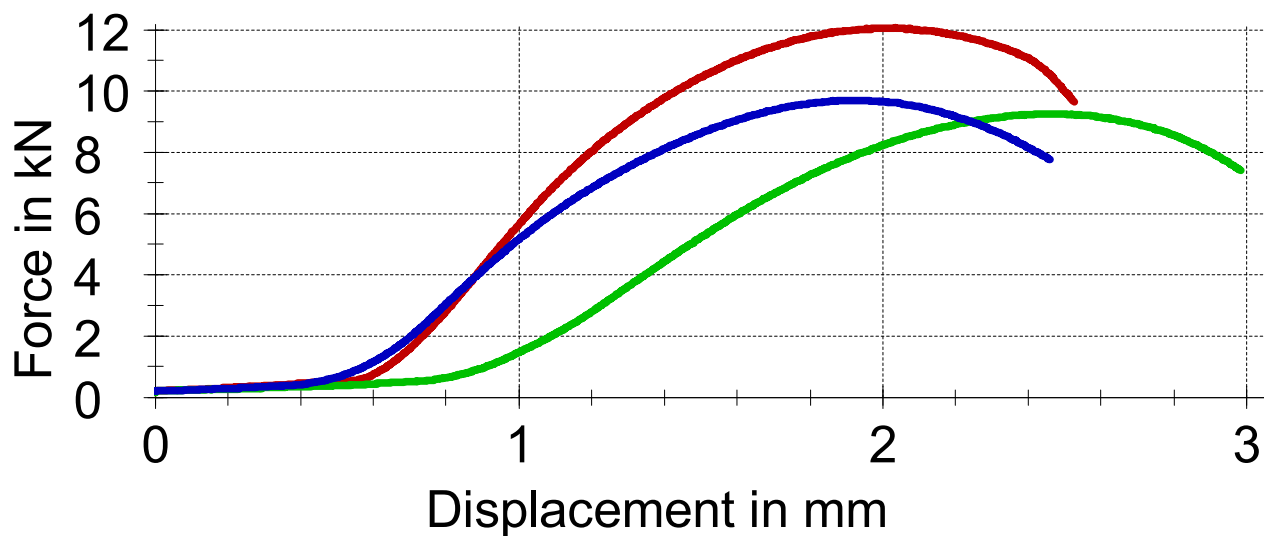
Test report

Customer : Aalto/CE/Soil Lab. Pre-treatment :
 Group : Tester : Manish Jaiswal
 Material : Inceneration slag + Fly ash + Cement Notes... :
 Specimen type : Cylindrical rammed earth (1:5)
 Pre-load : 200 N
 Test speed : 3 mm/min

Test results:

Legends	Nr	Specimen identifier	d_0 mm	h_0 mm	ρ_0 kg/m ³	Mass g	F_{max} kN	σ_M N/mm ²	dL at F_{max} mm
■	1	M_14_1	100,00	178,2	1139	2210	12,06	1,54	2,0
■	2	M_14_2	100,00	181,0	1294	2551	9,25	1,18	2,4
■	3	M_14_3	100,00	179,9	1292	2532	9,71	1,24	1,9

Series graph:



Statistics:

Series	ρ_0 kg/m ³	σ_M N/mm ²
n = 3		
\bar{x}	1242	1,32
s	89,26	0,19
v	7,19	14,55

02.10.24

Aalto-yliopisto
 Insinöörیتieteiden korkeakoulu
 Rakennustekniikan laitos

Test report

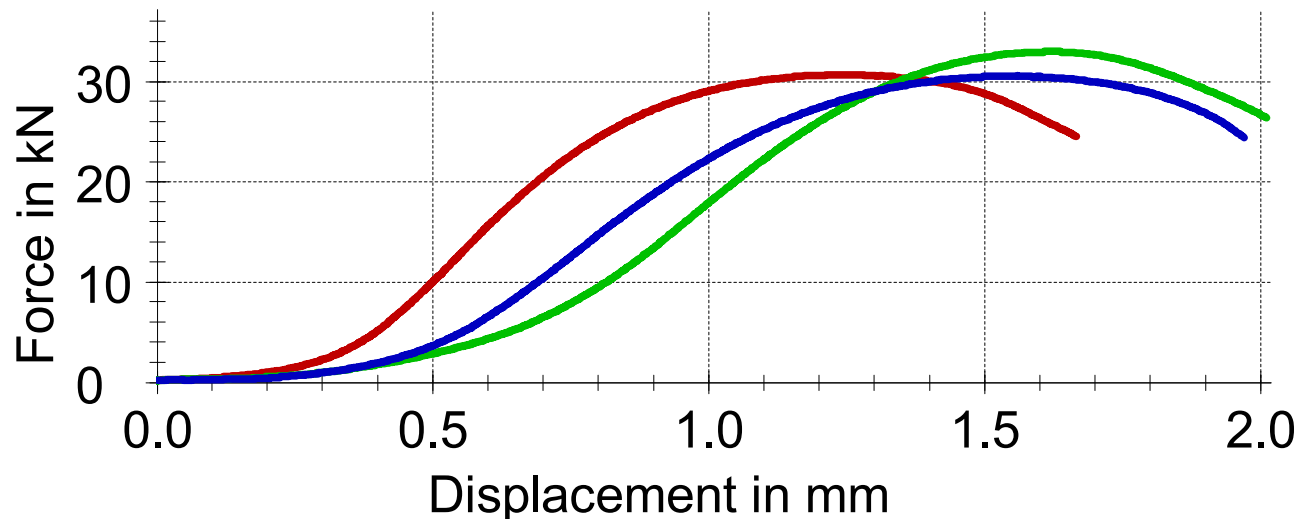
Customer : Aalto/CE/Soil Lab.
 Group :
 Material : Inceneration slag + Fly ash + Cement (1:4)
 Specimen type : Cylindrical rammed earth
 Pre-treatment :
 Tester : Otso Laurila
 Notes... :

Pre-load : 200 N
 Test speed : 3 mm/min

Test results:

Legends	Nr	Specimen identifier	d_0 mm	h_0 mm	ρ_0 kg/m ³	Mass g	F_{max} kN	σ_M N/mm ²	dL at F_{max} mm
■	1	M_15_1	100,00	177,6	1305	2523	30,69	3,91	1,2
■	2	M_15_2	100,00	173,8	1313	2485	33,00	4,20	1,6
■	3	M_15_3	100,00	174,0	1163	2205	30,56	3,89	1,6

Series graph:



Statistics:

Series	ρ_0 kg/m ³	σ_M N/mm ²
n = 3		
\bar{x}	1260	4,00
s	84,13	0,17
v	6,67	4,37

02.10.24

Aalto-yliopisto
Insinööritieteiden korkeakoulu
Rakennustekniikan laitos

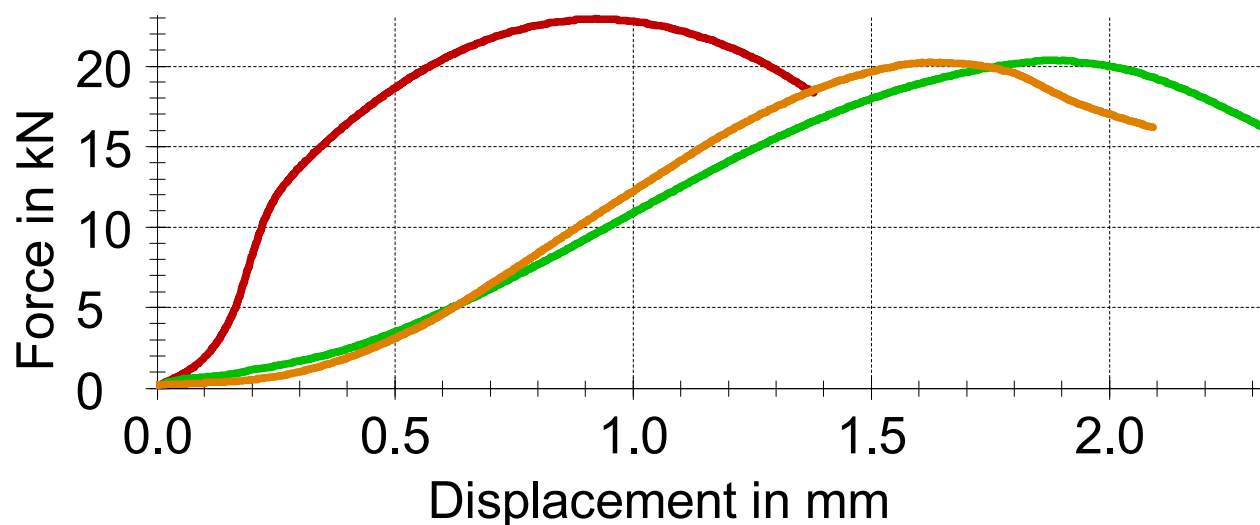
Test report

Customer : Aalto/CE/Soil Lab. Pre-treatment :
 Group : Tester : Manish Jaiswal
 Material : Inceneration slag + Fly ash + Cement Notes... :
 Specimen type : Cylindrical rammed earth
 Pre-load : 200 N
 Test speed : 3 mm/min

Test results:

Legends	Nr	Specimen identifier	d_0 mm	h_0 mm	ρ_0 kg/m ³	Mass g	F_{max} kN	σ_M N/mm ²	dL at F_{max} mm
■	1	M_16_1	100,00	176,5	1297	2493	22,92	2,92	0,9
■	2	M_16_2	100,00	180,5	1298	2553	20,35	2,59	1,9
■	4	M_16_3	100,00	179,8	1299	2545	20,25	2,58	1,6

Series graph:



Statistics:

Series	ρ_0 kg/m ³	σ_M N/mm ²
n = 3		
\bar{x}	1298	2,70
s	1,183	0,19
v	0,09	7,15

02.10.24

Aalto-yliopisto
Insinöörityöiden korkeakoulu
Rakennustekniikan laitos

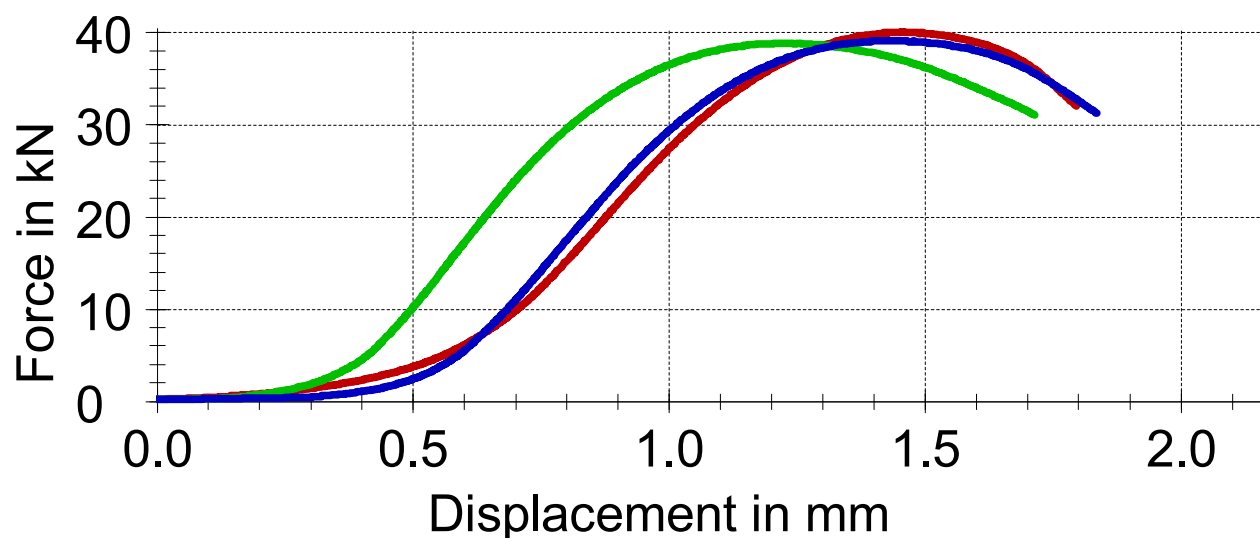
Test report

Customer : Aalto/CE/Soil Lab.
Group :
Material : Inceneration slag + Fly ash + Cement (1:4)
Specimen type : Cylindrical rammed earth
Pre-treatment :
Tester : Manish Jaiswal
Notes... :
Pre-load : 200 N
Test speed : 3 mm/min

Test results:

Legends	Nr	Specimen identifier	d_0 mm	h_0 mm	ρ_0 kg/m ³	Mass g	F_{max} kN	σ_M N/mm ²	dL at F_{max} mm
■	1	M_17_1	100,00	177,5	1306	2526	40,04	5,10	1,5
■	2	M_17_2	100,00	177,1	1313	2532	38,85	4,95	1,2
■	3	M_17_3	100,00	177,4	1311	2532	39,12	4,98	1,4

Series graph:



Statistics:

Series	ρ_0 kg/m ³	σ_M N/mm ²
n = 3		
\bar{x}	1310	5,01
s	3,542	0,08
v	0,27	1,58

03.10.24

Aalto-yliopisto
Insinööritieteiden korkeakoulu
Rakennustekniikan laitos

Test report

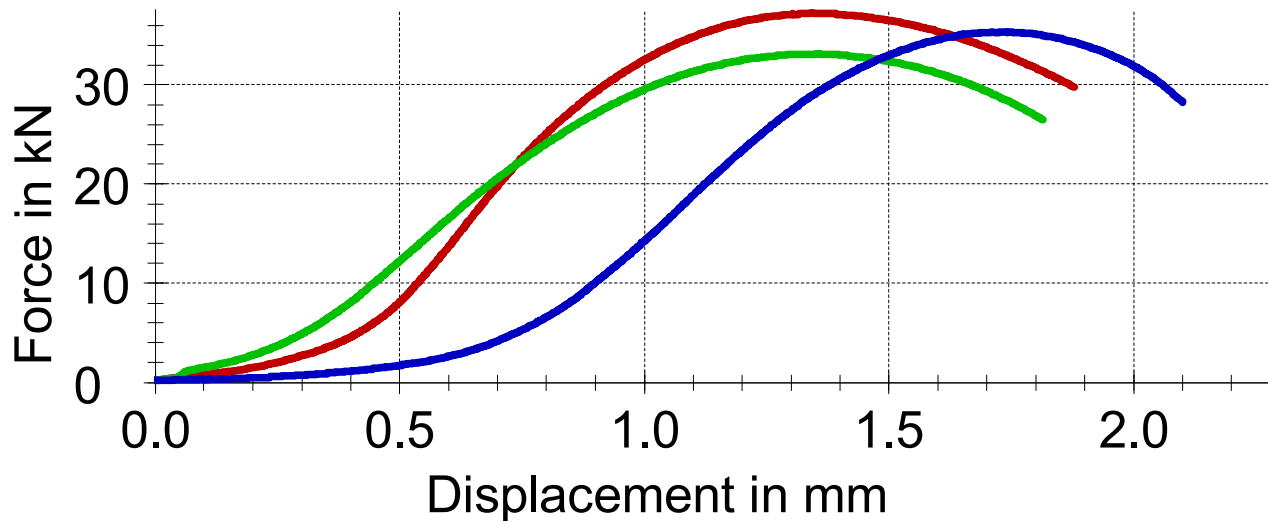
Customer : Aalto/CE/Soil Lab.
Group :
Material : Inceneration slag + Fly ash + Cement (1:5)
Specimen type : Cylindrical rammed earth
Pre-treatment :
Tester : Manish Jaiswal
Notes... :

Pre-load : 200 N
Test speed : 3 mm/min

Test results:

Legends	Nr	Specimen identifier	d_0 mm	h_0 mm	ρ_0 kg/m ³	Mass g	F_{max} kN	σ_M N/mm ²	dL at F_{max} mm
■	1	M_18_1	100,00	176,0	1289	2472	37,26	4,74	1,3
■	2	M_18_2	100,00	178,0	1285	2491	33,14	4,22	1,4
■	3	M_18_3	100,00	174,8	1295	2466	35,38	4,50	1,7

Series graph:



Statistics:

Series	ρ_0 kg/m ³	σ_M N/mm ²
n = 3		
\bar{x}	1290	4,49
s	4,965	0,26
v	0,38	5,84

18.10.24

Aalto-yliopisto
Insinööritieteiden korkeakoulu
Rakennustekniikan laitos

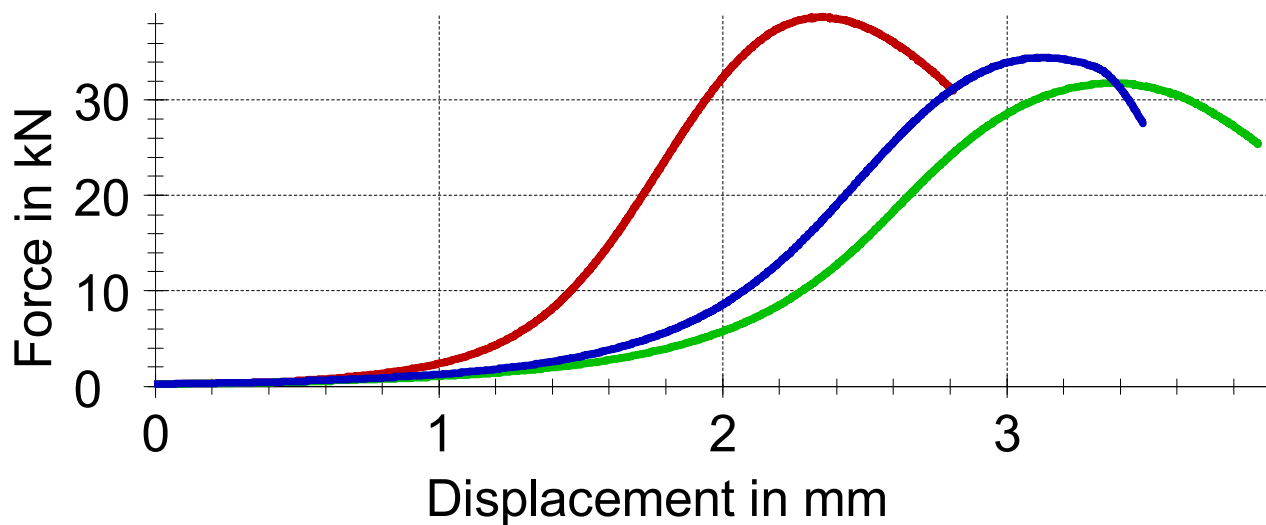
Test report

Customer : Aalto/CE/Soil Lab. Pre-treatment :
 Group : Tester : Manish Jaiswal
 Material : Inceneration slag + Fly ash + Cement Notes... :
 Specimen type : Cylindrical rammed earth
 Pre-load : 200 N
 Test speed : 3 mm/min

Test results:

Legends	Nr	Specimen identifier	d_0 mm	h_0 mm	ρ_0 kg/m ³	Mass g	F_{max} kN	σ_M N/mm ²	dL at F_{max} mm
■	1	M_19_1	100,00	176,1	1321	2534	38,72	4,93	2,3
■	2	M_19_2	100,00	178,8	1327	2584	31,79	4,05	3,4
■	3	M_19_3	100,00	175,1	1328	2533	34,47	4,39	3,1

Series graph:



Statistics:

Series	ρ_0 kg/m ³	σ_M N/mm ²
n = 3		
\bar{x}	1325	4,46
s	3,466	0,44
v	0,26	9,98

18.10.24

Aalto-yliopisto
Insinööritieteiden korkeakoulu
Rakennustekniikan laitos

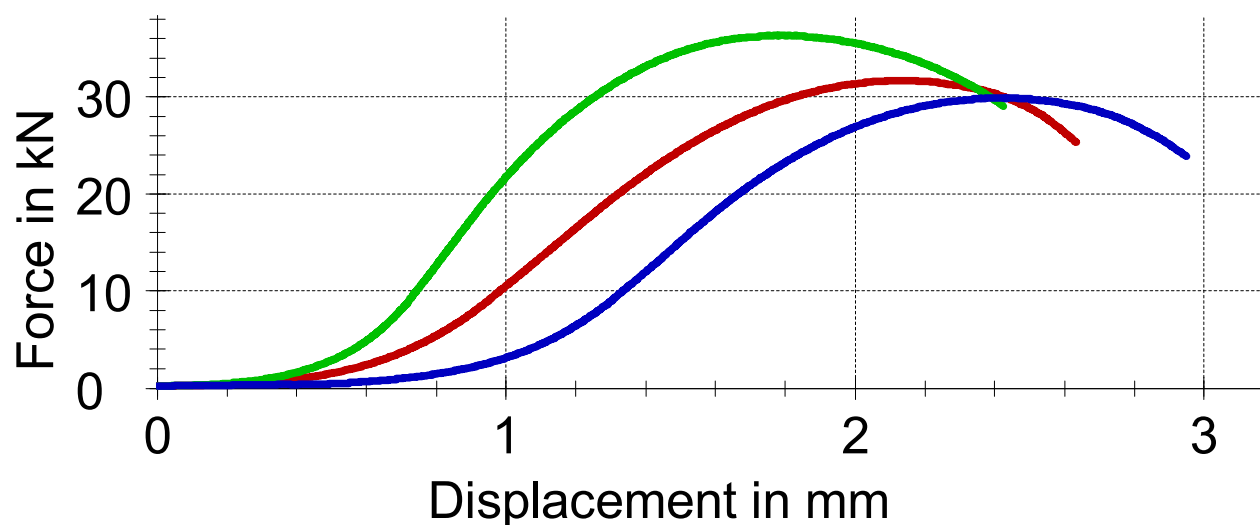
Test report

Customer : Aalto/CE/Soil Lab. Pre-treatment :
Group : Tester : Manish jaiswal
Material : Inceneration slag + Fly ash + Cement Notes... :
Specimen type : Cylindrical rammed earth
Pre-load : 200 N
Test speed : 3 mm/min

Test results:

Legends	Nr	Specimen identifier	d_0 mm	h_0 mm	ρ_0 kg/m ³	Mass g	F_{max} kN	σ_M N/mm ²	dL at F_{max} mm
■	1	M_20_1	100,00	178,9	1314	2560	31,68	4,03	2,2
■	2	M_20_2	100,00	176,8	1319	2540	36,33	4,63	1,8
■	3	M_20_3	100,00	178,5	1318	2563	29,87	3,80	2,4

Series graph:



Statistics:

Series	ρ_0 kg/m ³	σ_M N/mm ²
n = 3		
\bar{x}	1317	4,15
s	2,783	0,42
v	0,21	10,21

03.12.24

Aalto-yliopisto
Insinööritieteiden korkeakoulu
Rakennustekniikan laitos

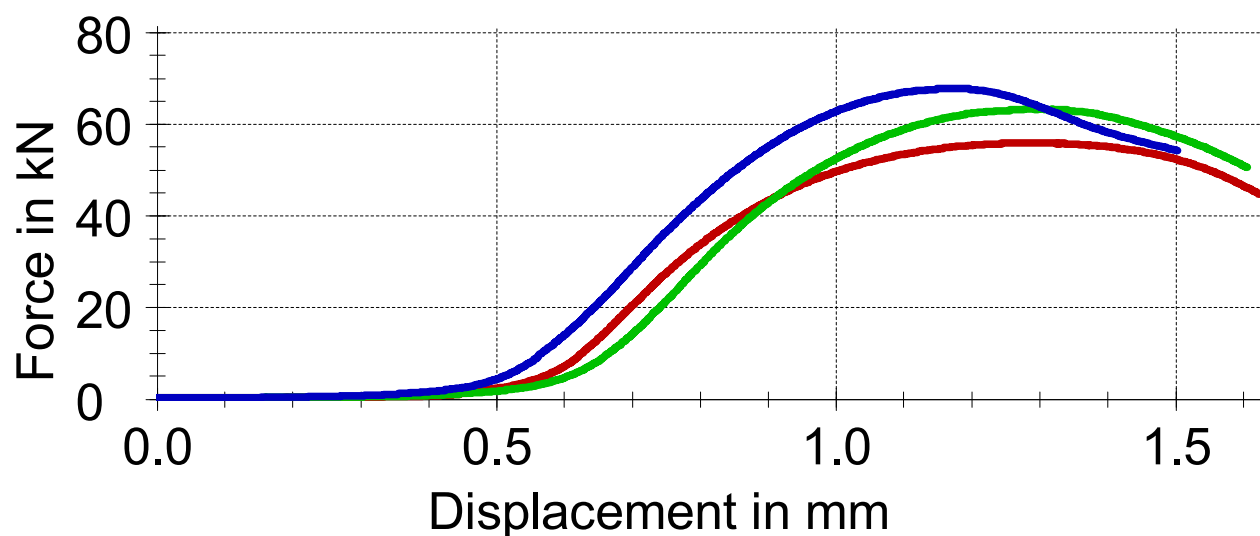
Test report

Customer : Aalto/CE/Soil Lab. Pre-treatment :
Group : Tester : Manish Jaiswal
Material : NS + CC + IS + FA + CEM W14% Notes... :
Specimen type : Cylindrical rammed earth
Pre-load : 200 N
Test speed : 1,5 mm/min

Test results:

Legends	Nr	Specimen identifier	d ₀ mm	h ₀ mm	ρ ₀ kg/m ³	Mass g	F _{max} kN	σ _M N/mm ²	dL at F _{max} mm
■	1	M_23_1	100,00	157,5	1346	2310	55,99	7,13	1,3
■	2	M_23_2	100,00	155,6	1323	2244	63,30	8,06	1,3
■	3	M_23_3	100,00	154,4	1316	2214	67,86	8,64	1,2

Series graph:



Statistics:

Series	ρ ₀ kg/m ³	σ _M N/mm ²
n = 3		
\bar{x}	1329	7,94
s	15,61	0,76
v	1,17	9,60

20.11.24

Aalto-yliopisto
Insinööritieteiden korkeakoulu
Rakennustekniikan laitos

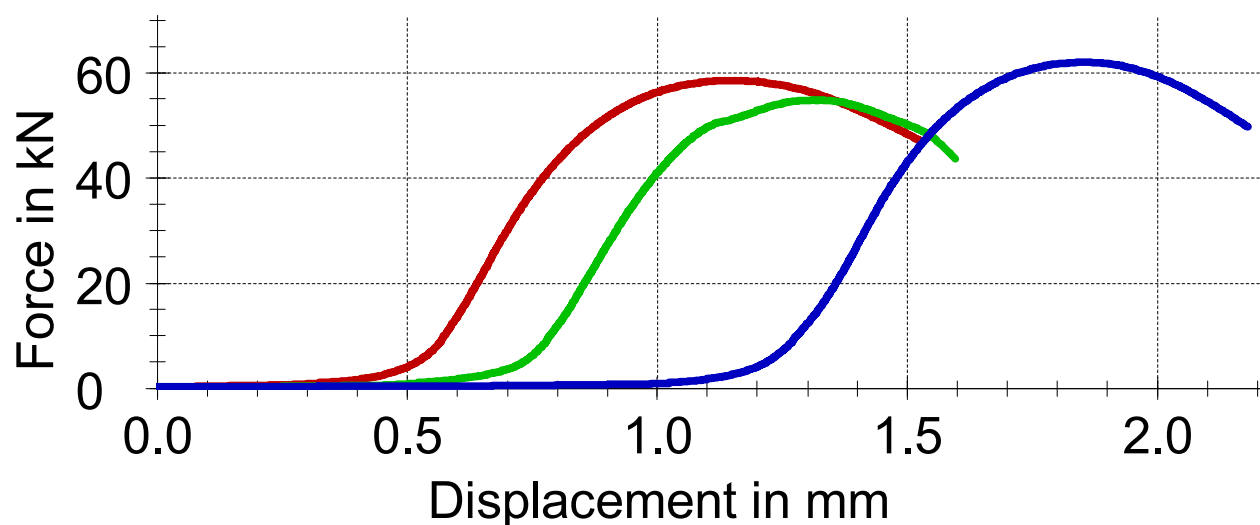
Test report

Customer : Aalto/CE/Soil Lab. Pre-treatment :
 Group : Tester : Manish Jaiswal
 Material : NS + CC + IS + FA + CEM + W14% Notes... :
 Specimen type : Cylindrical rammed earth
 Pre-load : 200 N
 Test speed : 2 mm/min

Test results:

Legends	Nr	Specimen identifier	d_0 mm	h_0 mm	ρ_0 kg/m ³	Mass g	F_{max} kN	σ_M N/mm ²	dL at F_{max} mm
■	1	M_23_4	100,00	157,3	1334	2286	58,54	7,45	1,2
■	2	M_23_5	100,00	156,7	1316	2246	54,86	6,98	1,3
■	3	M_23_6	100,00	156,6	1345	2295	62,10	7,91	1,8

Series graph:



Statistics:

Series	ρ_0 kg/m ³	σ_M N/mm ²
n = 3		
\bar{x}	1332	7,45
s	14,69	0,46
v	1,10	6,19

03.12.24

Aalto-yliopisto
Insinöörityöiden korkeakoulu
Rakennustekniikan laitos

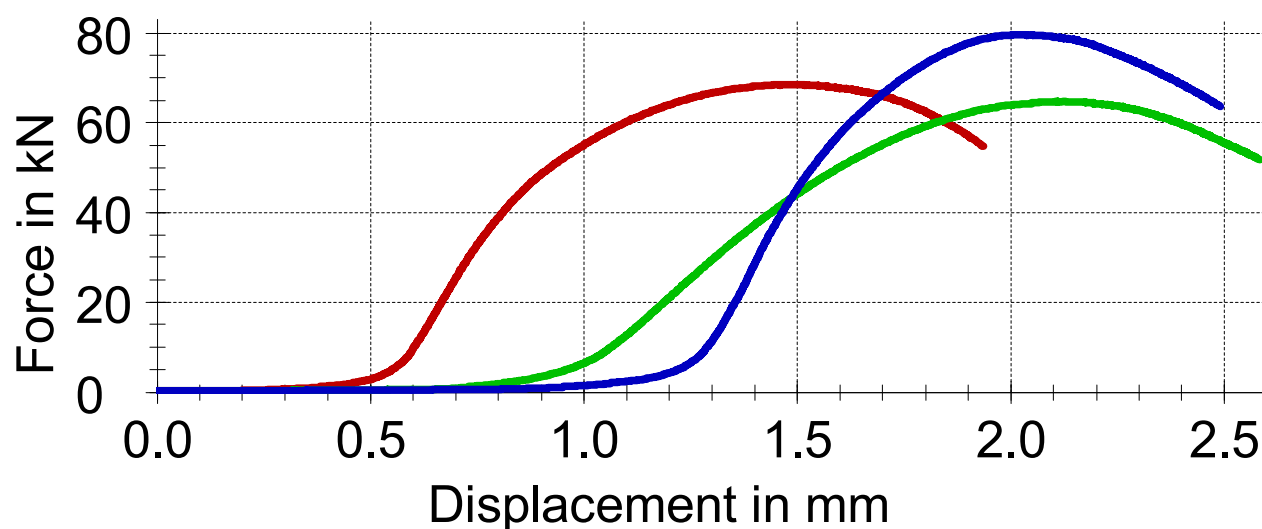
Test report

Customer : Aalto/CE/Soil Lab. Pre-treatment :
 Group : Tester : Manish Jaiswal
 Material : NS + CC + IS + FA + CEM W16% Notes... :
 Specimen type : Cylindrical rammed earth
 Pre-load : 200 N
 Test speed : 1,5 mm/min

Test results:

Legends	Nr	Specimen identifier	d_0 mm	h_0 mm	ρ_0 kg/m ³	Mass g	F_{max} kN	σ_M N/mm ²	dL at F_{max} mm
■	1	M_24_1	100,00	147,8	1390	2238	68,53	8,72	1,5
■	2	M_24_2	100,00	149,6	1377	2245	64,72	8,24	2,1
■	3	M_24_3	100,00	147,9	1377	2219	79,59	10,13	2,0

Series graph:



Statistics:

Series	ρ_0 kg/m ³	σ_M N/mm ²
n = 3		
\bar{x}	1382	9,03
s	7,619	0,98
v	0,55	10,89

20.11.24

Aalto-yliopisto
Insinöörیتieteiden korkeakoulu
Rakennustekniikan laitos

Test report

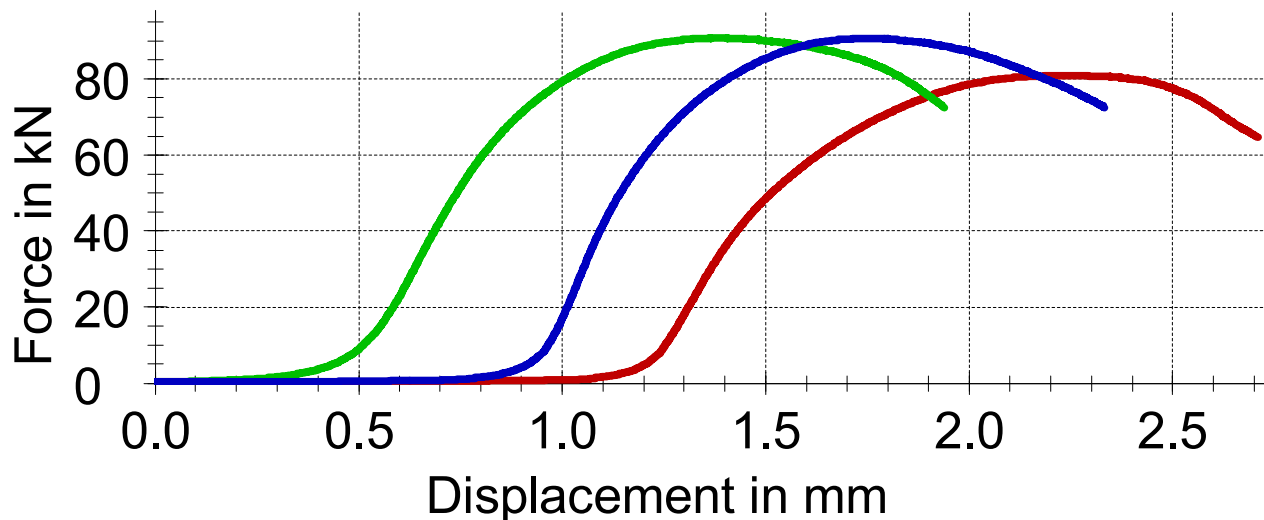
Customer : Aalto/CE/Soil Lab. Pre-treatment :
 Group : Tester : Manish Jaiswal
 Material : NS + CC + IS + FA + CEM + W16% Notes... :
 Specimen type : Cylindrical rammed earth

Pre-load : 200 N
 Test speed : 1,5 mm/min

Test results:

Legends	Nr	Specimen identifier	d_0 mm	h_0 mm	ρ_0 kg/m ³	Mass g	F_{max} kN	σ_M N/mm ²	dL at F_{max} mm
■	1	M_24_4	100,00	147,5	1374	2206	80,91	10,30	2,2
■	2	M_24_5	100,00	146,2	1385	2206	90,78	11,56	1,4
■	3	M_24_6	100,00	147,1	1375	2202	90,64	11,54	1,7

Series graph:



Statistics:

Series	ρ_0 kg/m ³	σ_M N/mm ²
n = 3		
\bar{x}	1378	11,13
s	6,483	0,72
v	0,47	6,47

03.12.24

Aalto-yliopisto
Insinööritieteiden korkeakoulu
Rakennustekniikan laitos

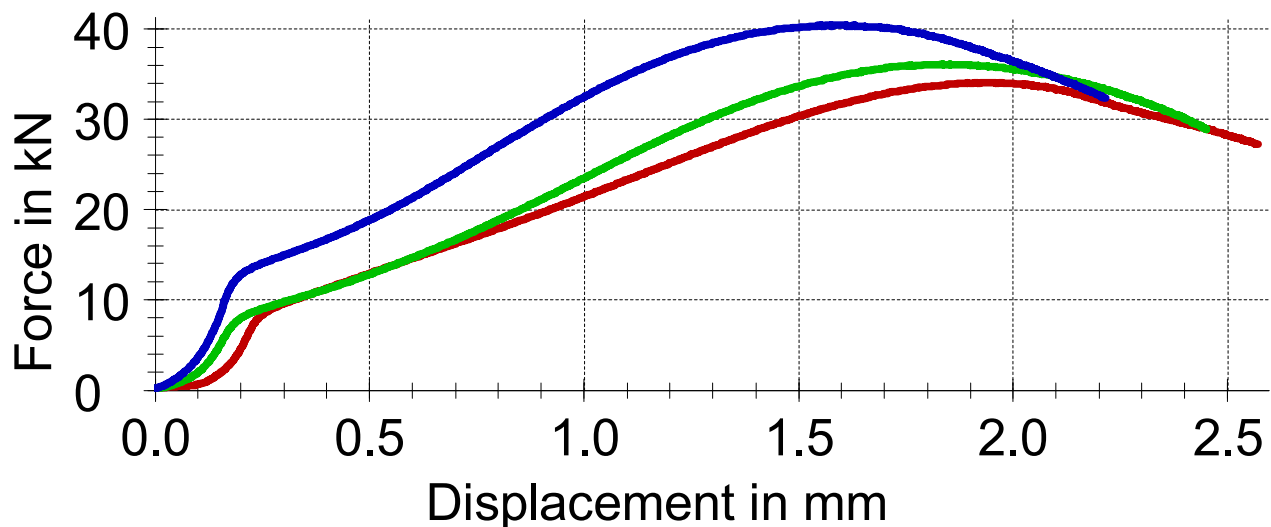
Test report

Customer : Aalto/CE/Soil Lab. Pre-treatment :
 Group : Tester : Manish Jaiswal
 Material : NS + CC + IS + FA + CEM W18% Notes... :
 Specimen type : Cylindrical rammed earth
 Pre-load : 200 N
 Test speed : 1,5 mm/min

Test results:

Legends	Nr	Specimen identifier	d_0 mm	h_0 mm	ρ_0 kg/m ³	Mass g	F_{max} kN	σ_M N/mm ²	dL at F_{max} mm
■	1	M_25_1	100,00	141,8	1448	2238	34,08	4,34	2,0
■	2	M_25_2	100,00	141,0	1452	2229	36,13	4,60	1,8
■	3	M_25_3	100,00	136,9	1478	2204	40,43	5,15	1,6

Series graph:



Statistics:

Series	ρ_0 kg/m ³	σ_M N/mm ²
n = 3		
\bar{x}	1459	4,70
s	16,17	0,41
v	1,11	8,80

20.11.24

Aalto-yliopisto
Insinööritieteiden korkeakoulu
Rakennustekniikan laitos

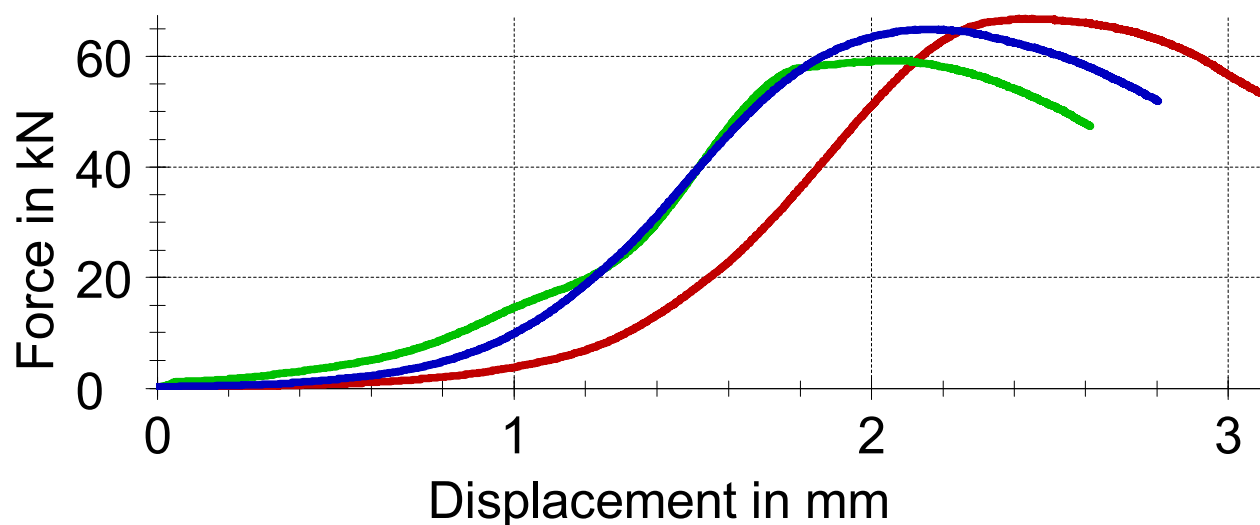
Test report

Customer : Aalto/CE/Soil Lab. Pre-treatment :
 Group : Tester : Manish jaiswal
 Material : NS + CC + IS + FA + CEM W18% Notes... :
 Specimen type : Cylindrical rammed earth
 Pre-load : 200 N
 Test speed : 1,5 mm/min

Test results:

Legends	Nr	Specimen identifier	d_0 mm	h_0 mm	ρ_0 kg/m ³	Mass g	F_{max} kN	σ_M N/mm ²	dL at F_{max} mm
	1	M_25_4	100,00	142,3	1416	2195	66,78	8,50	2,4
	2	M_25_5	100,00	140,8	1425	2184	59,24	7,54	2,1
	3	M_25_6	100,00	142,3	1419	2199	64,95	8,27	2,2

Series graph:



Statistics:

Series	ρ_0 kg/m ³	σ_M N/mm ²
n = 3		
\bar{x}	1420	8,10
s	4,465	0,50
v	0,31	6,18

04.12.24

Aalto-yliopisto
Insinööritieteiden korkeakoulu
Rakennustekniikan laitos

Test report

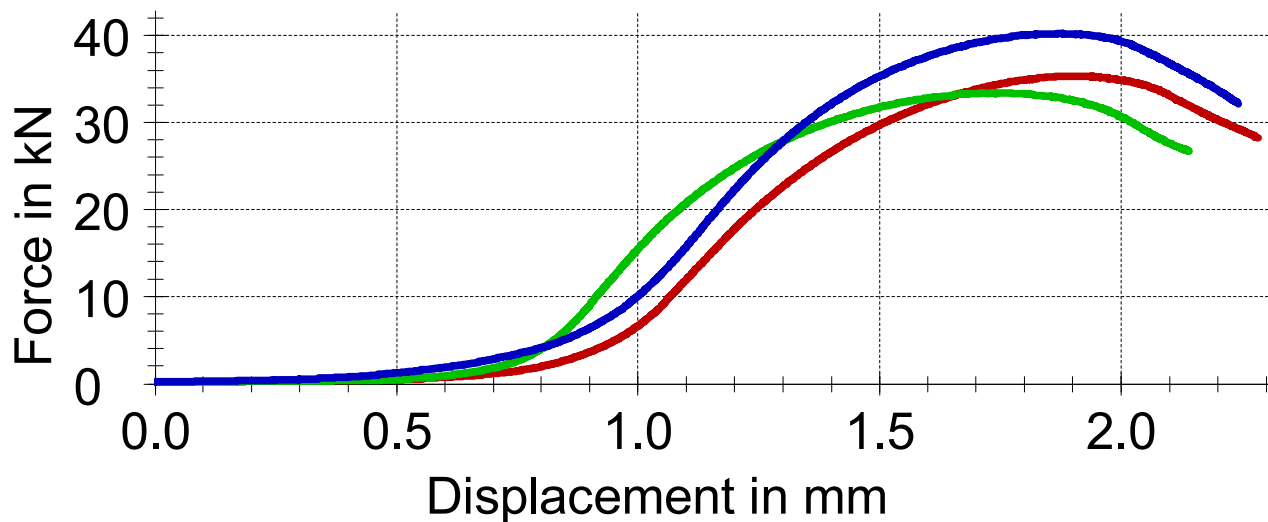
Customer : Aalto/CE/Soil Lab. Specimen type : Cylindrical rammed earth
Group : Pre-treatment :
Material : AGG + FA + CEM W8% Tester : Manish jaiswal
Specimen removal : Notes... :

Pre-load : 200 N
Test speed : 1,5 mm/min

Test results:

Legends	Nr	Specimen identifier	d_0 mm	h_0 mm	ρ_0 kg/m ³	Mass g	F_{max} kN	σ_M N/mm ²	dL at F_{max} mm
■	1	M_26_1	100,00	160,8	1393	2439	35,35	4,50	1,9
■	2	M_26_2	100,00	162,8	1405	2490	33,42	4,25	1,8
■	3	M_26_3	100,00	161,6	1407	2478	40,27	5,13	1,9

Series graph:



Statistics:

Series	ρ_0 kg/m ³	σ_M N/mm ²
n = 3		
\bar{x}	1402	4,63
s	7,85	0,45
v	0,56	9,73

21.11.24

Aalto-yliopisto
Insinööritieteiden korkeakoulu
Rakennustekniikan laitos

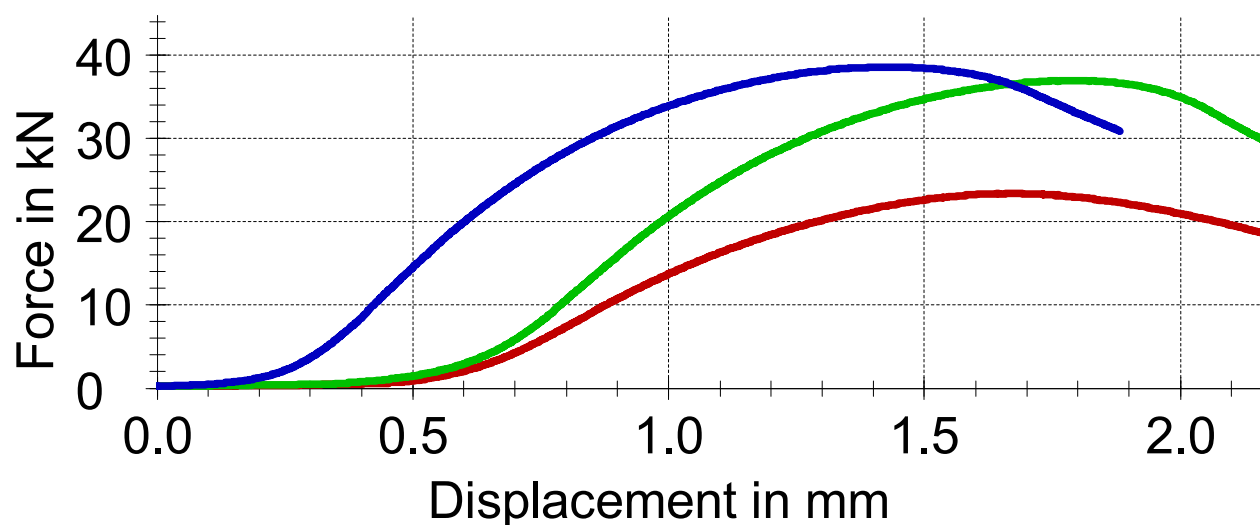
Test report

Customer : Aalto/CE/Soil Lab. Pre-treatment :
Group : Tester : Manish Jaiswal
Material : AGG + IS + FA + CEM W8% Notes... :
Specimen type : Cylindrical rammed earth
Pre-load : 200 N
Test speed : 2 mm/min

Test results:

Legends	Nr	Specimen identifier	d_0 mm	h_0 mm	ρ_0 kg/m ³	Mass g	F_{max} kN	σ_M N/mm ²	dL at F_{max} mm
■	1	M_26_4	100,00	161,8	1347	2374	23,39	2,98	1,7
■	2	M_26_5	100,00	161,8	1405	2476	36,97	4,71	1,8
■	3	M_26_6	100,00	161,4	1409	2478	38,62	4,92	1,5

Series graph:



Statistics:

Series	ρ_0 kg/m ³	σ_M N/mm ²
n = 3		
\bar{x}	1387	4,20
s	34,65	1,06
v	2,50	25,32

04.12.24

Aalto-yliopisto
Insinöörیتieteiden korkeakoulu
Rakennustekniikan laitos

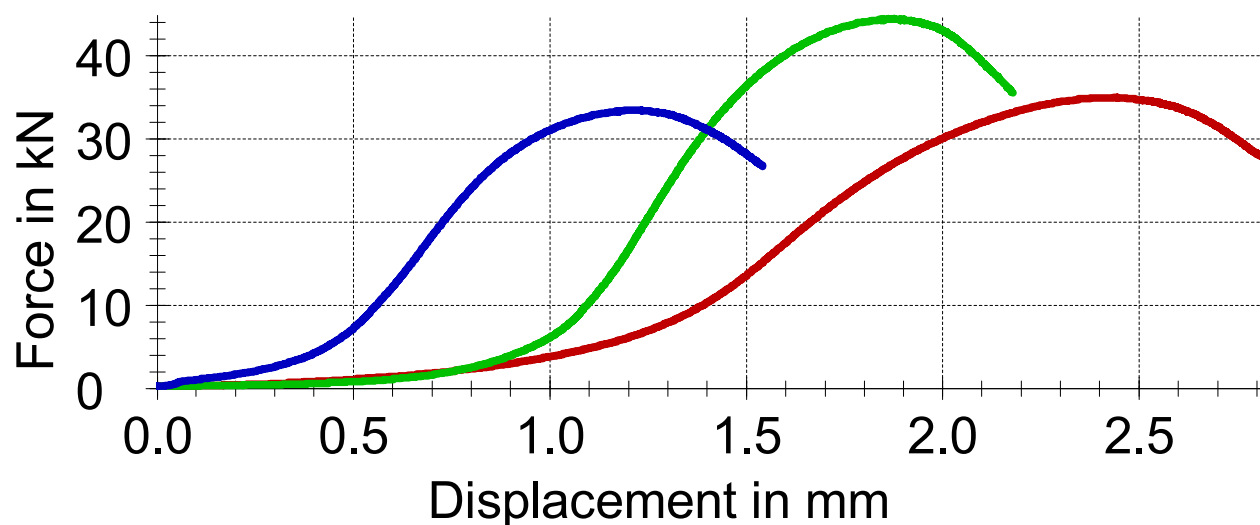
Test report

Customer : Aalto/CE/Soil Lab. Pre-treatment :
Group : Tester : Manish Jaiswal
Material : AGG + FA + CEM W10% Notes... :
Specimen type : Cylindrical rammed earth
Pre-load : 200 N
Test speed : 1,5 mm/min

Test results:

Legends	Nr	Specimen identifier	d_0 mm	h_0 mm	ρ_0 kg/m ³	Mass g	F_{max} kN	σ_M N/mm ²	dL at F_{max} mm
■	1	M_27_1	100,00	159,0	1402	2428	35,00	4,46	2,4
■	2	M_27_2	100,00	158,6	1403	2424	44,47	5,66	1,9
■	3	M_27_3	100,00	158,8	1382	2392	33,48	4,26	1,2

Series graph:



Statistics:

Series	ρ_0 kg/m ³	σ_M N/mm ²
n = 3		
\bar{x}	1396	4,79
s	11,58	0,76
v	0,83	15,81

21.11.24

Aalto-yliopisto
Insinöörityöiden korkeakoulu
Rakennustekniikan laitos

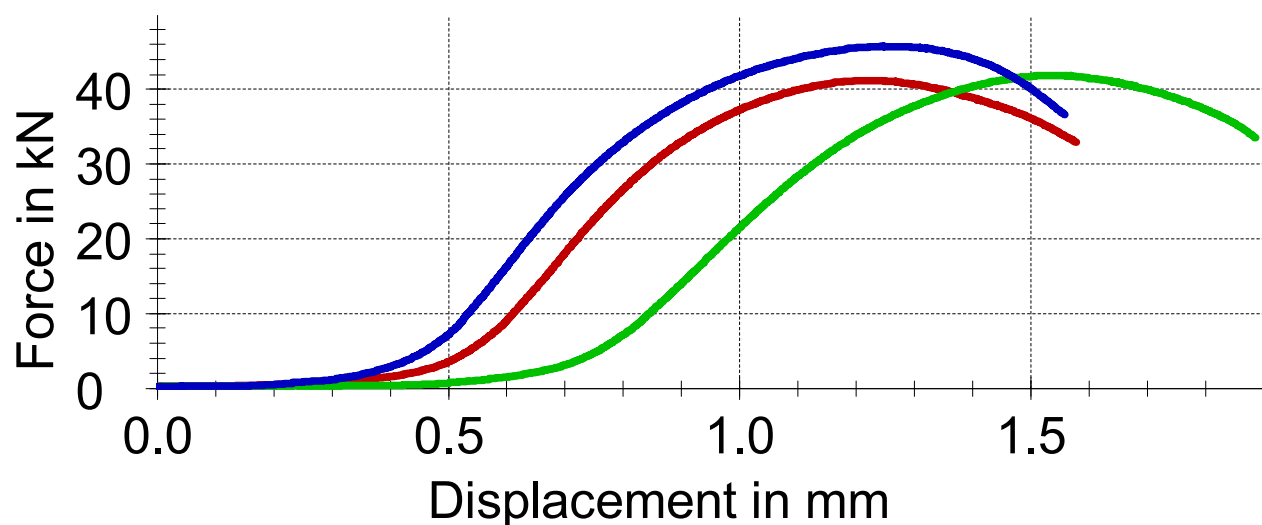
Test report

Customer : Aalto/CE/Soil Lab. Pre-treatment :
 Group : Tester : Manish Jaiswal
 Material : AGG + IS + FA + CEM W10% Notes... :
 Specimen type : Cylindrical rammed earth
 Pre-load : 200 N
 Test speed : 1,5 mm/min

Test results:

Legends	Nr	Specimen identifier	d ₀ mm	h ₀ mm	ρ ₀ kg/m ³	Mass g	F _{max} kN	σ _M N/mm ²	dL at F _{max} mm
■	1	M_27_4	100,00	157,4	1410	2417	41,18	5,24	1,2
■	2	M_27_5	100,00	158,3	1406	2424	41,90	5,34	1,5
■	3	M_27_6	100,00	158,2	1404	2419	45,77	5,83	1,2

Series graph:



Statistics:

Series	ρ ₀ kg/m ³	σ _M N/mm ²
n = 3		
\bar{x}	1407	5,47
s	2,91	0,31
v	0,21	5,75

04.12.24

Aalto-yliopisto
Insinöörیتieteiden korkeakoulu
Rakennustekniikan laitos

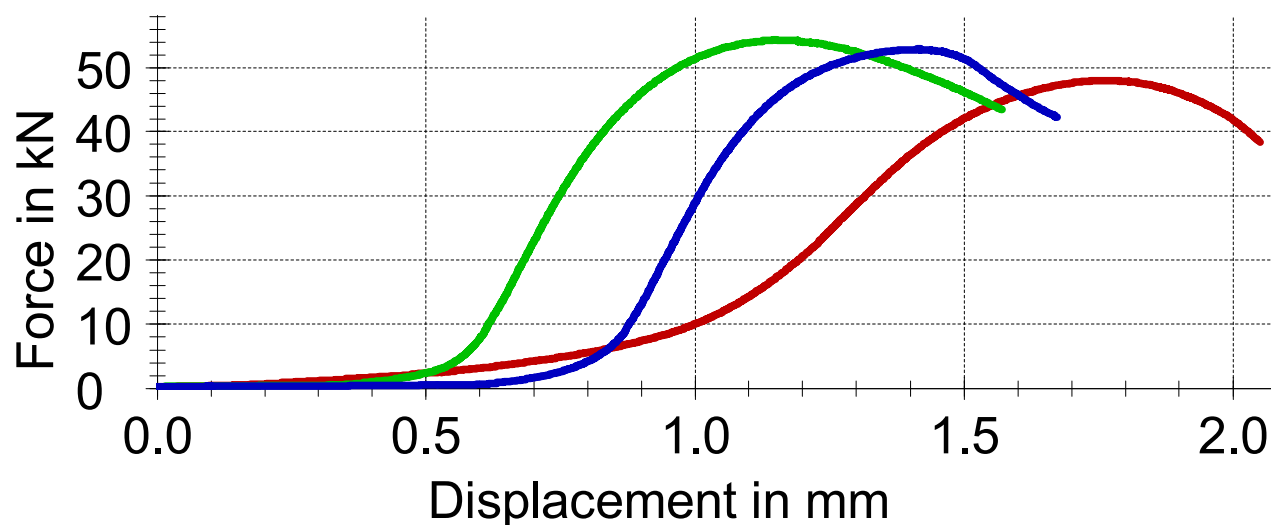
Test report

Customer : Aalto/CE/Soil Lab. Pre-treatment :
Group : Tester : Manish jaiswal
Material : AGG + FA + CEM W12% Notes... :
Specimen type : Cylindrical rammed earth
Pre-load : 200 N
Test speed : 1,5 mm/min

Test results:

Legends	Nr	Specimen identifier	d ₀ mm	h ₀ mm	ρ ₀ kg/m ³	Mass g	F _{max} kN	σ _M N/mm ²	dL at F _{max} mm
■	1	M_28_1	100,00	154,7	1395	2351	47,99	6,11	1,8
■	2	M_28_2	100,00	153,1	1364	2276	54,30	6,91	1,1
■	3	M_28_3	100,00	154,5	1372	2309	52,88	6,73	1,4

Series graph:



Statistics:

Series	ρ ₀ kg/m ³	σ _M N/mm ²
n = 3		
\bar{x}	1377	6,59
s	16,06	0,42
v	1,17	6,40

21.11.24

Aalto-yliopisto
Insinööritieteiden korkeakoulu
Rakennustekniikan laitos

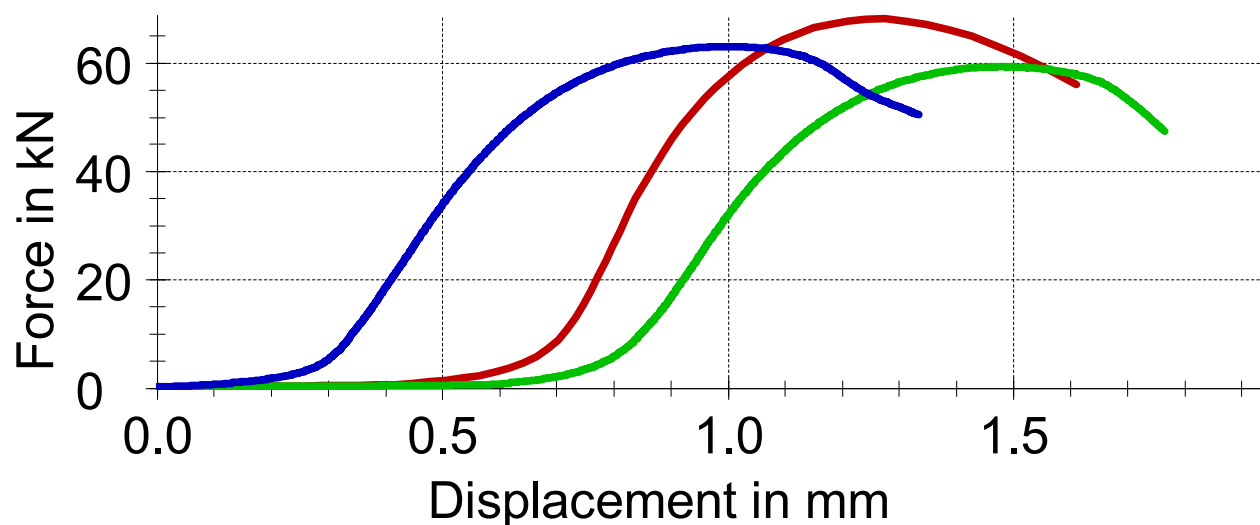
Test report

Customer : Aalto/CE/Soil Lab. Pre-treatment :
 Group : Tester : Manish Jaiswal
 Material : AGG + IS + FA + CEM W12% Notes... :
 Specimen type : Cylindrical rammed earth
 Pre-load : 200 N
 Test speed : 1,5 mm/min

Test results:

Legends	Nr	Specimen identifier	d_0 mm	h_0 mm	ρ_0 kg/m ³	Mass g	F_{max} kN	σ_M N/mm ²	dL at F_{max} mm
	1	M_28_4	100,00	152,8	1407	2341	68,21	8,69	1,3
	2	M_28_5	100,00	152,9	1403	2337	59,43	7,57	1,5
	3	M_28_6	100,00	151,6	1337	2208	63,15	8,04	1,0

Series graph:



Statistics:

Series	ρ_0 kg/m ³	σ_M N/mm ²
n = 3		
\bar{x}	1382	8,10
s	39,1	0,56
v	2,83	6,93

Pika

SEMENTTI CEMENT

Erittäin nopeasti kovettuva portlandsementti
CEM I 52,5 R

Pikasementti soveltuu nopean lujuudenkehityksensä ansiosta erittäin nopeaa muottikiertoa vaativaan elementti- ja betonituotantoon. Erityiskäyttökohteita ovat jännebetonit ja korkealujuusbetonit. Seostamalla Pikasementti soveltuu hyvin myös valmisbetonituotantoon.

Sementin ominaisuuksia

Vaatimukset (SFS-EN 197-1)

Puristuslujuus 2 vrk	≥ 30 MPa
Puristuslujuus 28 vrk	≥ 52,5 MPa
Sitoutumisaika	≥ 45 min
Tilavuudenpysyvyys	≤ 10 mm
Hehkutushäviö	≤ 5 %
Liukenematon jäännös	≤ 5 %
SO ₃	≤ 4,0 %
Kloridipitoisuus	≤ 0,10 %

Sementin koostumus

Vaatimukset (SFS-EN 197-1)

Klinkkeri	≥ 95 % ja ≤ 100 %
-----------	-------------------

Sementin ominaisuuksia

Vaatimukset (REACH N:o 1907/2006)

Cr6+	≤ 2 mg/kg
------	-----------

FINNSEMENTTI
A CRH COMPANY

Finnsementti Oy
FI-21600 Parainen, Puh. 0201 206 200
info@finnsementti.fi, etunimi.sukunimi@finnsementti.fi
semnet.fi, finnsementti.fi





TESTAUSSELOSTE 2023-41270
Korvaa testausselosteen samalla
numerolla päiväyksellä 10.1.2024.

1(1)
18.07.2024

Tilaaaja
2274241-9
317 HSY Jätehuolto, jätteen jalostus (kuona)

Maksaja
**317 HSY Helsingin seudun
ympäristöpalvelut -kuntayht
Ostolaskut**



PL 210
00066 HSY

PL 303
00066 HSY

Näytetiedot

Näyte	Jäte, 2-vaiheinen liukoisuustesti		
Näyte otettu	27.12.2023	Kellonaika	11.00
Vastaanotettu	29.12.2023	Kellonaika	12.35
Tutkimus alkoi	29.12.2023	Näytteenoton syy	Omaavonta

Näytteenottaja Tilaaajan toimesta
Viite Hannu Juntunen
Korvaavuuden syy: Näytteen nimi korjattu

Analyysi	Menetelmä	41270-1 Jäte, 2-vaiheinen liukoisuustesti 0-2 KM15	Yksikkö	MU %
2-vaiheinen ravistelutesti L/S=10L/kg	* SFS-EN 12457-3:2002	Liite 1		

MU % = mittausepävarmuus, joka pätee MetropoliLabin tuottamilla tuloksilla näytteille tyypillisellä pitoisuusalueella. Tarkemmat tiedot mittausepävarmuudesta on saatavilla laboratorion sivustalta. * = Akkreditoitu menetelmä

Yhteyshenkilö Nyandoto Were, 010 391 3427, ympäristöasiantuntija

Tiedoksi hannu.juntunen@hsy.fi;
jate.jalostus@hsy.fi;
matilda.seppinen@hsy.fi;
taru.leskela@hsy.fi

Laboratorio ei vastaa asiakkaan toimittamista tiedoista. Asiakkaan toimittamat tiedot voivat vaikuttaa tulosten oikeellisuuteen. Tulokset pätevät vain testatuille näytteille. Ellei testausselostella toisin ilmoiteta, tulokset pätevät laboratorion vastaanottamille näytteille ja näytteenottoon liittyvät tiedot ovat asiakkaan toimittamia. Testausselosteen osittainen kopiointi ei ole sallittua. Testausseloste on hyväksytty sähköisesti ja on pätevä ilman allekirjoitusta.

Postiosoite Viikinkaari 4
00790 Helsinki
metropolilab@metropolilab.fi

Puhelin +358 10 391 350

Faksi +358 9 310 31626

http://www.metropolilab.fi

Y-tunnus 2340056-8
Alv. Nro FI23400568



LIITE 1 testausselosteeseen 41270-1
Sivu 1 / (2)

KAKSIVAIHEINEN RAVITSELUTESTI UUTTOLIUKOKSEN JA KIINTEÄN JÄTTEEN SUHTEISSA 2 l / kg ja 8 l / kg *
Jäte, 2-vaiheinen ravitsemustesti
SFS-EN 12457-3:2002

LIMS-numero: 2023--41270-1+2

Ensimmäisen vaiheen liukoisuus
A2 = C2 * [(L2 / MD) + (MC / 100)]
(Merkinnot viitestandardin laskukaavoista)

Näyte: 0-2 KM15

L/S = 10 l/kg, Kumulaattivinen liukoisuus, mg / kg kuiva-ainetta
A2-10 = C2 * (VE1 / MD) + C8 * [(L2 + L8 - VE1) / MD + (MC / 100)]

Analyysi		Yksikkö		Mittausepävarmuus		VNA 331/2013 & T030/2021 kaatopaikka-kelpoisuuden enimmäispiitoisuudet:			
Analyysi	Liukoisuus	Yksikkö	Analyysi	Liukoisuus	Yksikkö	Mittausepävarmuus	Pysyvä jäte	Vaaraton jäte	Vaarallinen jäte
pH	10,8		pH *	11,2		0,5 pH-yks.			
Sähkönjoht.	970	mS/m	Sähkönjoht. *	180	mS/m	30 %			
As	< 0,01	mg/kg	As *	< 0,05	mg/kg	40 %	0,5	2	25
Ba	0,09	mg/kg	Ba *	0,25	mg/kg	40 %	20	100	300
Cd	< 0,002	mg/kg	Cd *	< 0,010	mg/kg	40 %	0,04	1	5
Cr	3,25	mg/kg	Cr *	3,97	mg/kg	40 %	0,5	10	70
Cu	0,39	mg/kg	Cu *	0,62	mg/kg	40 %	2	50	100
Hg	0,005	mg/kg	Hg *	0,010	mg/kg	40 %	0,01	0,2	2
Mo	0,87	mg/kg	Mo *	1,05	mg/kg	50 %	0,5	10	30
Ni	< 0,01	mg/kg	Ni *	< 0,05	mg/kg	40 %	0,4	10	40
Pb	< 0,01	mg/kg	Pb *	< 0,05	mg/kg	40 %	0,5	10	50
Sb	0,03	mg/kg	Sb *	0,22	mg/kg	40 %	0,06	0,7	5
Se	0,02	mg/kg	Se *	< 0,06	mg/kg	40 %	0,1	0,5	7
Zn	< 0,03	mg/kg	Zn *	0,37	mg/kg	40 %	4	50	200
V	0,03	mg/kg	V *	0,11	mg/kg	40 %	-	-	-
Cl	4,876	mg/kg	Cl *	4,752	mg/kg	40 %	800	15 000	25 000
F	5	mg/kg	F *	< 12	mg/kg	40 %	10	150	500
SO ₄	3 657	mg/kg	SO ₄ *	5 368	mg/kg	40 %	1 000	20 000	50 000
DOC	120	mg/kg	DOC *	< 169	mg/kg	40 %	500	800	1 000
TDS	13 002	mg/kg	TDS *	16 996	mg/kg	40 %	4 000	60 000	100 000

* = Akkreditoitu menetelmä Lisätietoja näytteen esikäsitelystä ja ravitsemustestistä: Wete Nyandoro, Yrmpäristöasiantuntija, puh. 010 3913 427

Postiosoite
Valikkokaari 4
00790 Helsinki
metropolilab@metropolilab.fi

Puhelin
+358 10 391 350
http://www.metropolilab.fi

Y-tunnus
2340056-8
AV. Nro
FI23400568



LITTE 1 testausselosteeseen 41270-1
Sivu 2 / (2)

Menetelmätiedot

pH	SFS 3021:1979
Sähkönjohtavuus	SFS-EN 27888:1994
Alkuaineet	SFS-EN ISO 17294-2:2016, ICP-MS
Ioni (Cl, F, SO ₄)	SFS-EN ISO 10304-1:2009
DOC	SFS-EN 1484:1997
TDS	SFS 3008:1990
Fenoli-indeksi	ISO 14402:1999 (CFA)

25-Sep-2024 09:39:48

PANalytical

Quantification of sample Lentotuhka

R.M.S.: 0.005

Result status: NoC;

Sum before normalization: 39.2 %

Normalised to: 100.0 %

Sample type: Loose powder

Compton validation factor: 0.75

Correction applied for medium: Yes

Correction applied for film: Yes

Used Compound list: Oxides

Results database: omnian_al_27_he

Results database in: c:\panalytical\superq\userdata

Compound	Conc.	Absolute
Name	(%)	Error (%)
1	SiO2	49.47 0.2
2	Al2O3	16.81 0.1
3	Fe2O3	12.76 0.1
4	CaO	9.10 0.09
5	K2O	4.29 0.06
6	TiO2	1.96 0.04
7	P2O5	1.73 0.04
8	MgO	1.02 0.03
9	SO3	0.83 0.03
10	SrO	0.61 0.02
11	Na2O	0.41 0.03
12	BaO	0.39 0.02
13	ZrO2	0.23 0.01
14	MnO	0.12 0.01
15	ZnO	0.06 0.007
16	Cr2O3	0.04 0.006
17	NiO	0.04 0.006
18	CuO	0.03 0.005
19	Co3O4	0.03 0.005
20	Cl	0.03 0.005
21	Rb2O	0.03 0.005
22	Ga2O3	0.01 0.003
23	Nb2O5	0.01 0.003
24	GeO2	0.01 0.002
25	Ac	0.00
26	Rn	0.00
27	PbO	0.00
28	OsO4	0.00
29	Dy2O3	0.00
30	CeO2	0.00
31	Y2O3	0.00
32	Kr	0.00
33	As2O3	0.00
34	V2O5	0.00

25-Sep-2024 09:41:48

PANalytical
Quantification of sample Lentotuhka

R.M.S.: 0.005
 Result status: NoC;
 Sum before normalization: 39.2 %
 Normalised to: 100.0 %
 Sample type: Loose powder
 Compton validation factor: 0.75
 Correction applied for medium: Yes
 Correction applied for film: Yes
 Used Compound list: Oxides
 Results database: omnian_al_27_he
 Results database in: c:\panalytical\superq\userdata

Compound	Conc.	Absolute
Name	(%)	Error (%)
1	SiO2	49.47 0.2
2	Al2O3	16.81 0.1
3	Fe2O3	12.76 0.1
4	CaO	9.10 0.09
5	K2O	4.29 0.06
6	TiO2	1.96 0.04
7	P2O5	1.73 0.04
8	MgO	1.02 0.03
9	SO3	0.83 0.03
10	SrO	0.61 0.02
11	Na2O	0.41 0.03
12	BaO	0.39 0.02
13	ZrO2	0.23 0.01
14	MnO	0.12 0.01
15	ZnO	0.06 0.007
16	Cr2O3	0.04 0.006
17	NiO	0.04 0.006
18	CuO	0.03 0.005
19	Co3O4	0.03 0.005
20	Cl	0.03 0.005
21	Rb2O	0.03 0.005
22	Ga2O3	0.01 0.003
23	Nb2O5	0.01 0.003
24	GeO2	0.01 0.002
25	Ac	0.00
26	Rn	0.00
27	PbO	0.00
28	OsO4	0.00
29	Dy2O3	0.00
30	CeO2	0.00
31	Y2O3	0.00
32	Kr	0.00
33	As2O3	0.00
34	V2O5	0.00